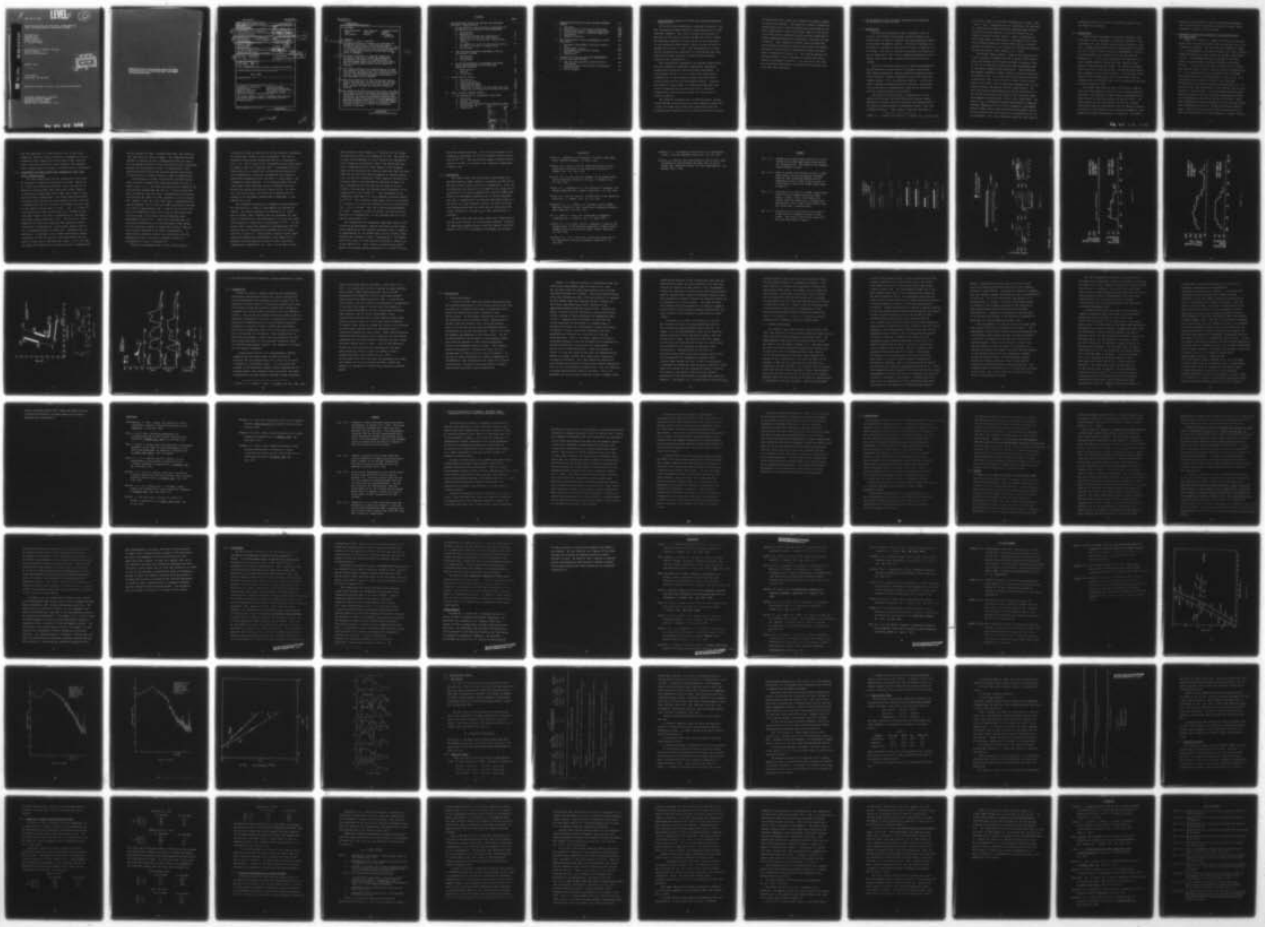
AD-A065 550 EMMANUEL COLL BOSTON MASS F/G 4/1
STUDY AND ANALYSIS OF EQUATORIAL IRREGULARITIES, TOTAL ELECTRON--ETC(U)
OCT 78 S BASU, S BASU, J JOHANSON F19628-76-C-0003
UNCLASSIFIED AFGL-TR-78-0263 NL

1 OF 2
AD
AD 65550




1 OF 2
AD
AO 65550
1.0
1.1
1.25
1.4
1.6
1.8
2.0
2.2
2.5
2.8
3.2
3.6
4.0
4.5
5.0
5.6
MICROCOPY RESOLUTION TEST CHART
NATIONAL BUREAU OF STANDARDS-1963-A

AFGL-TR-78-0263

LEVEL II

(12)

STUDY AND ANALYSIS OF EQUATORIAL IRREGULARITIES, TOTAL ELECTRON CONTENT, AND SCINTILLATIONS

Santimay Basu
Sunanda Basu
James Johanson
Eileen MacKenzie
M. Patricia Hagan

The Trustees of Emmanuel College
400 The Fenway
Boston, Massachusetts

AD A065550

DDC FILE COPY

D D C
RECEIVED
MAR 12 1979
C

October 1978

Final Report
1 July 1975 - 30 June 1978

Approved for public release; distribution umlimited.

AIR FORCE GEOPHYSICS LABORATORY
AIR FORCE SYSTEMS COMMAND
UNITED STATES AIR FORCE
HANSCOM AFB, MASSACHUSETTS 01731

79 03 09 036

Qualified requestors may obtain additional copies from the Defense Documentation Center. All others should apply to the National Technical Information Service.

UNCLASSIFIED

MIL-STD-847A
31 January 1973

SECURITY CLASSIFICATION OF THIS PAGE (When Data Entered)

REPORT DOCUMENTATION PAGE

READ INSTRUCTIONS BEFORE COMPLETING FORM

1. REPORT NUMBER: AFGL-TR-78-0263	2. GOVT ACCESSION NO. / 3. RECIPIENT'S CATALOG NUMBER
4. TITLE (and Subtitle): Study and Analysis of Equatorial Irregularities, Total Electron Content, and Scintillations.	5. TYPE OF REPORT & PERIOD COVERED: Final Rept. 01JUL75 - 30JUN78 (1 Jul 75-30 June 78.)
	6. PERFORMING ORG. REPORT NUMBER
7. AUTHOR(s): Santimay Basu, Sunanda Basu, James Johanson, Eileen MacKenzie, M. Patricia Hagan	8. CONTRACT OR GRANT NUMBER(s): F19628-76-C-0003
9. PERFORMING ORGANIZATION NAME AND ADDRESS: Emmanuel College, 400 The Fenway, Boston MA 02115	10. PROGRAM ELEMENT, PROJECT, TASK AREA & WORK UNIT NUMBERS: 46430401, 62101F 46430502
11. CONTROLLING OFFICE NAME AND ADDRESS: Air Force Geophysics Laboratory (PHP), Hanscom AFB, MA 01731, Contract Monitor: Herbert E. Whitney	12. REPORT DATE: October 1978
	13. NUMBER OF PAGES: 180 (182p.)
14. MONITORING AGENCY NAME & ADDRESS (if different from Controlling Office): 4643, 4643	15. SECURITY CLASS. (of this report): Unclassified
	15a. DECLASSIFICATION DOWNGRADING SCHEDULE

16. DISTRIBUTION STATEMENT (of this Report): 04, 05

A - Approved for public release; distribution unlimited.

17. DISTRIBUTION STATEMENT (of the abstract entered in Block 20, if different from Report)

TECH, OTHER

18. SUPPLEMENTARY NOTES

19. KEY WORDS (Continue on reverse side if necessary and identify by block number)

Ionospheric Irregularities	Invariant Latitude
Scintillations	Scintillations Modelling
Equatorial Electrojet	Total Electron Content (TEC)
Equatorial Spread-F	Plasmaspheric Content

20. ABSTRACT (Continue on reverse side if necessary and identify by block number)

This report embodies a study of Ionospheric Scintillations and the Total Electron Content as considered from the following aspects:

DD FORM 1 JAN 73 1473A EDITION OF 1 NOV 65 IS OBSOLETE

UNCLASSIFIED

SECURITY CLASSIFICATION OF THIS PAGE (When Data Entered)

128 950

UNCLASSIFIED
SECURITY CLASSIFICATION OF THIS PAGE(When Data Entered)

19. KEY WORDS

Radar Backscatter	Plume Structure	Irregularity Patch
Bubble	Scale Size	Lifetime
Power Spectra	M-value	Correlation coefficient

20. ABSTRACT

The following are among the topics studied:

(1) The nature of electrojet irregularities responsible for daytime VHF scintillations in the equatorial region. The times of onset and decay of VHF scintillations are shown to correspond closely with the times of onset and decay of type 2 irregularities deflected by 50 MHz radar and E_{sq} echoes on ionograms.

(2) The spatial localization of nighttime irregularities detected by scintillation and VHF radar backscatter measurements; The results on irregularity patch size and their minimum lifetime based on scintillation measurements at multiple ground stations and by aircraft are presented.

(3) The kilometer and meter scale irregularities in the nighttime equatorial F-region giving rise to VHF-UHF scintillations and VHF radar backscatter; The co-existence of large and small scale irregularities during various phases of their development has been examined.

(4) Modelling of equatorial and high latitude scintillations using a large data base, and also the detailed, individual magnetic storm picture; Solar flux level, seasonal variation, invariant latitude, and irregularity region are discussed.

(5) The variability of total electron content (TEC) as it limits the accuracy of satellite navigation and satellite detection radar systems as well as the correlation distance of TEC variability. The results of plasmaspheric electron content are presented and its importance in the determination of additional ionospheric group delay is assessed. A computer program developed for real time use by Air Weather Service to correct for non zero inclination of geostationary satellites is discussed.

UNCLASSIFIED
SECURITY CLASSIFICATION OF THIS PAGE(When Data Entered)

CONTENTS

		PAGE
I.	MULTITECHNIQUE STUDIES OF DAYTIME AND NIGHTTIME EQUATORIAL IRREGULARITIES	5
	1. ON THE NATURE OF THE ELECTROJET IRREGULARITIES RESPONSIBLE FOR DAYTIME VHF SCINTILLATIONS	
	1. Introduction	7
	2. Observations	9
	3. Comparison between the occurrence of scintillations and VHF radar echoes	10
	4. Comparison of scintillation, radar echoes, and E_{sq}	12
	5. Development of scintillations and evolution of type 1 and type 2 irregularities	13
	6. Conclusions	17
	2. THE LOCALIZED ORIGIN OF EQUATORIAL F-REGION IRREGULARITY PATCHES	
	1. Introduction	29
	2. Observations	31
	3. Discussions	39
	3. ON THE CO-EXISTENCE OF KILOMETER- AND METER-SCALE IRREGULARITIES IN THE NIGHTTIME EQUATORIAL F-REGION	45
	1. Observations	49
	2. Results	50
	3. Discussions	57
II.	SCINTILLATION STUDIES	
	1. Description	73
	2. Equatorial Model	74
	3. High-Latitude Model	77
	4. Comprehensive Model	80
	5. Comparison of Model with Millstone Hill Data	83
	6. Geometrical Considerations at High Latitudes	85
III.	TOTAL ELECTRON CONTENT STUDIES	113
	1. THE VARIABILITY OF IONOSPHERIC TIME DELAY	115
	1. Data Base	116
	2. Diurnal Variation	117
	3. Monthly Variations	119
	4. Distribution of Percentage Differences from Monthly Mean TEC	119
	5. Conclusions	120

ACCESSION for
NTIS [illegible] ☑
DDC [illegible] ☐
UNANNOUNCED ☐
JUSTIFICATION
BY
DISTRIBUTION/AVAILABILITY CODES
Dist. AVAIL. and/or SPECIAL
A

2. CORRELATION DISTANCE OF MEAN DAYTIME ELECTRON CONTENT 131

1. Data Base 132
2. Significance of Correlation Coefficient 134
3. Correlation Results: Longitude Separation 136
4. Correlation Results: Latitude Separation 138
5. Discussions 140
6. Summary of Results 141

3. THE CONTRIBUTION OF THE PLASMASPHERE TO TOTAL TIME DELAY 159

1. Available Plasmaspheric Electron Content Data 160
2. Experimental Results 161
3. Plasmaspheric Group Delay During Magnetic Storms 163
4. Conclusions 163

4. CONVERSION OF FARADAY ROTATION MEASUREMENTS TO TOTAL ELECTRON CONTENT 169

1. Non-zero Geostationary Satellite Orbit Inclination 169
2. Computer Program for Diurnal M Calculation Called ROPLOK 171
3. Use of Program 172

I. MULTITECHNIQUE STUDIES OF DAYTIME AND NIGHTTIME EQUATORIAL IRREGULARITIES

VHF scintillation measurements performed at Huancayo, Peru near the magnetic equator indicate a weak daytime and a strong nighttime component. The level of daytime scintillation is typically of the order of 10 dB at 40 MHz and 1 dB at 140 MHz. The nighttime component of scintillation, on the other hand, is very strong and often attains levels in excess of 25 dB at 140 MHz and 6-8 dB at 1.5 GHz. The characteristics of ionospheric irregularities responsible for both daytime and nighttime scintillations have been studied by multitechnique probing of the irregularities.

The irregularities responsible for daytime scintillations have been explored by conducting simultaneous ionospheric sounding and oblique VHF radar backscatter experiments. In the following section I.1, it is shown that plasma density irregularities in the electrojet region cause VHF scintillations during the day near the magnetic equator. Simultaneous presence of E_{sq} echoes on ionograms and VHF radar backscatter establishes the excitation of type 2 electrojet irregularities covering scale lengths of a few meters to several kilometers.

The nighttime irregularities of electron density causing intense VHF-UHF scintillations have been studied by conducting a series of 50 MHz radar backscatter measurements from the Jicamarca Radio Observatory of the Instituto Geofisico del Peru

in conjunction with a large scale ground and airborne campaign to study scintillations. The equatorial F-region irregularity patches that arise in the post-sunset period are shown to contain irregularities in the scale length range of a few meters to at least several kilometers having east-west dimensions of several hundred kilometers and extending to altitudes as high as 1000 km. Such irregularity patches cause saturated UHF scintillations and intense coherent radar backscatter echoes. The spatial localization of irregularity patches and their drift is discussed in Section I.2. The lifetime patches containing kilometer scale irregularities causing VHF scintillations are examined in Section I.3 in relation to the lifetime of patches containing 3-m irregularities that give rise to 50 MHz radar backscatter.

I.1 ON THE NATURE OF THE ELECTROJET IRREGULARITIES RESPONSIBLE FOR DAYTIME VHF SCINTILLATIONS*

I.1.1 INTRODUCTION

Scintillation measurements made at Huancayo, Peru, by using 41- and 140-MHz transmissions of ATS-6 indicate that scintillation is almost a regularly occurring phenonemon during the day near the magnetic equator. The level of daytime scintillation is typically of the order of 10 dB at 41 MHz and 1 dB at 140 MHz. The level of daytime scintillation is indeed very low in comparison to the level of nighttime equatorial scintillation, which often shows saturation in excess of 25 dB at 140 MHz.

In view of the much lower level of daytime than nighttime scintillation the characteristics of daytime scintillation have remained unexplored, whereas equatorial nighttime scintillation caused by F region irregularities has been extensively studied (Aarons, 1977, and references therein). In the equatorial ionosphere during daytime the electrojet region generates plasma density irregularities; these may be associated with the observed daytime scintillations.

The nature of electron density irregularities in the equatorial electrojet has been extensively explored, experimentally by the radar spectral techniques and theoretically in the light of plasma instability mechanisms (Farley, 1974, and references therein). These studies reveal the existence of

---

* Basu, S., J. Aarons, B.B. Balsley, J. Geophys. Res., 82,5262,1977.

two distinct types of electrojet irregularities, namely, types 1 and 2. Type 1 irregularities are considered to be generated by a modified two-stream instability mechanism when the electron drift velocity relative to the ions exceeds the ion acoustic velocity of about 360 m/s. Type 2 irregularities, on the other hand, are generated by the gradient drift instability mechanism when the electron drift velocity exceeds a velocity of about 30 m/s in a region of steep density gradient (Farley and Balsley, 1973; Balsley et al., 1976).

The present paper attempts a study of the characteristics of the electrojet irregularities and is based on VHF scintillation measurements and ionograms obtained at Huancayo, Peru, as well as on concurrent oblique VHF radar measurements made at the nearby Jicamarca Radar Observatory. These different measurements examined a common E region scattering volume near the Huancayo site. It is known that scintillations arise from irregularities with scale sizes of the order of the Fresnel radius $(\lambda z)^{\frac{1}{2}}$, where λ is the exploring wavelength and z is the distance between the observer and the irregularities. For ATS-6 observations from Huancayo and Fresnel dimensions at 41 and 140 MHz with 110-km slant range of the electrojet region corresponded to approximately 1 and 0.5 km, respectively. The study of E_{sq} on ionograms obtained simultaneously at Huancayo provided information on 30- to 80-m irregularity wavelengths, whereas 50-MHz oblique radar backscatter measurements used in the work revealed the existing types of irregularities at the 3-m wavelength. This study therefore covers the wide range of

irregularity scale sizes from a few meters to about 1 km in the equatorial electrojet.

I.1.2 OBSERVATIONS

Scintillation measurements were made at Huancayo, Peru (latitude, 11.96°S; longitude, 75.34°W; dip latitude, 0.6°N), by receiving 41- and 140-MHz transmissions of the ATS 6 satellite. During the period of study the subionospheric location (11.7°S, 75.7°W) of the scintillation measurements, referred to 100-km height, was situated only 50 km away from the Huancayo site. A 30-ft (9-m) paraboloid was employed to receive 140-MHz signals from the satellite, whereas a yagi antenna system was used for 41 MHz. The signals were amplified in low noise receiving systems, and the detected signals were recorded on strip chart recorders. The amplitude fluctuations of the recorded signal were scaled every 15 min to determine the scintillation index SI by following the procedure outlined by Whitney (1974).

The 50-MHz radar spectral data on electrojet irregularities were simultaneously obtained at the Jicamarca Radio Observatory. The technique of radar spectral measurements has been discussed in detail by Balsley and Farley (1973). The radar antenna was oriented eastward so that the E region scattering volume was approximately over the Huancayo station. In addition to the radar and scintillation measurements, ionograms were obtained simultaneously at Huancayo. The confi-

79 03 09 036

urations of scintillation, radar and ionosonde measurements were such that there measurements explored a roughly common ionospheric volume at E region height.

I.1.3 COMPARISON BETWEEN THE OCCURRENCE OF SCINTILLATIONS AND VHF RADAR ECHOES

Figure I.1.1 indicates a comparison of the time intervals during which the VHF radar echoes and scintillations at 41 and 140 MHz were observed. The first four bar diagrams in Figure I.1.1, corresponding to the period February 1-8, 1974, indicate a comparison between the radar echoes and 140-MHz scintillation activity. The unshaded diagrams correspond to the radar echoes, and the hatched ones denote 140-MHz scintillation activity. It may be observed that scintillations are present only when the radar is able to detect electrojet irregularities. It is to be pointed out that the recorded level of 140-MHz scintillation was low, varying between 0.8 and 1.5 dB. It is interesting to note that on February 4 the electrojet irregularities are absent during the morning period, as is indicated by the radar measurements; scintillations are also conspicuous by their absence. In the afternoon period the radar showed the presence of weak electrojet irregularities without any corresponding scintillation activity at 140 MHz. These weak irregularities probably generated a level of scintillation below the detectable limit of 140-MHz scintillation measurements. Since for a given electron density deviation ΔN the level of scintillation at a lower frequency is higher, the use

of a low frequency, such as 41 MHz, during the period will probably indicate the presence of scintillation. As was mentioned earlier, our observations indicate that during the daytime a typical scintillation level of only 1 dB at 140 MHz corresponds to about 10 dB at 41 MHz. A close examination of the times of onset and decay of 140-MHz scintillation activity with respect to radar echoes indicates that the scintillation activity at 140 MHz occurs slightly after the radar echoes are observed and that scintillations also cease prior to the decay of radar echoes. The weak irregularities during the onset and decay of the electrojet do not generate measurable scintillation at 140 MHz. Unfortunately, scintillation measurements at 41 MHz were not available on these days.

Scintillations at 140 MHz observed on February 1, immediately before 2000 LT without any associated radar echo are attributed to the postsunset F region irregularities. On this day the nighttime scintillations started at 1945 LT and continued until 0445 LT on the next day.

Between February 18 and March 5, 1975, scintillation measurements could be made at the lower frequency of 41 MHz (shown as black bars in Fig. I.1.1), and it may be noted that the time synchronism between the radar echoes and the scintillation is excellent. The weakest irregularity amplitudes detectable with the radar give rise to immediate scintillation effects at the lower frequency. The comparative study of radar echoes and VHF scintillation illustrated by Figure I.1.1 indicates that daytime scintillation is related to the electrojet irregularities

and that the irregularities with wavelengths of the order of 1 km (corresponding to the Fresnel radius) as explored by scintillation measurements coexist with the short-wavelength (3 m) irregularities detected by the 50-MHz radar.

I.1.4 COMPARISON OF SCINTILLATION, RADAR ECHOES, AND E_{sq}

We shall next illustrate the behavior of q-type sporadic E (E_{sq}) echoes on February 20 in relation to the 41-MHz scintillation and to the VHF radar echoes. The data in the upper section of Fig. I.1.2 show that both the scintillation activity and the radar echo ceased at about 1820 LT. A more detailed study of the radar echo indicates that type 2 electrojet irregularities were present between 1800 and 1815 LT but disappeared at about 1820 LT. The bottom section of this figure shows the ionogram sequence between 1800 and 1830 LT. The presence of E_{sq} echoes in the first two frames may be observed, but in the final frame, obtained at 1830 LT, E_{sq} is found to disappear. Such a correlation between these events has been found to exist on other days. The comparisons show that VHF scintillation, type 2 radar echo, and E_{sq} echoes appear and disappear together. An extensive study showing the close relationship between the E_{sq} echoes and type 2 radar echoes has recently been carried out (Balsley et al., 1976).

Our results show that daytime VHF scintillations occur essentially simultaneously with these two ionospheric features. This establishes that 3-m type 2 irregularities are synchronized

with the appearance of irregularities at 30- to 80-m wavelengths as viewed by the E_{sq} signature on ionograms as well as kilometer-sized irregularities which cause 41-MHz scintillations. Thus this correlative study indicates that gradient drift irregularities cover about a 3-decade range in wavelength.

I.1.5 DEVELOPMENT OF SCINTILLATIONS AND EVOLUTION OF TYPE 1 AND TYPE 2 IRREGULARITIES

The radar observations provide information on the nature of electrojet irregularities observed at 50 MHz. Balsley et al. (1976) have found that both type 1 and 2 are equally important in giving 50-MHz radar backscatter echoes, whereas at frequencies higher/lower than 50 MHz, type 1/type 2 irregularities tend to predominate. The 50-MHz radar observations discussed herein outline the time evolution of type 1 and type 2 irregularities and also classify the strength of either type of echo simply as being weak or strong. Fig. I.1.3 shows the time variation of scintillation index SI at 140 MHz and the evolution of type 1 and type 2 irregularities as observed by the 50-MHz radar on February 2, 1975. The levels of 1 and 2 marked on the radar plots represent the presence of weak or strong type 2 irregularities, respectively, whereas levels 3 and 4 correspond to weak or strong type 1 irregularities, respectively. On February 2 the 140-MHz scintillation becomes discernible at 0915 LT, when the radar echo reveals the presence of strong type 2 and weak type 1 echo. At 1210 LT, when the radar echo indicates the cessation of type 1 irregularities

and the presence of type 2 irregularities only, the scintillation index does not show any change. This signifies that the presence or absence of type 1 irregularities does not introduce any marked variation of the scintillation level, indicating thereby that the presence of type 1 irregularities is not required for VHF scintillation activity and that the scintillation activity is probably related to type 2 irregularities.

The evolution of 41-MHz scintillations and radar echoes from electrojet irregularities observed on March 9, 1975, is shown in Fig. I.1.4. The radar observations were limited to the time interval between 0800 and 1520 LT. It may be noted that prior to 0850 LT, when only type 2 irregularities were present, the scintillation index at 41 MHz remained at a level of about 50%. However, after this time, when type 1 irregularities became discernible, the SI level at 41 MHz registered an increase to a level of approximately 60%. A drop of the SI level from 40% to 25% immediately after 1330 LT may be noted when type 1 activity ceased. On the basis of multifrequency radar measurement, Balsley et al. (1976) have concluded that the electrojet irregularities at long wavelengths ($\sim$40m) giving rise to backscatter echoes at frequencies of about 4 MHz are very strongly dominated by the type 2 irregularities. It seems that the observed increase on scintillation with the appearance of type 1 activity is probably related to a strengthening of type 2 irregularities.

During the development phase of VHF scintillations a

scintillation index of about 50% at 41 MHz typically corresponds to strong type 2 echoes at meter wavelengths. This may be observed in March 9 data during 0815-0845 LT, illustrated in Fig. I.1.4. The SI value of 50% corresponds to the theory based S_4 index of about 0.25 (Whitney, 1974). A knowledge of the S_4 index allows us to compute the electron density deviation in the irregularities if realistic assumptions can be made regarding the irregularity layer thickness L, slant range z, and irregularity power spectrum. It has been mentioned that the slant range of the electrojet region to Huancayo for ATS-6 observations during the period was about 110 km. The thickness (L) of this layer, over which the irregularities are assumed to be distributed undiminished in magnitude, is considered to be 5 km.

The assumption regarding the irregularity power spectrum has been based on a series of experimental and theoretical results. The rocket experiments of Prakash et al. (1970), made at Thumba, India, indicate that the wavenumber (k) spectrum of irregularities with wavelengths of 1-15 m in the nighttime equatorial E region may be represented as $k^{-3\pm1}$. Ott and Farley (1974) showed from dimensional considerations that the spectral index of irregularities averaged over all k space should be at least k^{-3}. These results, based on rocket experiments and dimensional considerations, were found to be in agreement with the numerical studies of type 2 electrojet irregularities (McDonald et al., 1975). On the basis of the

above results we have assumed a k^{-4} spectrum for the irregularities with an outer scale dimension of 2 km. The choice of an outer scale dimension of 2 km is based on the theoretical work of Rognlien and Weinstock (1975), who showed that electrojet irregularities with scale lengths in the kilometer range can be postulated under daytime conditions when the scale length of the zero-order density gradient is typically about 6 km. By the use of Rufenach's (1975) equation relating scintillation index to electron density deviation of power law type irregularities we find that the S_4 index of 0.25 at 41 MHz is obtained when the electron density deviation of the irregularities is $\Delta N = 6 \times 10^9$ m^{-3}. This corresponds to an irregularity amplitude of 6% for an ambient ionization density of 10^{11} m^{-3}. The irregularity amplitudes need to be increased by a factor of 5 to cause an equivalent level of scintillation ($S_4 = 0.25$) at 140 MHz. Thus the scintillation measurements at 41 MHz, compared to those at 140 MHz, are more sensitive detectors of irregularities, as was discussed earlier in connection with Figure I.1.1.

Our computations of irregularity amplitudes based on VHF scintillation measurements indicate that when the rms irregularity amplitude in the kilometer wavelength range is found to be approximately 4%, the 50-MHz radar is able to detect simultaneously the presence of type 2 irregularities. The highest level of S_4 index at 41 MHz during the daytime is found to be of the order of 0.5. Such a level of scintillation corresponds to an electron density deviation $\Delta N = 1.6 \times 10^{10}$ m^{-3} with

the above assumed parameters. This value corresponds to rms irregularity amplitudes of 16% for an ambient ionization density of 10^{11} m^{-3}. Thus the observed range of daytime scintillations at 41 MHz is consistent with irregularity ampltiudes of about 5-15%.

I.1.6 CONCLUSIONS

The study reveals that daytime VHF scintillations are generated when E_{sq} echoes appear on ionograms and when the 50-MHz radar detects type 2 electrojet irregularities. Since VLF scintillations are sensitive to kilometer-sized irregularities E_{sq} monitors 30- to 80-m irregularities, and the 50-MHz radar detects 3-m wavelength irregularities, it may be concluded that type 2 irregularities covering the wavelength range of a few meters to a few kilometers coexist. We have also found that during periods when the radar does not detect any electrojet irregularity, neither E_{sq} nor VHF scintillation is observed.

We have shown that when type 2 meter wave irregularities and VHF scintillations are simultaneously observed, irregularity amplitudes ranging between 5% and 15% (ambient ionization density of 10^{11} m^{-3}) at kilometer wavelengths are obtained.

REFERENCES

Aarons, J., Equatorial scintillations: A review, IEEE Trans. Trans. Antennas Propagat., in press, 1977.

Balsley, B.B., and D.T. Farley, Radar observations of two-dimensional turbulence in the equatorial electrojet, J. Geophys. Res., 78, 7471, 1973.

Balsley, B.B., A. Rey, and R.F. Woodman, On the plasma instability mechanisms responsible for E_{sq}, J. Geophys. Res., 81, 1319, 1976.

Farley, D.T., Irregularities in the equatorial ionosphere: The Berkner Symposium, Rev. Geophys. Space Phys., 12, 285, 1974.

Farley, D.T., and B.B. Balsley, Instabilities in the equatorial electrojet, J. Geophys. Res., 78, 227, 1973.

McDonald, B.E., T.P. Coffey, S.L. Ossakow, and R.N. Sudan, Numerical studies of type 2 electrojet irregularity development, Radio Sci., 10, 247, 1975.

Ott, E., and D.T. Farley, The k spectrum of ionospheric irregularities, J. Geophys. Res., 79, 2469, 1974.

Prakash, S.P., S.P. Gupta, and B.H. Subbaraya, A study of the irregularities in the nighttime equatorial E-region using a Langmuir probe and plasma nose probe, Planet. Space Sci., 18, 1307, 1970.

Rognlien, T.D., and J. Weinstock, Theoretical properties of two-dimensional electrojet turbulence, Radio Sci., 10, 239, 1975.

Rufenach, C.L., Ionospheric scintillation by a random phase screen: A spectral approach, Radio Sci., 10, 155, 1975.

Whitney, H., Notes on the relationship of scintillation index to probability distributions and their uses in system design, Rep. AFCRL-TR-74-0004, Air Force Cambridge Res. Lab., Bedford, Mass., 1974.

FIGURES

Fig. I.1.1. Comparison of scintillation activity at 41 and 140 MHz with 50-MHz radar echoes from electrojet irregularities. The breaks in the diagrams signify absence of data.

Fig. I.1.2. Decay of 41-MHz scintillation activity, 50-MHz radar echoes, and E_{sq} on Huancayo ionograms. Note the time synchronism between the disappearance of E_{sq} at 1830 LT and the decay of scintillation activity and 50-MHz radar echoes at 1820 LT.

Fig. I.1.3. Variation of the level of 140-MHz scintillation (SI%) with the strength and type of radar echoes. Levels 1 and 2 in the radar plot signify weak and strong type 2 irregularities, respectively, while levels 3 and 4 denote weak and strong type 1 irregularities.

Fig. I.1.4. Variation of the scintillation level (SI%) of 41 MHz with the strength and type of radar echoes. The various levels in the radar plot have been described in Figure 3.

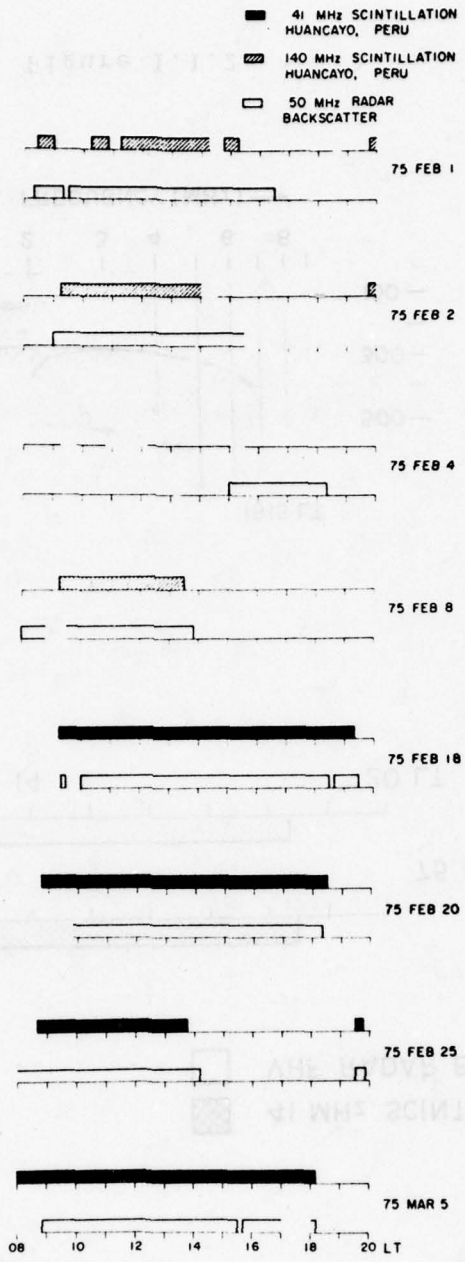

41 MHz SCINTILLATION
HUANCAYO, PERU
140 MHz SCINTILLATION
HUANCAYO, PERU
50 MHz RADAR
BACKSCATTER
75 FEB 1
75 FEB 2
75 FEB 4
75 FEB 8
75 FEB 18
75 FEB 20
75 FEB 25
75 MAR 5
08
10
12
14
16
18
20 LT

Figure I.1.1

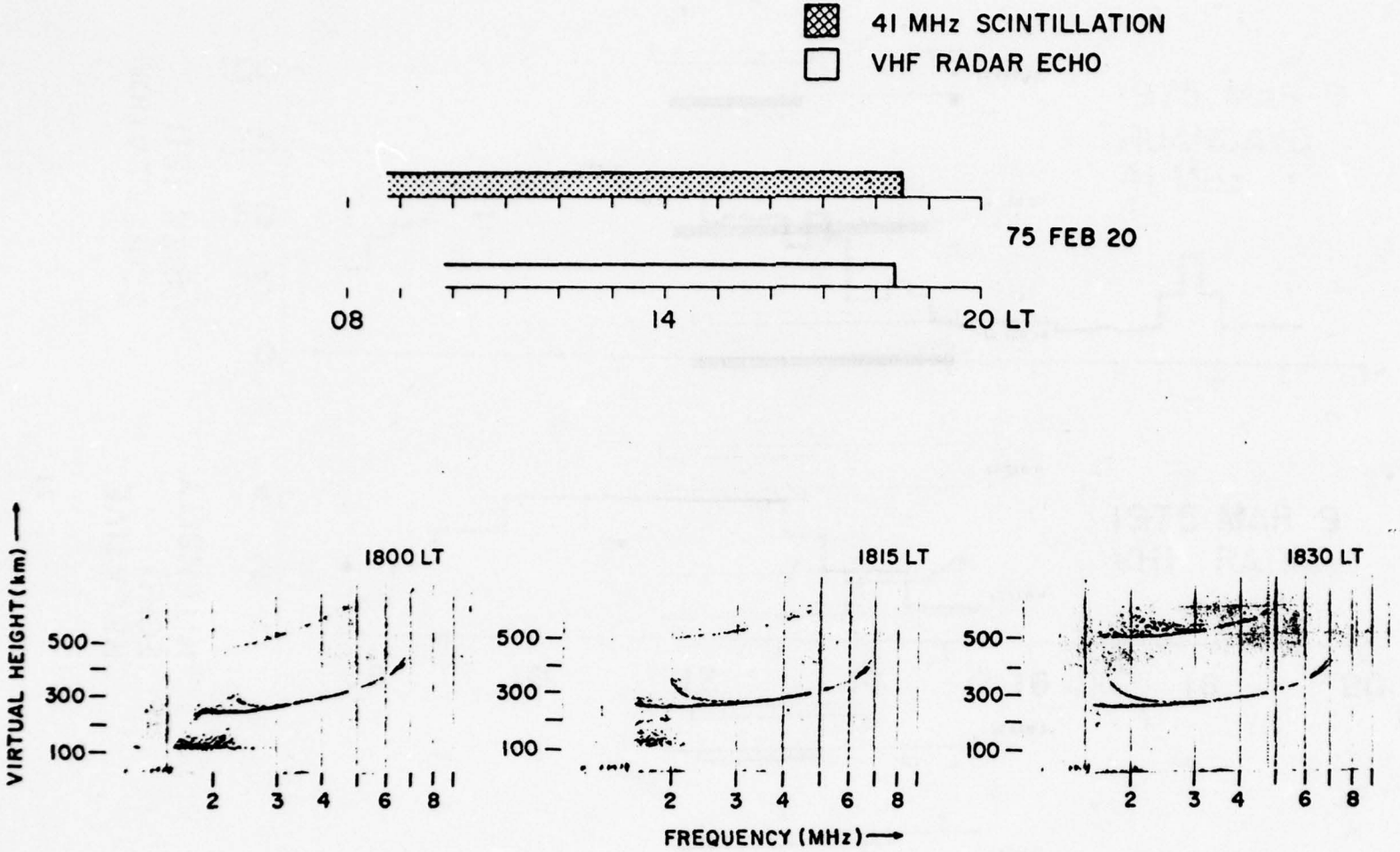


Figure I.1.2

AFGL PHOTO 56-616

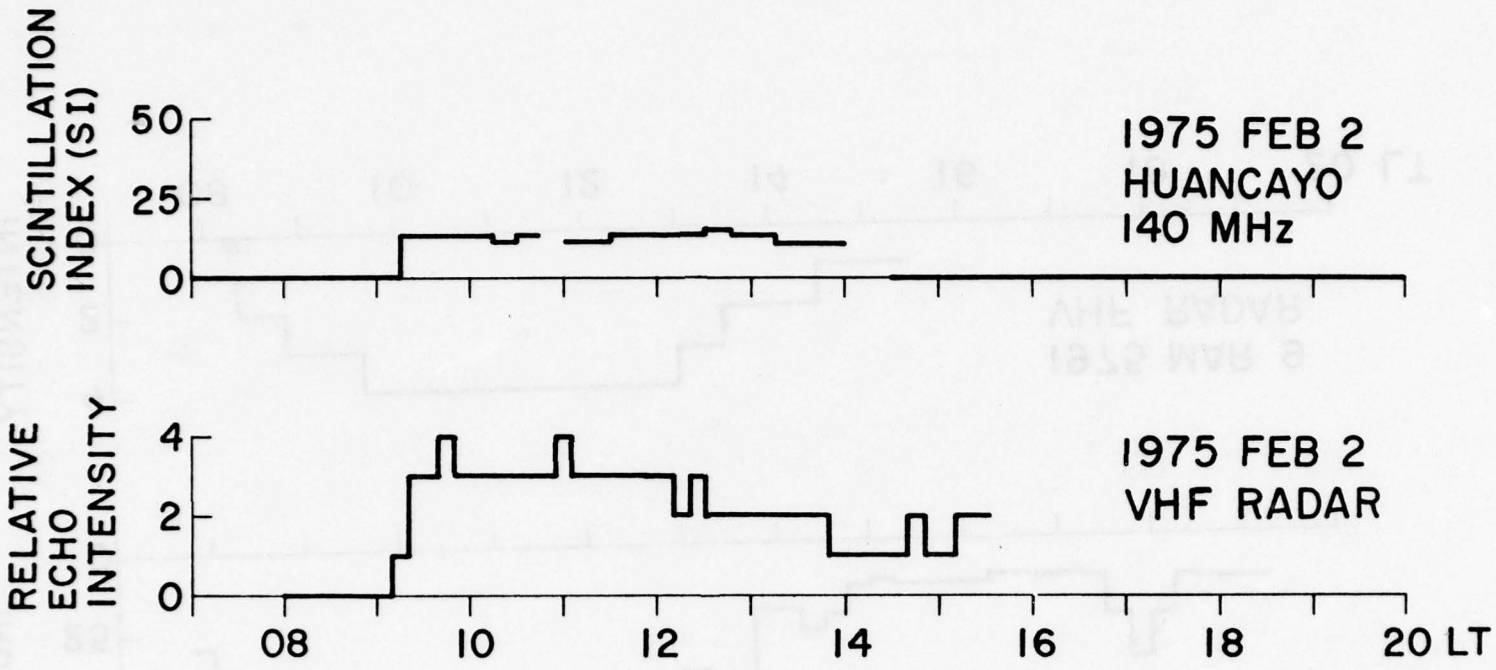

SCINTILLATION INDEX (SI)
50
25
0
1975 FEB 2
HUANCAYO
140 MHz
RELATIVE ECHO INTENSITY
4
2
0
1975 FEB 2
VHF RADAR
08
10
12
14
16
18
20 LT

Figure I.1.3

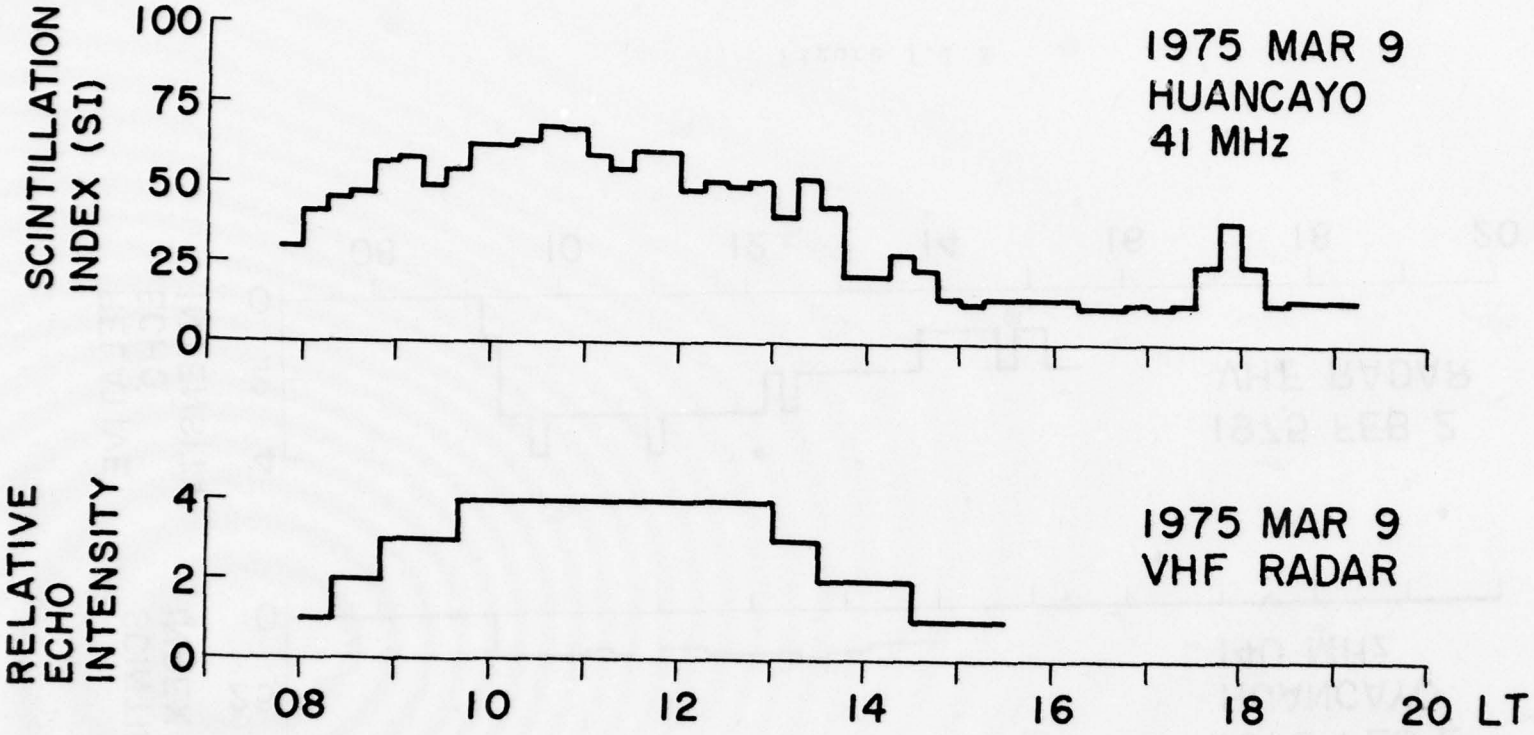

SCINTILLATION INDEX (SI)
100
75
50
25
0
1975 MAR 9
HUANCAYO
41 MHz
RELATIVE ECHO INTENSITY
4
2
0
1975 MAR 9
VHF RADAR
08
10
12
14
16
18
20 LT

Figure I.1.4

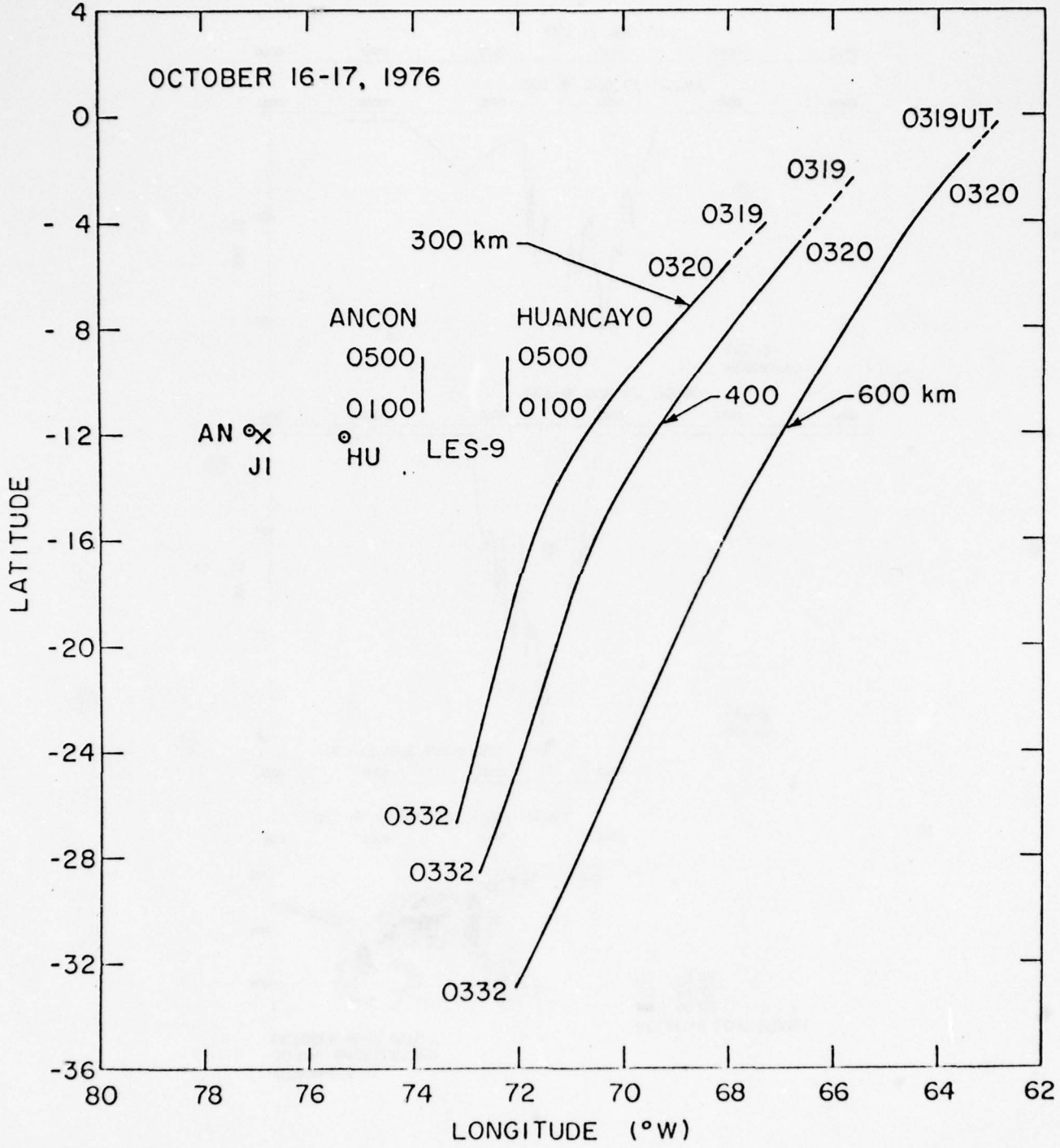

OCTOBER 16-17, 1976
0319UT
0319
0320
0319
0320
300 km
0320
ANCON
HUANCAYO
0500
0500
0100
0100
400
600 km
AN
JI
HU
LES-9
0332
0332
0332
LATITUDE
LONGITUDE (°W)
4
0
- 4
- 8
-12
-16
-20
-24
-28
-32
-36
80
78
76
74
72
70
68
66
64
62

Figure I.2.1

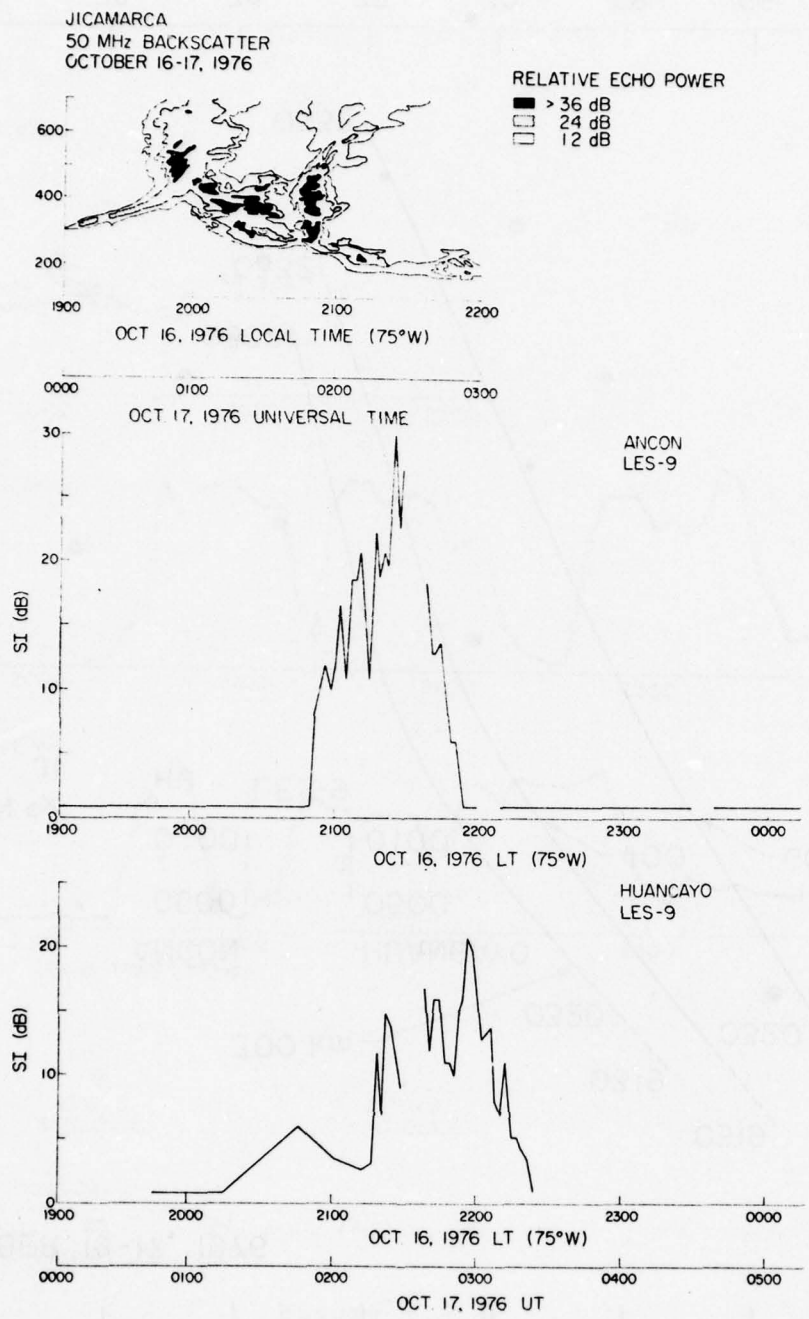

JICAMARCA
50 MHz BACKSCATTER
OCTOBER 16-17, 1976
RELATIVE ECHO POWER
> 36 dB
24 dB
12 dB
600
400
200
1900
2000
2100
2200
OCT 16, 1976 LOCAL TIME (75°W)
0000
0100
0200
0300
OCT 17, 1976 UNIVERSAL TIME
ANCON
LES-9
SI (dB)
30
20
10
0
1900
2000
2100
2200
2300
0000
OCT 16, 1976 LT (75°W)
HUANCAYO
LES-9
SI (dB)
20
10
0
1900
2000
2100
2200
2300
0000
OCT 16, 1976 LT (75°W)
0000
0100
0200
0300
0400
0500
OCT 17, 1976 UT

Figure I.2.2

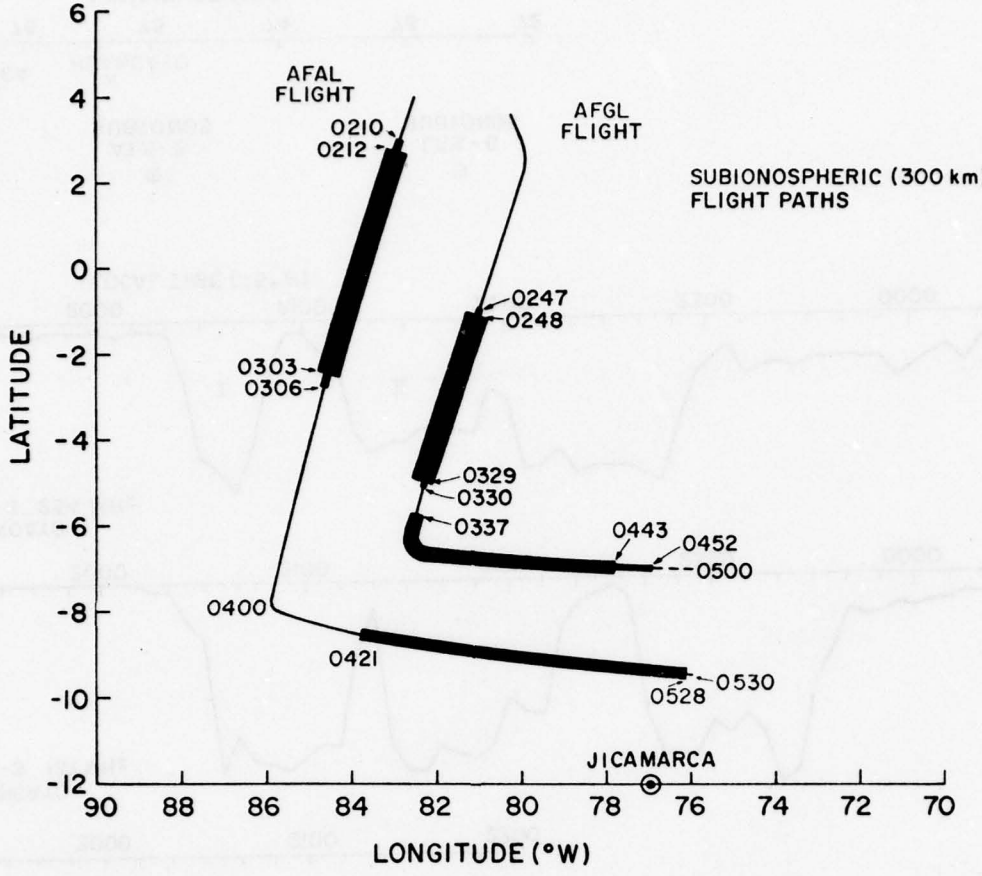


Figure I.2.3a

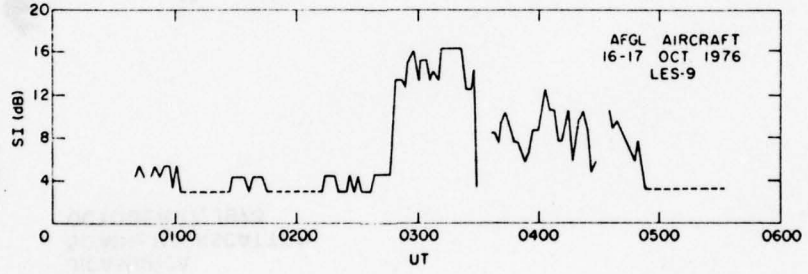


Figure I.2.3b

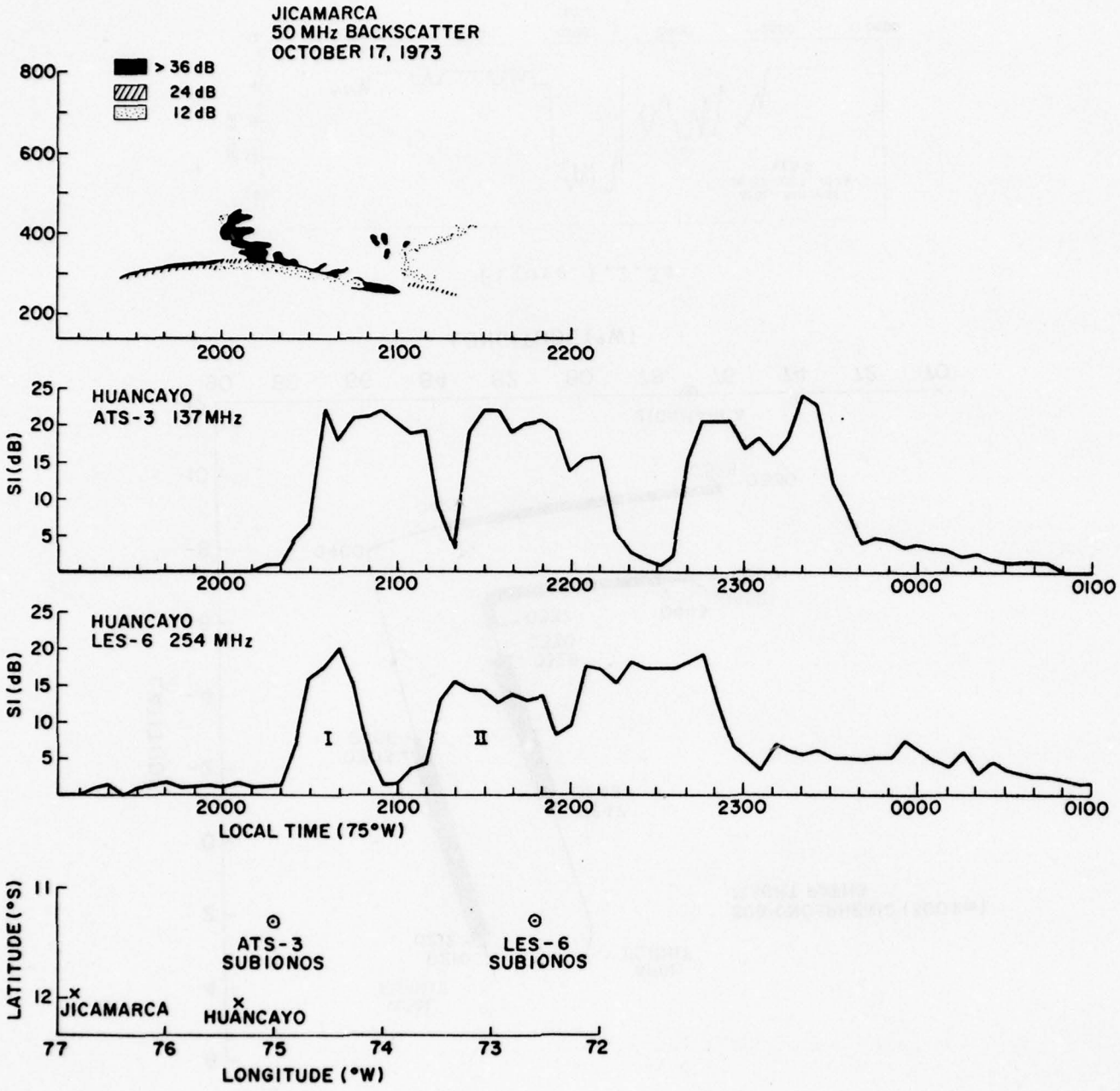

JICAMARCA
50 MHz BACKSCATTER
OCTOBER 17, 1973
> 36 dB
24 dB
12 dB
800
600
400
200
2000
2100
2200
HUANCAYO
ATS-3 137MHz
SI(dB)
25
20
15
10
5
2000
2100
2200
2300
0000
0100
HUANCAYO
LES-6 254 MHz
SI(dB)
I
II
LOCAL TIME (75°W)
LATITUDE(°S)
11
12
ATS-3
SUBIONOS
LES-6
SUBIONOS
JICAMARCA
HUANCAYO
77
76
75
74
73
72
LONGITUDE (°W)

Figure I.2.4

I.2 THE LOCALIZED ORIGIN OF EQUATORIAL F-REGION IRREGULARITY PATCHES*

I.2.1 INTRODUCTION

Theoretical studies, computer modeling, and experimental observations through radar backscatter, rocket and satellite in-situ measurements have provided a greater insight into the formation of those equatorial irregularities which lead to deep scintillation of UHF and microwave transmissions through the ionosphere (see review by Basu and Kelley, 1977 and references therein). The picture that emerges from these studies points to large-scale irregularity structures, tilted usually to the west, having an E-W dimension of up to several hundred kilometers, extending to altitudes as high as 1000 km and containing a Hierarchy of irregularity scale sizes in the range of several tens of kilometers to a few meters. Such irregularities of ionization are thought to result from the generation of large-scale plasma depletions in the bottomside ionosphere, which rise rapidly upward against gravity, like "bubbles" or "plumes", into the topside ionosphere.

Scintillation activity in a transionospheric VHF/UHF communication link results when the electron density deviation (ΔN) of irregularities with a scale size of about a kilometer is sufficiently large. It is well-known that at night in the equatorial F-region strong irregularities of electron density with different scale sizes exist, and these irregularities are most commonly observed to have a monotonic

---

* Aarons, J., J. Buchau, S. Basu, J. Geophys. Res.,83, 1659, 1978.

power law spectrum (McClure and Hanson, 1973; Dyson et al., 1974). By considering the above irregularity power spectrum, Basu and Basu (1976) demonstrated that the in-situ ΔN measurements are compatible with the simultaneous ground-based scintillation observations at 6 GHz. In view of the above studies, one can assume the co-existence of irregularities in the scale size range of several tens of kilometers to several meters although the in-situ observations referenced above indicate that in certain (exceptional) cases, irregularities may have most of their spectral power either above or below a scale size of the order of one kilometer. In general, then, microwave fadings are likely to be associated with the plume structure seen on 50 MHz backscatter as predicted by Woodman and LaHoz (1976). Under those backscatter conditions when the plumes do not extend far into the topside ionosphere but still the product of thickness and ΔN is large, microwave fadings may also result. Most of the theoretical studies deal with the generation and motion of the small-scale structures within a large scale bubble or patch (Woodman and LaHoz, 1976; McClure et al., 1977). In this paper it will be shown that the generation of a large-scale bubble can be very localized and that a bubble can maintain its integrity for several hours during its eastward motion.

I.2.2 Observations

A. Ground Measurements

A series of 50 MHz radar backscatter observations from the Jicamarca Observatory of the Instituto Geofisico del Peru was made over a period of two weeks in conjunction with a large scale ground and airborne campaign to study scintillations. On the ground, observations were made of the synchronous satellite beacon, LES-9, transmitting at 249 MHz, from two different sites, Ancon and Huancayo, both in Peru and also of the orbiting Wideband satellite transmissions at 137 MHz from Huancayo. Figure I.2.1 shows the geometry and geography of the observations. The 400 km sub-ionospheric intersections of the propagation paths from Ancon and Huancayo to LES-9 and sub-ionospheric tracks of the Wideband transit are shown. The Jicamarca vertical intersection is farthest west while the two oblique paths to LES-9 are to the east of Jicamarca. If the time of sunset determined the timing of appearance of irregularities then the Huancayo path should first observe scintillations, followed by Ancon and finally Jicamarca would record backscatter from irregularities.

Figure I.2.2 shows the results of simultaneous radar and scintillation measurements made on October 16-17, 1976. The top panel shows the range-time-intensity plot of 50 MHz backscatter obtained at Jicamarca. Since the original digital power maps (Woodman and LaHoz, 1976) are difficult to reproduce we have redrawn these and displayed the echo intensity at only three logarithmic power levels, relative to the approximate maximum incoherent scatter level. The next two panels illustrate the time variation of scintillation index, SI(dB), recorded at Ancon and Huancayo on propagation paths to LES-9. Comparing the three panels, we find that the initial appearance of backscatter in Jicamarca radar is followed by the onset of scintillations at Ancon and finally at Huancayo; clearly a localized irregularity patch was generated over Jicamarca or to the west of it and has moved eastwards. This is, of course, based on the usually justifiable assumption that the kilometer sized irregularities causing scintillations coexist with 3m irregularities giving rise to 50 MHz backscatter. Using the geometry of Figure I.2.1 and the timing of the onset of irregularities we measure an average eastward drift speed of the irregularity structure as 100 m/sec. The cross-correlation analysis of scintillation data acquired at Ancon using antennas separated by 366 m in the E-W direction on October 16-17, 1976, also provides an average eastward drift speed of 116 m/sec. This is in agreement with the previously reported values of Woodman (1972).

Combining the duration of the scintillation event with the observed drift speed, the patch dimension in the east-west direction is found to be about 400 km. The correspondence between the radar map of Jicamarca and scintillation measurements at Huancayo with a delay of 90 minutes indicates that the irregularity structure retained its integrity between the two stations for at least 1½ hours. The total of three hours between the first appearance of a plume at Jicamarca and the end of scintillation at Huancayo indicate that the total lifetime of the irregularity patch may be at least 3 hours.

On October 16-17, 1976, scintillations of the 137 MHz transmissions from the orbiting Wideband satellite were recorded at Huancayo between 0320 to 0332 UT. In Figure I.2.1 the sub-ionospheric tracks of the satellite transit referred to three ionospheric heights, 300, 400 and 600 km are shown. The portion of the track marked by the solid line indicates the presence of scintillation while the dotted line indicates the absence of any scintillation. Considering the 400 km track, we find that scintillations were extant between 66°W to 72°W. If we assume that the irregularity structure front (eastern edge) causing the onset of LES-9 scintillations at Huancayo had reached the 66°W location at 0320 UT, a drift speed of 160 m/sec for the irregularity patch is obtained. This speed is considerably higher than that derived previously for the patch during its passage from Ancon and Huancayo. From Figure I.2.1, we find that in view of the low

elevation angle of the transit, the sub-ionospheric tracks for the three altitudes are considerably displaced. This poses problems in locating the irregularity structure and deriving the drift speed. For example, if we consider the 300 km track, a drift speed of 110 m/sec, more in accord with the previously derived drift speed, may be obtained. The latitudinal extent of the track exhibiting scintillations is found to be about 20°. Owing to the low elevation angle of the satellite, there exists the possibility of the satellite encountering discrete irregularity patches and, hence, it is difficult to arrive at a definite conclusion regarding the latitudinal extent of a single patch.

B. Airborne Measurements

Two aircraft were used to observe scintillations from LES-9, one from the Air Force Avionics Laboratory (AFAL) and the other from the Air Force Geophysics Laboratory (AFGL). The subionospheric flight paths of the AFAL and AFGL aircraft are shown in the top panel of Figure I.2.3. The heavy lined portions of the track signify the presence of scintillations in excess of 12 dB, the moderately heavy lines indicate 6-8 dB scintillations while the thin lines represent the absence of any scintillations. In the bottom panel of the diagram, we show the time variation of scintillation as recorded by the AFGL aircraft. The aircraft flew on parallel paths such that the initial portions of either subionospheric track were inclined at about 10° to the east of the magnetic meridian while the later portion of the track was approximately in the magnetic east-west direction. From the bottom panel

as well as the flight path map, it may be noted that the AFGL aircraft encountered two scintillation events, the initial event being in excess of 12 dB and the later event having a level of about 8 dB. The subionospheric flight map of the AFAL aircraft shows that it also encountered one strong and one weak irregularity patch. The propagation path from the AFAL aircraft to LES-9 seems to have entered the eastern edge of a strong irregularity patch at 0210 UT and emerged from it at 0306 UT. Strong scintillations as high as 25 dB were recorded by the AFAL aircraft during some periods between 0212 and 0303 UT. The AFGL aircraft flying to the east of the AFAL aircraft recorded strong scintillatons between 0248 and 0329 UT. If we consider that the eastern edge of the strong irregularity patch initially detected by the AFAL aircraft at 0212 UT drifted eastwards to the subionospheric location of the AFGL aircraft propagation path at 0248 UT, then an eastward drift speed of 100 m/sec is obtained. Further, if we assume that the irregularity patch extended southwards all the way to the magnetic equator then the ends of the first scintillation event recorded by both aircraft are to be related to the passage of the western edge of the patch. Considering the duration of the scintillation event with the derived drift speed, an east-west patch dimension ranging from 250-300 km is obtained. This is consistent with the typical data from the AE-C satellite presented by McClure et al., (1977). The irregularity patch detected by the AFGL aircraft was located approximately 10° north and 4° west of Jicamarca, the position of which is indicated in the diagram. Irregularities of km scale size are expected to be field aligned and these field lines pass over the equator at altitudes of approximately

600 km. Considering the drift speed of 100 m/sec, these field lines should have drifted eastwards to the Jicamarca meridian at about 0400 UT. The radar map obtained at Jicamarca does not, however, exhibit the presence of any 3 m irregularities at this time. It is not clear whether the absence of 3 m irregularities is related to the decay of the patch during its passage to the Jicamarca meridian or the irregularity power spectrum had little spectral power at the meter wavelength end. Comparison of irregularity spectral power at km and meter wavelengths in the equatorial ionosphere is being actively pursued (Woodman and Basu, 1977).

Over the magnetic east-west portion of the flight paths weak scintillations were recorded by both aircraft. The measurements indicate that the AFGL aircraft encountered 8 dB scintillation levels whereas the AFAL aircraft encountered 6 dB levels, although the latter path was closer to the magnetic equator. Since the two aircraft did not cross the same meridian at the same time, it is difficult to separate the spatial and temporal variation and make comments on the latitude variation of the irregularity strength. During the eastward flight, the AFGL and AFAL aircraft crossed the Jicamarca meridian at 0450 UT and 0520 UT respectively and detected about 6 dB scintillations. The Jicamarca radar did not detect any 3 m irregularity structure at this time. This is not surprising in view of the low level of scintillations observed.

The initial appearance of plumes in the early part of the night at the westernmost location of Jicamarca as observed on October 16-17, 1976, should be viewed as an exception rather than the rule. In general, the activity on a given night starts on the eastward propagation path before that on the west. The illustration shown in Bandyopadhyay and Aarons (1970), indicates that, for only 20% of the time, satellite scintillations on a westward propagation path start before an eastward propagation path.

In order to illustrate this aspect of the problem, we compare simultaneous radar backscatter and scintillation measurements made on October 17, 1973, three years earlier than the present set of observations. The bottom panel of Fig. I.2.4 shows that on this night radar backscatter measurements were made at Jicamarca (Woodman and LaHoz, 1976) and simultaneous scintillation measurements were made at Huancayo with the 137 MHz transmissions from ATS-3 and at 254 MHz using LES-6. The sub-ionospheric locations of ATS-3 and LES-6 referred to an ionospheric height of 350 km are indicated in the diagram. The top panel shows the range-time-intensity plots of 3m irregularity structure obtained with the 50 MHz radar at Jicamarca. It may be observed that a thin irregularity structure evolved at 1925 LT persisting until about 2000 LT when a plume structure developed. The second panel shows the development of 137 MHz scintillation at Huancayo, the sub-ionospheric location of ATS-3 being 1.9° to the east of Jicamarca. It may be noted that scintillations on ATS-3 developed after 2010 LT and a sharp increase from 6dB to 22dB occurred after 2030 LT. Comparing the top two panels, it

is found that scintillations immediately to the east of Jicamarca occurred after the development of irregularity structure over Jicamarca. If we assume that the plume structure observed over Jicamarca drifted eastwards to cause the sudden increase of scintillation on ATS-3, a drift speed of 116 m/sec is obtained. If we now observe the third panel which shows the development of 254 MHz scintillation on LES-9, the sub-ionospheric location being far to the east with a longitude separation of 4°16' from Jicamarca, we find that the onset of LES-6 scintillation occurred slightly earlier than ATS-3 scintillation at Huancayo. This scintillation structure (marked A in Fig. I.2.4) observed on the LES-6 propagation path cannot be associated with the drifting irregularity structure observed over Jicamarca, but must have been caused by an independent irregularity structure developing to the east of the Huancayo ATS-3 ray path. In fact, the second scintillation structure observed on LES-6 propagation path after 2100 LT (marked B in Fig. I.2.4) could be associated with the plume structure at Jicamarca and the first scintillation structure on ATS-3 if we assume an average drift speed of about 130 m/sec. Comparing the set of observations made on October 16-17, 1976, discussed in detail above with the set obtained nearly 3 years earlier also discussed above, we conclude that on certain nights a single irregularity structure may evolve and while drifting eastwards may cause scintillations to occur as long as it persists or a series of irregularity patches may evolve and while drifting eastwards may give rise to a series of

scintillation structures. Thus the location of generation of the irregularities, their drift and their lifetimes dictate the time evolution of the scintillations observed at a given ground station in the equatorial region.

I.2.3 Discussions

Our results indicate that intense 3 m irregularity patches detected by the radar are associated with strong scintillation events. Thus, in general, the km-sized irregularities are obtained when the 3 m irregularities are present which is, of course, predicted by the theory. Although not covered in this preliminary report, we have found cases, in particular, during the post-midnight period, when patches containing km-sized irregularities were obtained without any associated radar event. It seems that on occasion the turbulent energy fails to cascade down to meter scale sizes. We expect to obtain more information in this regard from radar and scintillation measurements performed on a common ionospheric volume during March, 1977.

We have shown that the radar backscatter and scintillation measurements are consistent with an eastward drift speed of irregularity patches at about 100 m/sec. The scintillation observations as well as trans-equatorial propagation experiments indicate that irregularity patches can move past a fixed propagation path within a few tens of minutes to a maximum of 100 minutes, the latter figure being reported by Röttger (1976). Combining the drift speed with the duration of the scintillation event, east-west patch dimensions of several hundred kilometers are obtained. This is consistent with the recently published in-situ results (McClure et al., 1977).

We have shown that the radar map corresponding to a single scintillation patch may exhibit considerable structure. The simple scintillation event observed on October 16-17, 1976, was associated with the radar event showing two plumes joined by a thick region of intense irregularities at low altitudes.

The generation of irregularity patches is indeed very localized as revealed by multistation scintillation measurements made with an east-west ionospheric separation as small as 175 km. The lifetime of the large scale irregularity patches has been shown to be at least several hours.

The localized nature of irregularity formation and the dimensions of the patch indicate that very large scale global patterns of winds and tides cannot be used to determine the physical conditions necessary for the generation of the irregularities.

Acknowledgements

We thank the staff of the Instituto Geofísico del Perú for their help in recording the data and hospitality towards the visiting scientists. In addition, the assistance of John Mullen, Herbert Whitney (Air Force Geophysics Laboratory) and Allen Johnson (Air Force Avionics Laboratory) in making the observations and reducing their data is gratefully acknowledged. This work was partially supported by National

Science Foundation grants DES-71-00555 and ATM76-17351 and by National Aeronautics and Space Administration Grants NGL44-004-026 and NGL-004-13.

References

Bandyopadhyay, P. and J. Aarons, The equatorial F-layer irregularity extent as observed from Huancayo, Peru, Radio Sci., 5, 931-938, 1970.

Basu, S. and S. Basu, Correlated measurements of scintillations and in-situ F-region irregularities from Ogo-6, Geophys. Res. Lett., 3, 681-684, 1976.

Basu, S. and M. C. Kelley, Review of equatorial scintillation phenomena in the light of recent developments in the theory and measurement of equatorial irregularities, J. Atmos. Terr. Phys., 1977 (to appear).

Dyson, P. L., J. P. McClure and W. B. Hanson, In-situ measurements of the spectral characteristics of F-region ionospheric irregularities, J. Geophys. Res., 79, 1495-1502, 1974.

McClure, J. P. and W. B. Hanson, A catalog of ionospheric F-region irregularity behaviour based on Ogo-6 retarding potential analyzer data, J. Geophys. Res., 78, 7431-7440, 1973.

McClure, J. P., W. B. Hanson and J. H. Hoffman, Plasma bubbles and irregularities in the equatorial ionosphere, J. Geophys. Res., 82, 2650-2656, 1977.

Röttger, J., The macro-scale structure of equatorial spread-F irregularities, J. Atmos. Terr. Phys., 38, 97-101, 1976.

Woodman, R.F., East-west ionospheric drifts at the magnetic equator, Space Research XII, Akademie-Verlag, Berlin, 968-974, 1972.

Woodman, R.F. and C. LaHoz, Radar observations of F-region equatorial irregularities, J. Geophys. Res., 81, 5447-5466, 1976.

Woodman, R. F. and S. Basu, Comparison between in-situ spectral measurements of equatorial F-region irregularities and backscatter observations at 3 m wavelength (abstract), EOS Trans. AGU, 58, 449, 1977.

FIGURES

Fig. I.2.1. Geometry of radar backscatter and scintillation measurements on October 16-17, 1976. The ground locations of Jicamarca (JI), Ancon (An) and Huancayo (Hu) are indicated. The subionospheric locations (400 km) of LES-9 observations from Ancon and Huancayo between 0100 and 0500 UT are shown. The subionospheric tracks of the Wideband satellite between 0319 and 0332 UT referred to 300, 400 and 600 km are also shown.

Fig. I.2.2. Temporal variation of the 50 MHz radar backscatter observed at Jicamarca and scintillation index, SI(dB), of the 249 MHz transmissions from LES-9 satellite recorded at Ancon and Huancayo on October 16-17, 1976.

Fig. I.2.3. Scintillation measurements of the 249 MHz transmissions from the LES-9 satellite made on October 16-17, 1976 with aircraft flown by the Air Force Geophysics Laboratory(AFGL) and the Air Force Avionics Laboratory(AFAL). The top panel exhibits the subionospheric (300 km) flight paths of the two aircraft and the bottom panel shows the temporal variation of scintillation index, SI(dB), recorded by the AFGL aircraft.

Fig. I.2.4. Comparison of the 50 MHz radar backscatter map obtained at Jicamarca on October 17, 1973 and scintillation measurements made at Huancayo with the 137 and 254 MHz transmissions from ATS-3 and LES-9 satellites respectively.

I.3 ON THE CO-EXISTENCE OF KILOMETER- AND METER-SCALE IRREGULARITIES IN THE NIGHTTIME EQUATORIAL F-REGION

The detection of spread-F, ionospheric scintillations and VHF radar backscatter in the nighttime equatorial ionosphere shows that irregularities with scale lengths as large as several kilometers and as small as a few meters may arise in the equatorial F-region. In view of its importance in communications channel modeling as well as the development of theories of irregularity generation, the problem of co-existence of irregularities with different scale lengths in a common ionospheric volume has recently engaged the attention of many workers.

As early as 1970, Farley et al.(1970) stated that strong irregularities observed by the Jicamarca radar were in general associated with scintillations. When the digital power mapping technique became available (Woodman and La Hoz, 1976) a preliminary comparison of such radar maps and scintillations during November-December, 1975 made by Basu et al., (1977) indicated that plume-like structures on the maps were associated with intense scintillations in the VHF range at a nearby location.

Using the Atmospheric Explorer satellite, AE-C, McClure et al., (1977) observed that large scale bubbles of depleted ion concentration in the nighttime equatorial F-region are associated with small scale irregularities. These measurements

provided the incentive for a more carefully coordinated equatorial irregularity campaign conducted in Peru in October, 1976. During this campaign, simultaneous VHF radar backscatter and ionospheric scintillation measurements were made near the magnetic equator in which the ionospheric volume explored by the radar and scintillation experiments had a minimum separation of nearly 300 km. The analysis of results obtained on one night when a single plume structure was observed by the Jicamarca radar showed that the irregularity patch in which 3-m irregularities were detected by the 50 MHz radar in the post-sunset period drifted eastwards and caused onsets of scintillations on two propagation paths located to the east of Jicamarca (Aarons et al., 1978). This result implied that the patch contained both 3-m and km-scale irregularities which caused radar backscatter and scintillations respectively and the kilometer scale irregularities persisted in a patch for at least several hours during the transit of the patch to various propagation paths involved in the scintillation experiment. Owing to the separations encountered it was not possible to conclude whether the 3-m irregularities persisted in the patch at later periods of time when scintillations were detected.

In course of the above campaign, scintillation measurements were made on October 29, 1976, with the ATS-6 satellite when the propagation path of the satellite to the Huancayo ground station intersected the ionospheric height at a point where the radar was performing backscatter measurements. The results of these simultaneous measurements over a common volume discussed by Woodman and Basu (1978) indicate that the temporal variations of 3-m and kilometer scale irregularities were identical establishing thereby the co-existence of irregularities with scale lengths covering nearly four decades.

A careful study of the radar maps published by Woodman and LaHoz (1976) and the maps acquired by us during October, 1976, however indicates that the extended 3-m irregularity structures with which strong scintillations are associated, in general arise shortly after sunset. On the other hand, strong scintillation events are detected quite often even after midnight. Basu and Aarons (1977) concluded that during the October campaign there was a statistical preponderance of scintillation structures as compared to the extended 3-m irregularity structures. This seemed to indicate the possibility of having two types of equatorial irregularities: one type with significant spectral power at both km- and m- scales and the second with considerable power at kilometer scale lengths with little or no power at 3-m.

The second equatorial campaign in March, 1977 was planned to provide more definitive answers to the important problem of co-existence of km- and m-scales in the various phases of irregularity development and decay. The most important improvement during this campaign was the availability of scintillation and radar backscatter data pertaining to a common ionospheric volume for an extended period. We were also able to make scintillation measurements at closely spaced points both to the west and east of Jicamarca so that the evolution and decay of the drifting patches could be adequately monitored. With this unique data set we were able to demonstrate that it is possible to have two kinds of equatorial irregularities such as mentioned above. In this paper we shall discuss the results obtained on one day which seems to be fairly typical of the entire observation period. The implications of these measurements are also discussed in the context of current theories for the generation of equatorial irregularities.

I.3.1 OBSERVATIONS

On the night of March 19-20, 1977, 50 MHz radar backscatter observations were performed at Jicamarca (11.95°S, 76.86°W) near the magnetic equator in Peru. Radar power maps corresponding to three scattering volumes separated in the east-west direction by 6% of altitude were acquired by three antennas as discussed in Basu et al. (1977). We shall present the maps obtained with the westernmost radar beam. When referred to 400-km altitude, the above location corresponds to a position which is approximately 30 km to the west of Jicamarca. Simultaneous 137 MHz scintillation measurements were made at Ancon (11.71°S, 77.15°W) with GOES-1 satellite. The intersection of the propagation path from Ancon to GOES-1 with an ionospheric height of 400 km was located only 10 km to the east of the field line passing through the volume illuminated by the westernmost radar beam. However, the N-S separation of the two volumes was approximately 50 km. In view of the field aligned nature of equatorial F-region irregularities, the relatively large N-S separation may not be of serious concern while the much smaller E-W separation assures that the two experiments were exploring a nearly common ionospheric volume.

Scintillation measurements were also performed with a host of geostationary satellites, LES-8, LES-9, ATS-3, not only at Ancon but at Huancayo (11.97°S, 75.34°W) as well. The intersections of the propagation paths from these satellites to the two ground stations with

an ionospheric height of 400 km are indicated in Figure 1. The subionospheric locations are specified in the diagram by the station name (A for Ancon and H for Huancayo) followed by the abbreviated name of the satellite. The ground stations at Jicamarca, Ancon and Huancayo performing the radar and scintillation observations are shown by the dotted circles. Figure I.3.1 also shows the subionospheric (400 km) tracks of the orbiting Wideband satellite as viewed from Ancon and Huancayo on March 19-20. The Ancon station was equipped with coherent phase locked loop receivers and recorded both phase and amplitude scintillations at VHF (138 MHz), seven closely spaced frequencies at UHF centered at 413 MHz and L-band (1239 MHz) from the Wideband satellite (Fremouw et al., 1978). The station at Huancayo recorded only the amplitude scintillations of the transmissions at 138 and 413 MHz.

I.3.2 RESULTS

In Figure I.3.2 we show the results of simultaneous 50 MHz radar backscatter observations at Jicamarca and 137 MHz scintillation measurements at Ancon with GOES-1 satellite made on March 19, 1977, between 1900-2300 LT. The top panel shows radar power map of 3-m irregularites indicating the temporal variation of their range and intensity. The range scale is provided by the ordinate on the left hand side of the diagram while the tone of the map signifies the intensity of the backscattered echoes in the range of 6 to 48 dB above the approximate maximum incoherent scatter level. A complete description of the digital power mapping technique has been

outlined in Woodman and Lalloz (1976). The bottom panel shows the temporal variation of scintillation index in dB, SI(dB), scaled manually from the chart records at 2 minute intervals (Whitney et al., 1969).

The top panel in Figure I.3.2 shows that the radar started to detect weak irregularities in thin layers for the first time in the evening at 1938 LT. The first plume structure developed shortly thereafter at about 1950 LT. A series of plume developments occurred up to 2040 LT, with the later plumes having a low extent in altitude. Later, the backscatter echoes arose from progressively thinner irregularity layers. Between 2110 LT to 2210 LT weak, patchy backscattering regions above a weak and thin layer were observed. From the bottom panel, we find that the sharp onset of strong scintillations was very well matched in time with the development of strong 3-m irregularities at 1950 LT. Soon after onset, scintillation levels as high as 20 dB were encountered. It is interesting to note that although the plume structures were absent after 2040 LT and the 3-m irregularity structures were thinning out, high level of scintillation was maintained upto 2114 LT. It is also difficult to associate the large increase of scintillation observed after 2114 LT with the weak and patchy 3-m irregularities. The first scintillation structure ended at 2230 LT when the radar map was totally free of all traces of 3-m irregularities in the F-region. A study of the above event indicated that in the generation phase during the late evening hours, the kilometer and meter-sized irregularities evolve together and co-exist whereas in the later phase

approximately an hour after the onset, the meter-sized irregularities decay but the large scale irregularities responsible for scintillations continue to retain their high spectral intensities.

Another distinctive event was recorded later during this night and is illustrated in figure I.3.3. From the bottom panel we see that the second scintillation event of the evening was detected at Ancon on its propagation path to GOES-1 satellite at 2300 LT. The scintillation event was rather strong attaining levels as high as 22 dB at 137 MHz and decayed at about 0100 LT. A study of the top panel indicates that only very weak 3-m irregularity structures were detected between 2300 and 0000 LT and none at all between 0000 and 0100 LT. It appears that the irregularity structures detected during the late nighttime hours had little spectral power at short scale lengths although the spectral power at large scale lengths remained high giving rise to saturated VHF scintillations.

In order to investigate if the irregularity power spectra in the scale length range responsible for amplitude fluctuations have undergone any change, we obtained the power spectra of amplitude scintillations for both these cases, namely strong VHF scintillations in the presence of 3-m irregularities as illustrated in Figure I.3.4a and strong scintillations in the absence of 3-m irregularities shown in Figure I.3.4b. The scintillation data acquired on FM analog tapes were digitized at 36 samples/sec and the spectra for 7.5 minute data samples were obtained by the use of an FFT algorithm. The structure obtained around 3 Hz was generated by a subharmonic of the satellite spin and the multilobed satellite antenna pattern.

Considering that the 95% confidence interval of power estimate is approximately 6 dB, the average high frequency (ν) slopes of the power spectra in Figures I.3.4a and I.3.4b are very close to ν^{-4}. The diffraction scale length (Λ) on ground is related to the frequency scales (ν) in Figures I.3.4a and I.3.4b by the drift speed (v) of the irregularities as $\Lambda = (v/\nu)$.

However, the S_4 index of scintillation corresponding to Figures I.3.4a and I.3,4b were respectively 0.83 and 0,73 so that both the spectra pertained to strong scatter conditions. Under such conditions, it is not possible to relate the diffraction scale lengths on ground to irregularity scale lengths in the ionosphere in a precise manner (Yeh et al., 1975). Thus, even though drift speed measurements are available from spaced receiver scintillation observations performed at the nearby ground station at Ancon (Whitney, 1978), it is not possible to derive the irregularity characteristics from the scintillation spectra.

The similarity in the spectral forms in Figures 4a and 4b can only indicate in general terms that no drastic variation of irregularity power spectra occurred in the scale length range ($\sim$ 1 km to 100 m) which is responsible for VHF scintillations.

It is interesting to note that while the second scintillation event (cf. Figure I.3.3)at VHF was being recorded at Ancon on the propagation path to the GOES-1 satellite, a transit of the Wideband satellite occurred. The subionospheric tracks of the satellite as viewed from Ancon and Huancayo have been illustrated in Figure I.3.1 and designated as A(DNA) and H(DNA) respectively. We shall primarily discuss A(DNA) results acquired with the SRI International receiver providing both phase and amplitude scintillation data over a wide range of frequencies. Scintillations both in

amplitude and phase were recorded throughout the transit but we shall concentrate our attention to the interval 0427 UT (corresponding to 75°W time of 2327 LT) and 0428 UT, labelled on the track. Careful magnetic field line mapping indicated that at 0427.5 UT, the 400 km subionospheric location of the A(DNA) intersected the field line passing over Jicamarca. In Figure I.3.5, we illustrate the amplitude scintillation index, S_4, and r.m.s. phase fluctuation, $\phi_{r.m.s.}$ at the observing frequencies during a 20 sec interval beginning 0427.5 UT. The inverse frequency (f) dependence of $\phi_{r.m.s.}$, expected theoretically, is indicated by the solid line passing through the data point corresponding to 413 MHz, the UHF carrier frequency. For a 3-dimensional irregularity power spectrum of power-law exponent, 4, the amplitude scintillation index S_4 is expected to show $f^{-1.5}$ dependence (Rufenach, 1974) under weak scatter conditions. This is indicated by the dotted line. The data points agree well with the theoretical curves except for the S_4 data point at VHF which obviously violates weak scatter conditions. It should be noted that even significant L band scintillation was recorded at this time while in the VHF band an S_4 index of 0.78 was obtained. Fremouw et al., (1978) have noted that in the L band $S_4 \geq .02$ may be considered significant for these Wideband measurements. It may be observed from Figure I.3.3 that during the above scintillation event, only weak (<12 dB) and very fragmentary signatures of the backscatter echoes could be recorded.

Woodman and Basu (1978) have recently made a quantitative comparison of 360 MHz scintillation and 50 MHz radar backscatter measurements at Jicamarca. They postulated a gaussian type of

cut-off near the ion gyro-radius which is on the order of 3-m at F-region heights to bring scintillation and backscatter measurement into agreement. They showed that an S_4 index of 0.4 at 360 MHz may correspond to the observed 40 dB radar backscatter from an irregularity layer of thickness 200 km. Similar computations made in the present case under study, indicates that S_4 = 0.18 at 413 MHz should have been accompanied by at least 26 dB radar backscatter from a similarly extended irregularity layer, in contrast to the observed 12 dB backscatter from fragmentary patches. This result implies that the irregularity structures observed near midnight are characterized by a spectral cut-off at wavelengths longer than the ion gyro-radius, probably in the vicinity of tens of meters.

In Figure I.3.6, we illustrate the results of all scintillation measurements made on this night at the two ground stations, Ancon and Huancayo, with various geostationary satellites. The panels from top to bottom in Figure I.3.6 are arranged in the order of decreasing west longitude of the subionospheric position of scintillation measurements. From Figure I.3.1, it may be noted that subionospheric locations of these measurements spanned a longitude interval of nearly 12^{o} near the magnetic equator. The initial gap in the results shown in panel 1 of Figure I.3.6 was caused by an interruption of beacon transmission from LES-8 satellite. The remaining panels (2 through 7) indicate that the onset of scintillations at different locations occurred between 00 UT and 01 UT. Considering the different longitudes of all

these subionospheric locations, the onset of scintillations is found to have occurred within 4 minutes of 19h 40m (local). The local time dependence of scintillation onset on this night should not, however, be taken as a general rule, as we have observed cases when the irregularity generation has been localized in space rather than in local time (Aarons et al.,1978). In view of the consistent eastward drift speed of irregularity patches at night, the temporal variation of scintillation at an equatorial station is dictated by the localized generation (in space or time), eastward drift of irregularity patches, and the lifetime of these drifting patches. The successive panels of Figure I.3.6 have to be viewed in this context.

I.3.3 DISCUSSIONS

We have provided evidence for the existence of at least two phases of irregularity evolution in the equatorial F region. In the development phase during the post-sunset hours, irregularities covering the scale length range of tens of kilometers to 3-m evolve simultaneously. Near saturated VHF-UHF scintillations are observed in this phase when strong radar backscatter is detected from an extended altitude range. The recently compiled statistics of L band (1.54 GHz) scintillations observed at Huancayo also indicate that the occurrence maximum of gigahertz scintillations is obtained in this development phase (Mullen et al., 1978). The evolution of such thick irregularity layers takes place within tens of minutes. The generation of irregularities covering 3-4 decades of scale lengths has been explained by invoking a hierarchy of instability mechanisms starting at the long wavelength end with the gravitational Rayleigh-Taylor instability (Haerendel, 1974; Hudson and Kennel, 1975; Costa and Kelley, 1978a,b). The generation of irregularity patches extended both in altitude and in the E-W direction has recently been explained by Kelley and Ott (1978) by adopting the theoretical analysis of a rising ionospheric bubble presented by Ott (1978). Motivated by the sudden "bite outs" of plasma density observed by in situ measurements (Kelley et al., 1976; Morse et al., 1977; Hanson and Sanatani, 1973; McClure et al., 1977), Ott (1978) used a sharp boundary model and showed that the basic equations applicable to the rising bubble are identical to those governing the behavior of a

THIS PAGE IS BEST QUALITY PRACTICABLE
FROM COPY FURNISHED TO DDC

2-dimensional fluid. Using these results Kelley and Ott (1978) showed that upwelling plasma depleted regions or bubbles continually stir the medium and not only fill the wake with density irregularities in the presence of density gradients but also the regions (in the E-W direction) between the bubbles through a cascading process.

Following the development phase, the meter-scale irregularities are observed to decay while significant kilometer scale structures persist and continue to produce strong scintillations at VHF. Kelley and Ott (1978) have shown that in the late phase, the dissipation scale moves to smaller k values so that the smallest scale structures disappear first.

The irregularity structures that cause scintillations around local midnight are conspicuous by the absence of any significant spectral power at 3-m scale lengths. However, sufficient spectral power is available at long scale lengths to cause not only strong VHF/UHF scintillations but L band scintillations as well. It is of some interest to note that 6300 Å airglow measurements made on board the aircraft flown by the Air Force Geophysics Laboratory indicated the presence of regions with depleted ionization near Jicamarca corresponding to both the early evening and near midnight scintillation events (J. Bachau, private communication, 1978). Thus, it is possible to detect ionization depletions and strong scintillations in the absence of extended 3-m irregularity structures or "plumes". A similar irregularity structure was detected on March 30, 1977, at 2314 LT (75°W time), which caused as high as 7 dB (S_4 = .36)

scintillation at L band and 1 dB (S_4 = .07) at S band and yet failed to give rise to any appreciable VHF radar backscatter. It is important to note that even after considering the sharp cut-off near the ion gyro-radius proposed by Woodman and Basu (1978), the above scintillation levels are expected to be associated with a relatively thick layer of moderately strong 3-m irregularities. Thus it seems that the irregularity structures which exist near midnight are characterized by a spectral cut-off in the vicinity of tens of meters.

The nature of the irregularity spectrum at short scale-lengths needs much further study. It will be worthwhile to make observations of GHz scintillations in close proximity to Jicamarca to determine the relationship of irregularity scale lengths $\sim$ 100 m with the 3-m scale length during the various phases of irregularity evolution. In addition, rocket measurements of fully developed topside irregularity spectrum would be extremely useful in bridging the gap between the above scale length regimes.

ACKNOWLEDGMENTS

We thank Dr. J. Aarons, Mr. H. Whitney, and Mr. J.P. Mullen of AFGL for guidance and helpful cooperation. We appreciate the cooperation of J. Buchau of AFGL and A. Johnson of AFAL in making their aircraft observations available to us. We acknowledge the assistance and hospitality of the personnel of the Instituto Geofisico del Peru during the equatorial irregularity campaigns. We gratefully acknowledge the help of Dr. J.P. McClure of the University

THIS PAGE IS BEST QUALITY PRACTICABLE
FROM COPY FURNISHED TO DDC

of Texas at Dallas in placing the Jicamarca radar maps at our disposal. We also thank Dr. M.D. Cousins of SRI International for providing the Wideband satellite results obtained at Ancon. We thank Dr. Ben B. Balsley of National Oceanic and Atmospheric Administration, Boulder, Colorado for providing oblique VHF radar observations of electrojet irregularities.

REFERENCES

Aarons, J., J. Buchau, Santimay Basu and J.P. McClure, The localized origin of equatorial F-region irregularity patches, J. Geophys. Res., 83, 1659, 1978.

Basu, Sunanda, J. Aarons, J.P. McClure, C. LaHoz, A. Bushby and R.F. Woodman, Preliminary comparisons of VHF radar maps of F-region irregularities with scintillations in the equatorial region, J. Atmos. Terr. Phys., 39, 1251, 1977.

Basu, Santimay and J. Aarons, Equatorial irregularity campaigns: Part I, Correlated scintillation and radar backscatter measurements in October, 1976 Air Force Geophysics Laboratory Technical Report, AFGL-TR-77-0264, 1977.

Costa, E. and M.C. Kelley, On the role of steepened structures and drift wave instability with wavelengths near the ion gyroradius, J. Geophys. Res., 83, 4359, 1978a.

Costa, E. and M.C. Kelley, Linear theory for collisionless drift mode waves with wavelengths near the ion gyro-radius, J. Geophys. Res., 83, 4365, 1978b.

Farley, D.T., B.B. Balsley, R.F. Woodman and J.P. McClure, Equatorial spread F: Implications of VHF radar observations, J. Geophys. Res., 75, 7199, 1970.

Fremouw, E.J., R.L. Leadabrand, R.C. Livingston, M.D. Cousins, C.L. Rino, B.C. Fair, and R.A. Long, Early results from the DNA Wideband satellite experiment-Complex signal scintillation, Radio Sci., 13, 167, 1978.

Haerendel, G., Theory of equatorial spread-F, report, Max-Planck Institut fur Physik und Astrophysik, Garching, West Germany, 1974.

THIS PAGE IS BEST QUALITY PRACTICABLE
FROM COPY FURNISHED TO DDC

THIS PAGE IS BEST QUALITY PRACTICABLE
FROM COPY FURNISHED TO DDC

Hanson, W.B. and S. Sanatani, Large N_i gradients below the equatorial F peak, J. Geophys. Res., 78, 1167, 1973.

Hudson, M.K. and C.F. Kennel, Linear theory of equatorial spread-F, J. Geophys. Res., 80, 4581, 1975.

Kelley, M.C., G. Haerendel, H. Kappler, A. Valenzuela, B.B. Balsley, D.A. Carter, W.L. Ecklund, C.W. Carlson, B. Hausler and R. Torbert, Evidence for a Rayleigh-Taylor type instability and upwelling of depleted density regions during equatorial spread-F, Geophys. Res. Lett., 3, 448, 1976.

Kelley, M.C. and E. Ott, Two-dimensional turbulence in equatorial spread-F, submitted to J. Geophys. Res., 1978.

McClure, J.P., W.B. Hanson and J.H. Hoffman, Plasma bubbles and irregularities in the equatorial ionosphere, J. Geophys. Res., 82, 2650, 1977.

Morse, F.A., B.C. Edgar, H.C. Koons, C.J. Rice, W.J. Heikkila, J.H. Hoffman, B.A. Linsley, J.D. Winningham, A.B. Christensen, R.F. Woodman, J. Pomalaza and N.R. Teixeira, Equion: An ionospheric irregularity experiment, J. Geophys. Res., 82, 578, 1977.

Mullen, J.P., A. Bushby, J. Lanat and J. Pantoja, Gigahertz scintillation at the magnetic equator, Proceedings of the 1978 Symposium on the Effect of the Ionosphere on Space and Terrestrial Systems, Naval Research Laboratory, Washington, D.C., January, 1978.

Ott, E., Theory of Rayleigh-Taylor bubbles in the equatorial ionosphere, J. Geophys. Res., 83, 2066, 1978.

Rufenach, C.L., Wavelength dependence of radio scintillation: Ionosphere and interplanetary irregularities, J. Geophys. Res., 79, 1562, 1974.

Whitney, H.E., J. Aarons and C. Mailk, A proposed index for measuring ionospheric scintillations, Planet. Space Sci., 17, 1069, 1969.

Whitney, H.E., Spaced receiver measurements of intense equatorial scintillations, Proceedings of 1978 Symposium on the Effect of the Ionosphere on Space and Terrestrial Systems, Naval Research Laboratory, Washington, D.C., January, 1978.

Woodman, R.F. and C. LaHoz, Radar observations of F-region equatorial irregularities, J. Geophys. Res., 81, 5447, 1976.

Woodman, R.F. and Sunanda Basu, Comparison between in-situ spectral measurements of equatorial F-region irregularities and backscatter observations at 3m wavelength, Geophys. Res. Lett., 5, 869, 1978.

Yeh, K.C., C.H. Liu and M.Y. Youakim, A theoretical study of the ionospheric scintillation behavior caused by multiple scattering, Radio Sci., 10, 97, 1975.

THIS PAGE IS BEST QUALITY PRACTICABLE
FROM COPY FURNISHED TO DDC

LIST OF FIGURES

Figure I.3.1. Subionospheric positions (referred to an altitude of 400 km) of scintillation measurements on March 19-20, 1977. The ground stations at Ancon (A) and Huancayo (H) performing scintillation observations and Jicamarca (J) making radar backscatter observations are indicated in the diagram. The satellites LES-8, ATS-3, GOES-1 and LES-9 are abbreviated as L-8, A-3, G, L-9, respectively.

Figure I.3.2. Temporal variation of 50 MHz radar backscattered power obtained at Jicamarca and scintillation index, SI(dB), of 137 MHz transmissions from Goes-1 satellite recorded at Ancon on March 19, 1977 during 1900-2300 LT.

Figure I.3.3. Comparison of radar backscattered power and scintillation index, SI(dB) as in **Fig. I.3.2, on** March 19-20, 1977 during 2300-0200 LT. Note that weak and patchy 3-m irregularities shown in the top panel are associated with intense scintillation activity in the bottom panel.

Figure I.3.4a. Power spectrum of 137 MHz scintillations (S_4=0.83) recorded at Ancon by the use of Goes-1 transmissions between 0200-0207.5 UT on March 20, 1977 (2100-2107.5 LT on March 19, 1977). The power spectrum corresponds to the period when intense 50 MHz radar backscatter was obtained.

Figure I.3.4b. As in Figure I.3.4a for the period 0411-0418.5 UT on March 20, 1977 (2311-2318.5 LT on March 19) when S_4=0.73 was recorded. The period of scintillation corresponds to weak and patchy 50 MHz radar backscattered power.

Figure I.3.5. The frequency dependence of r.m.s. phase, ϕ_{RMS}, and S_4 index of Wideband satellite data recorded at Ancon on March 19, 1977 between 2327.5 and 2327.8 LT.

Figure I.3.6. Temporal variation of scintillation index, SI(dB), recorded at Ancon and Huancayo on March 19-20, 1977 by the use of transmissions from various geostationary satellites. The panels are arranged in order of decreasing west longitude of ionospheric intersection points of the various ray paths as shown in Figure I.3.1.

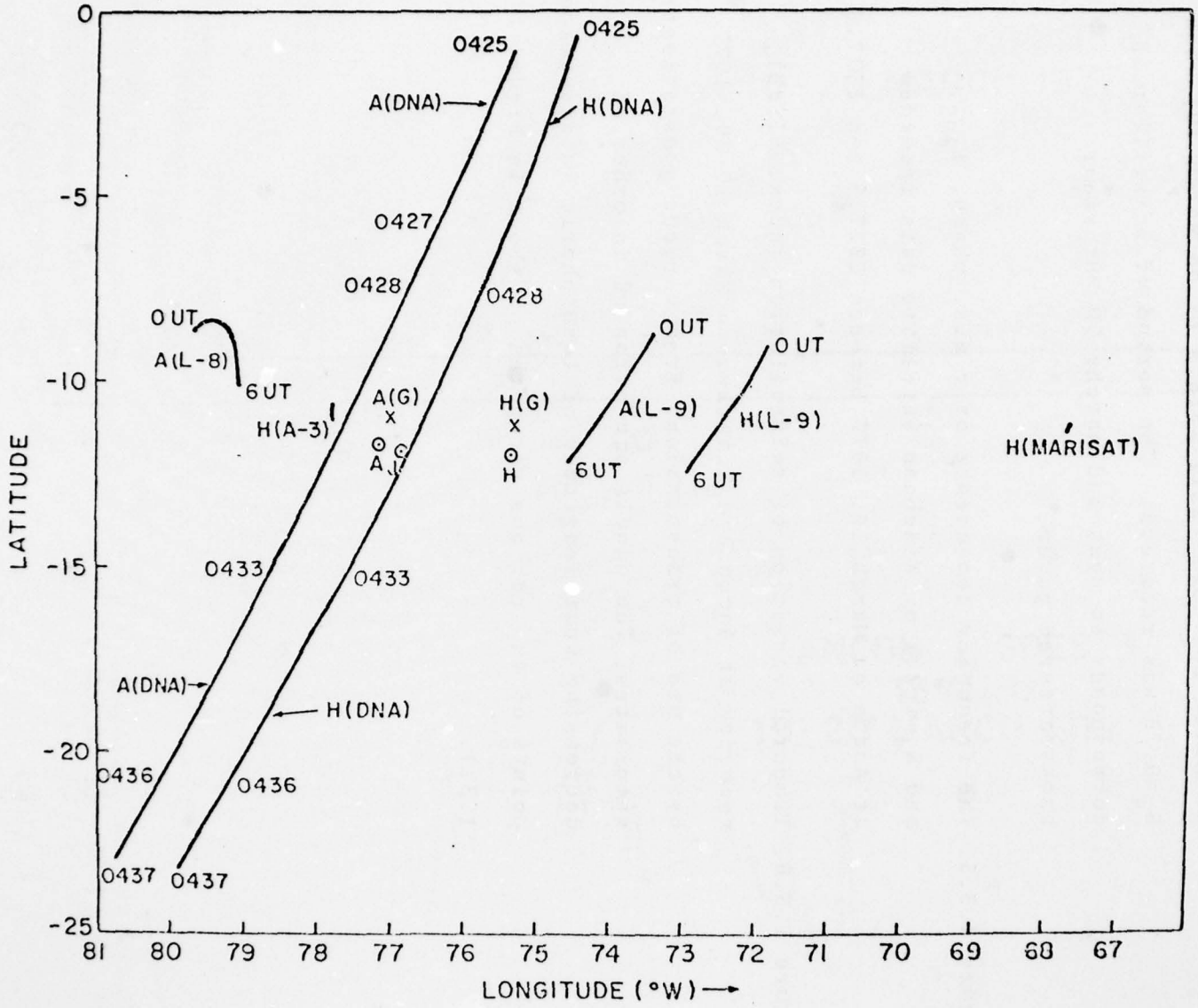
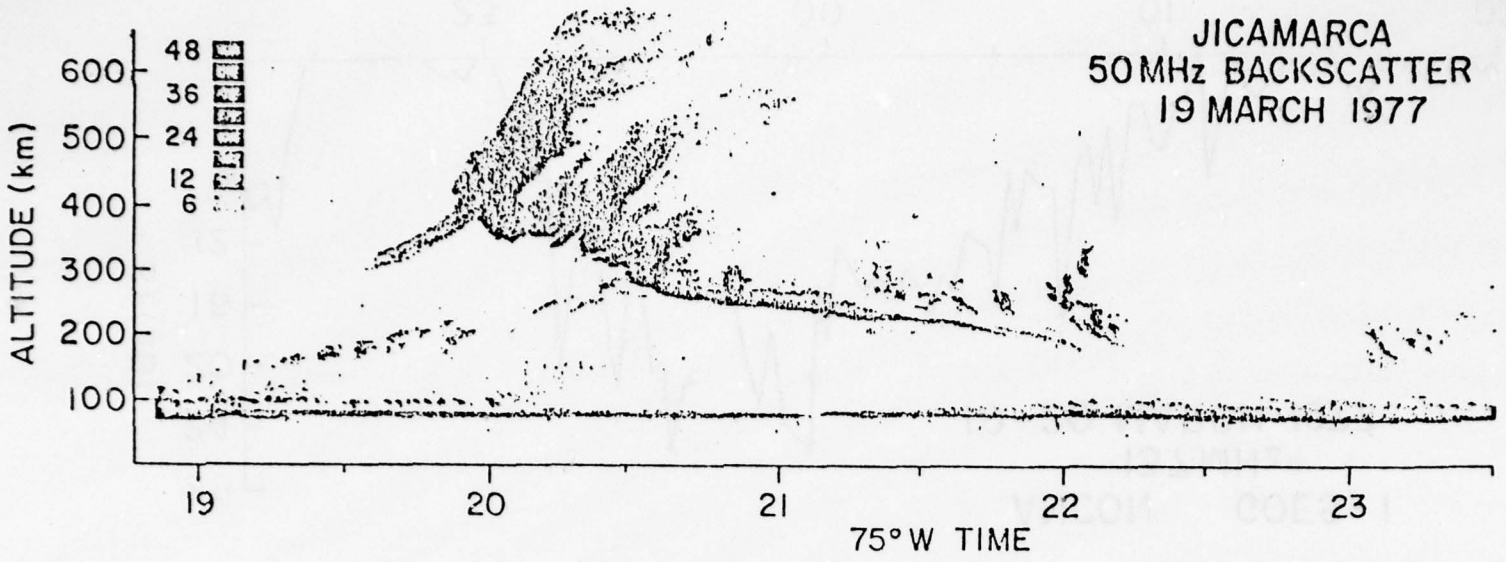

0
-5
-10
-15
-20
-25
LATITUDE
81
80
79
78
77
76
75
74
73
72
71
70
69
68
67
LONGITUDE (°W)
0425
0425
A(DNA)
H(DNA)
0427
0428
0428
0 UT
A(L-8)
6 UT
H(A-3)
A(G)
H(G)
0 UT
A(L-9)
6 UT
0 UT
H(L-9)
6 UT
H(MARISAT)
0433
0433
A(DNA)
H(DNA)
0436
0436
0437
0437

Figure I.3.1.


JICAMARCA
50 MHz BACKSCATTER
19 MARCH 1977
ALTITUDE (km)
600
500
400
300
200
100
48
36
24
12
6
19
20
21
22
23
75° W TIME

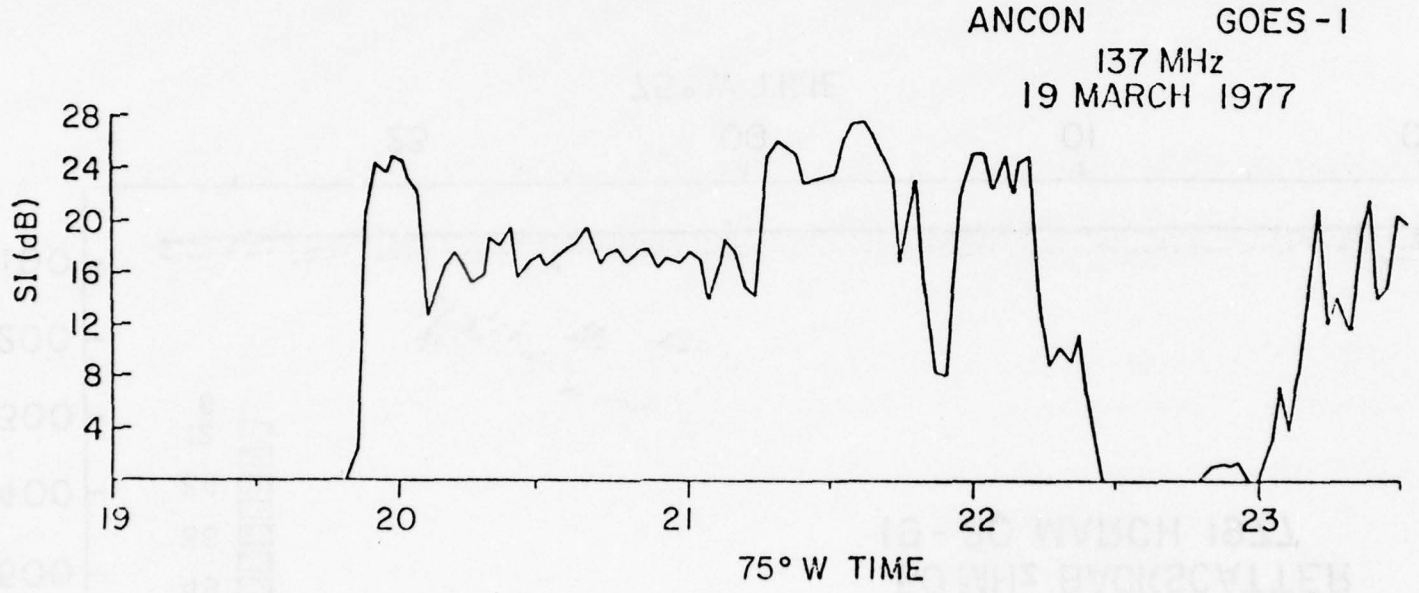
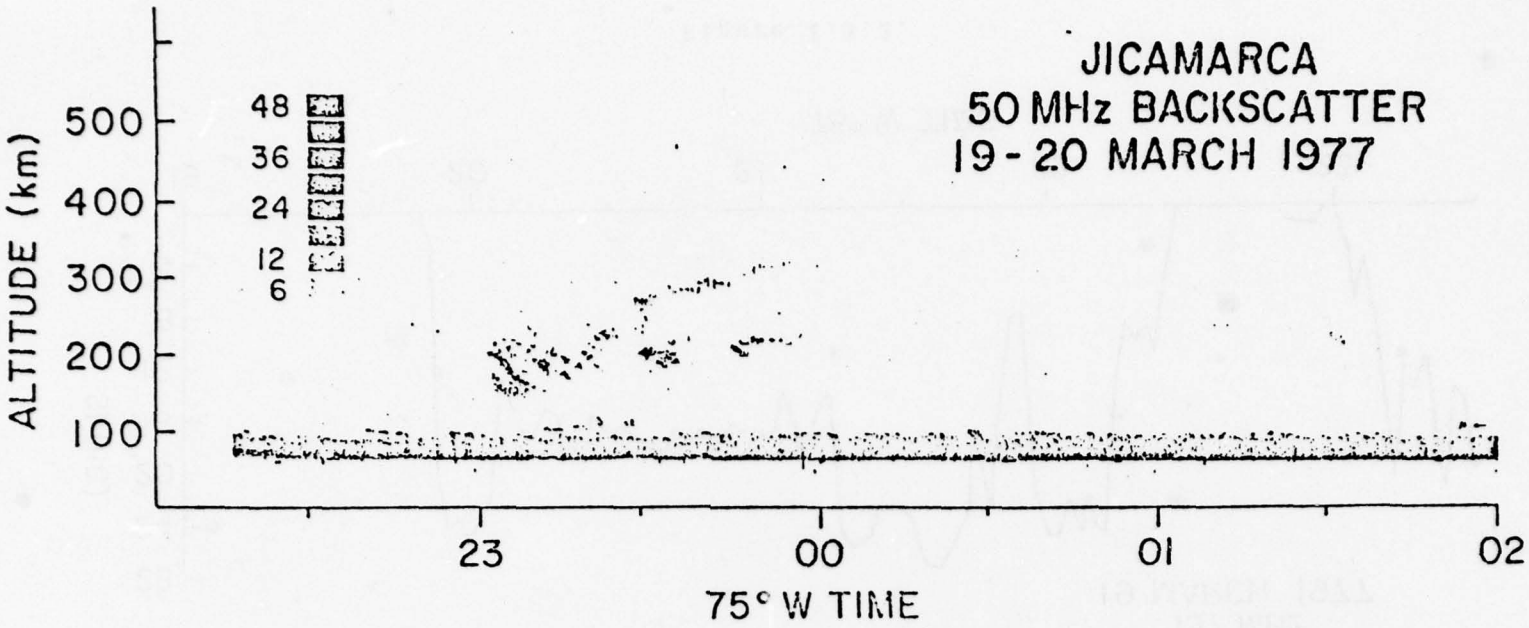

ANCON GOES-1
137 MHz
19 MARCH 1977
SI (dB)
28
24
20
16
12
8
4
19
20
21
22
23
75° W TIME

Figure I.3.2.


JICAMARCA
50 MHz BACKSCATTER
19 - 20 MARCH 1977
ALTITUDE (km)
500
400
300
200
100
48
36
24
12
6
23
00
01
02
75° W TIME

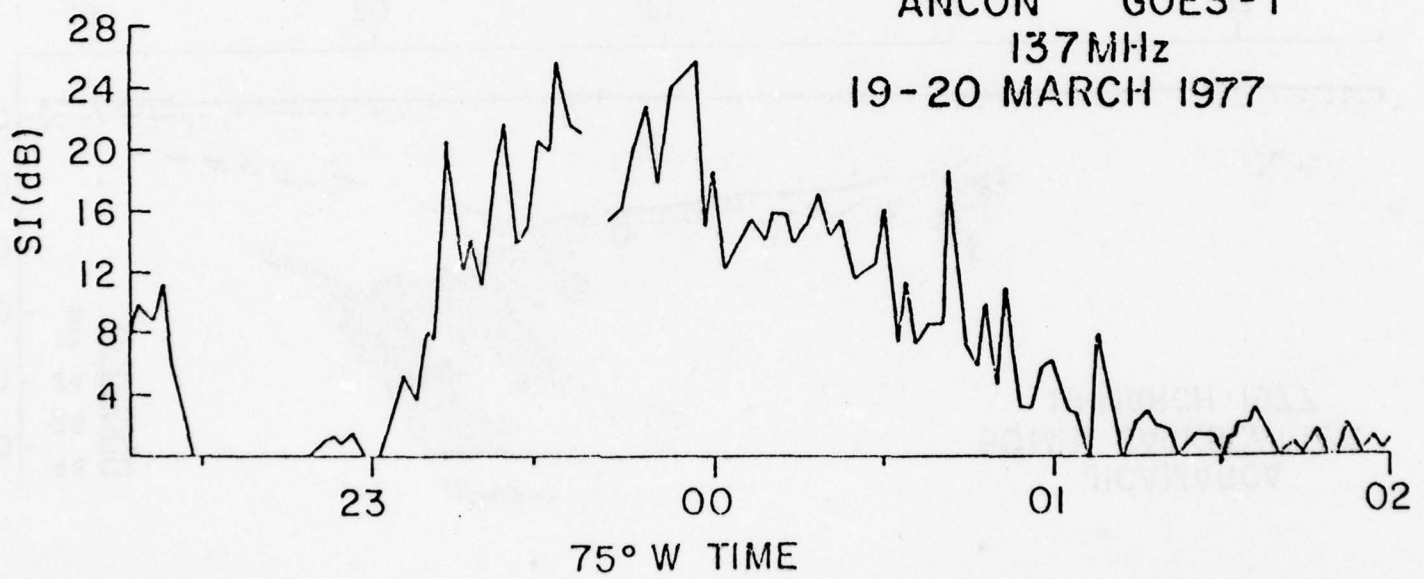

ANCON GOES - 1
137 MHz
19 - 20 MARCH 1977
SI (dB)
28
24
20
16
12
8
4
23
00
01
02
75° W TIME

Figure I.3.3.

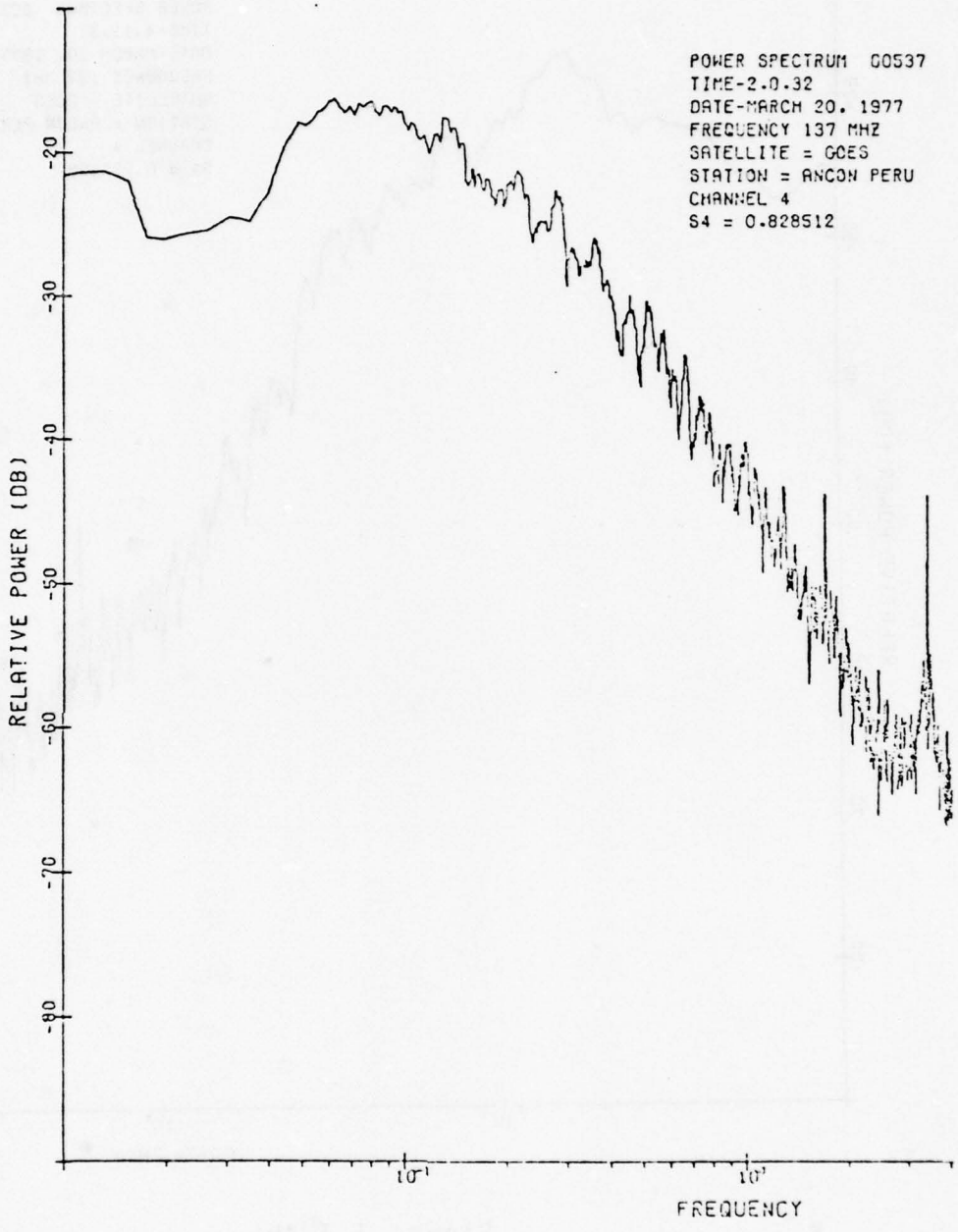

POWER SPECTRUM 00537
TIME-2.0.32
DATE-MARCH 20. 1977
FREQUENCY 137 MHZ
SATELLITE = GOES
STATION = ANCON PERU
CHANNEL 4
S4 = 0.828512
RELATIVE POWER (DB)
-20
-30
-40
-50
-60
-70
-80
10⁻¹
10⁰
FREQUENCY

Figure I.3.4a.

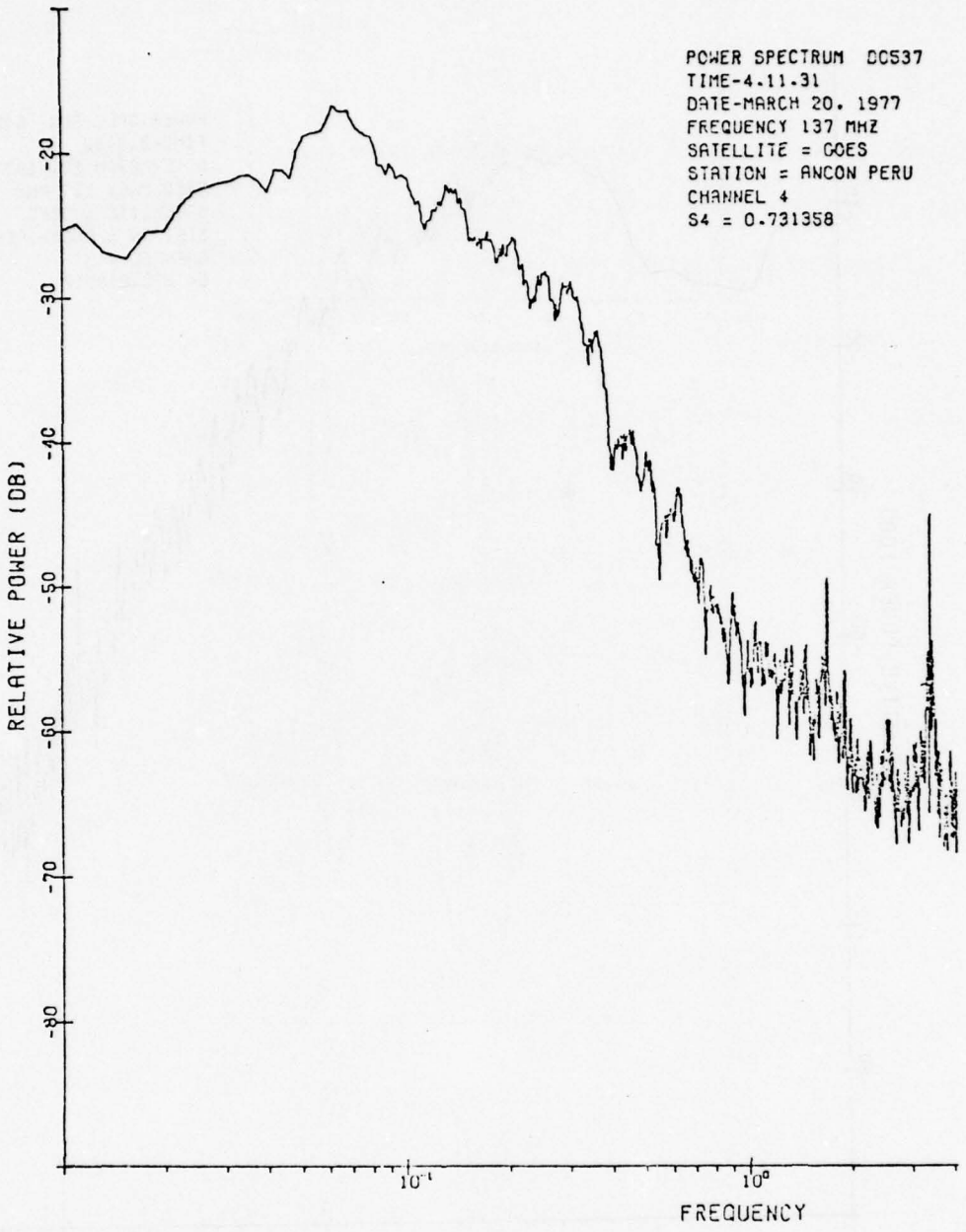

POWER SPECTRUM DC537
TIME-4.11.31
DATE-MARCH 20, 1977
FREQUENCY 137 MHZ
SATELLITE = GOES
STATION = ANCON PERU
CHANNEL 4
S4 = 0.731358
RELATIVE POWER (DB)
-20
-30
-40
-50
-60
-70
-80
10^{-1}
10^{0}
FREQUENCY

Figure I.3.4b.

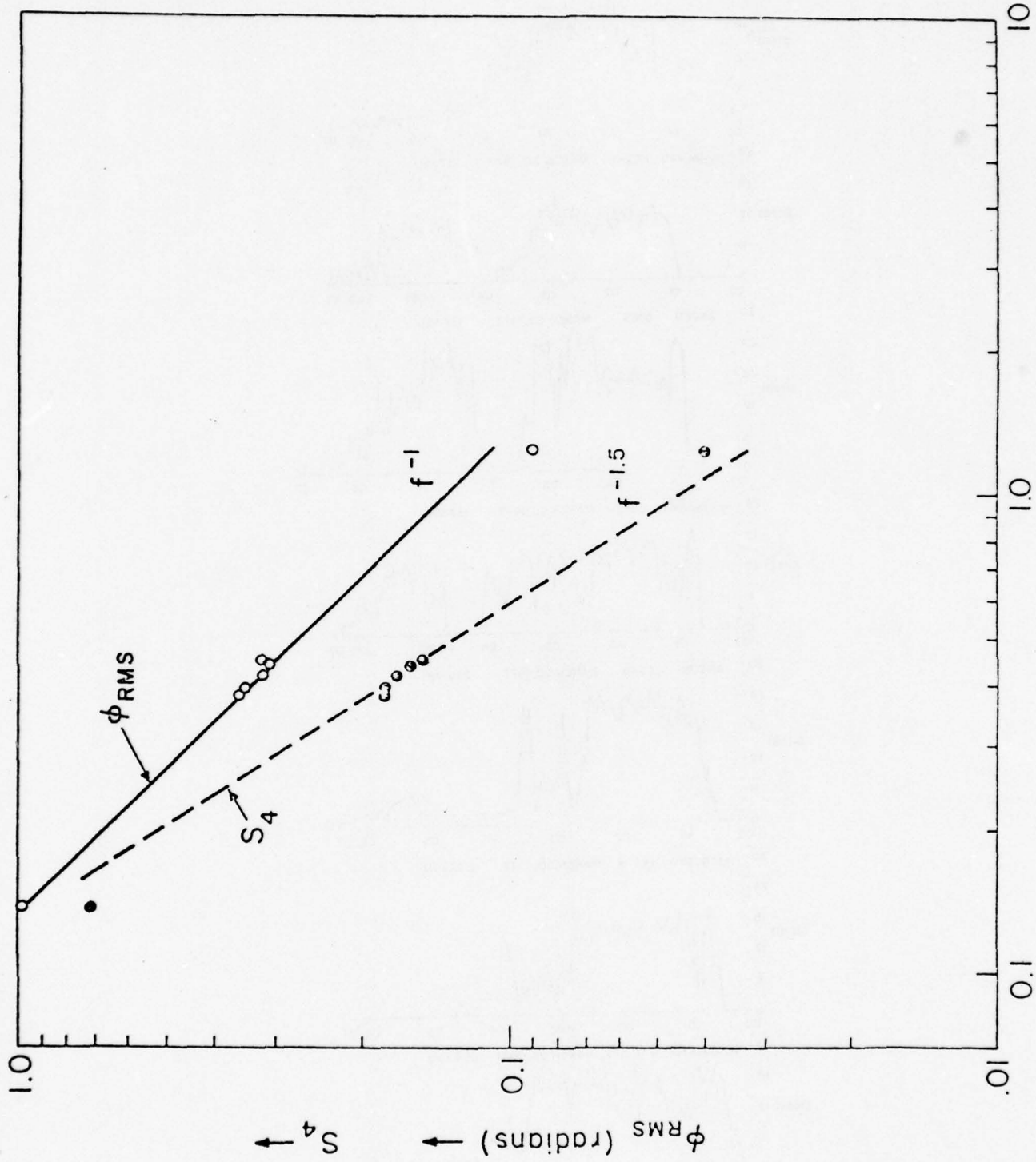


Figure I.3.5.

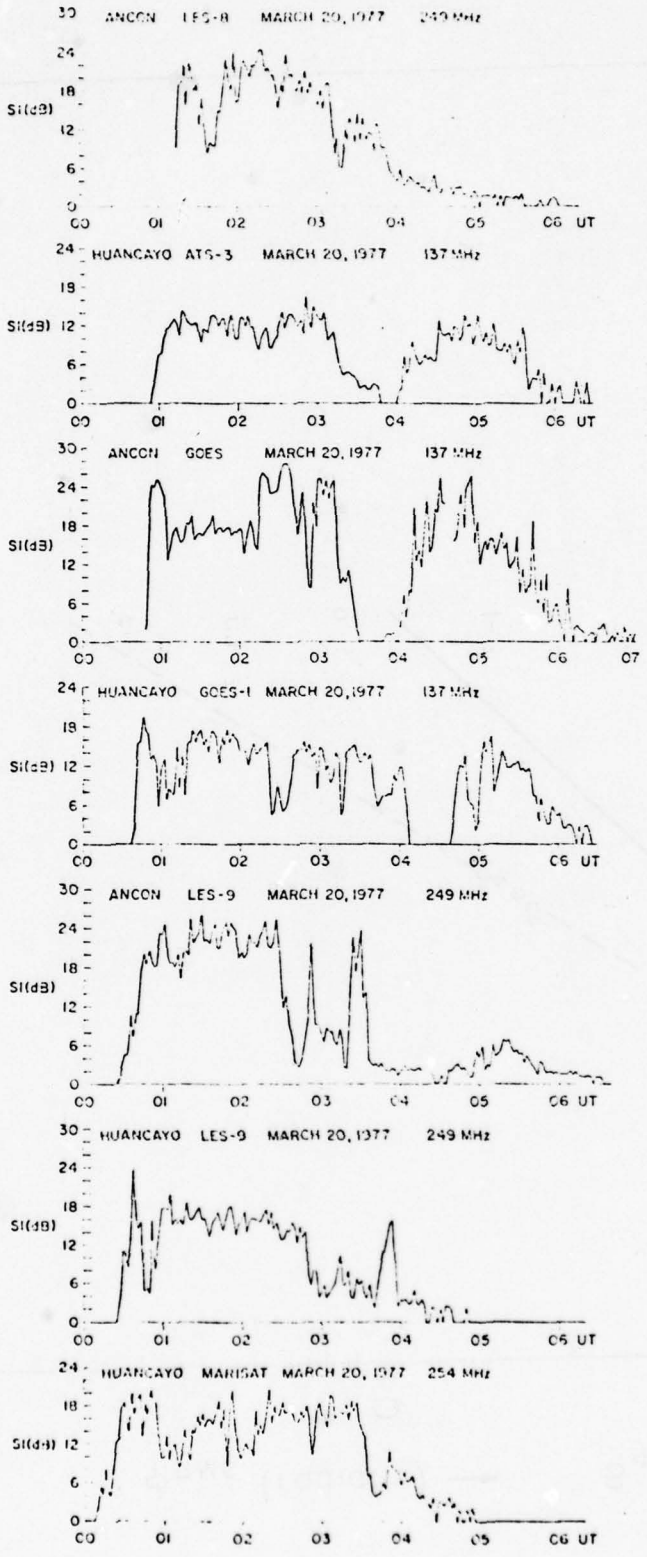

ANCON LES-8 MARCH 20, 1977 249 MHz
HUANCAYO ATS-3 MARCH 20, 1977 137 MHz
ANCON GOES MARCH 20, 1977 137 MHz
HUANCAYO GOES-1 MARCH 20, 1977 137 MHz
ANCON LES-9 MARCH 20, 1977 249 MHz
HUANCAYO LES-9 MARCH 20, 1977 249 MHz
HUANCAYO MARISAT MARCH 20, 1977 254 MHz
SI(dB)
00 01 02 03 04 05 06 07 UT

Figure I.3.6.

II. SCINTILLATION STUDIES

II.1 Description

The study of scintillations has been directed in two general areas. The first has been to utilize the large available data base by developing a model for scintillations at both high and equatorial latitudes; the second, to examine in detail certain periods, such as magnetic storm periods. The general aspects of scintillation which lead to a model will be discussed first.

The data base, in both equatorial and high latitude cases, were composed of 15-minute observations of the ATS-3 and for the case of Huancayo, also the LES-6 satellite beacon. These were reduced by the method of Whitney et al. (1969), where the definition of SI is:

$$SI = (P_{max}-P_{min})/(P_{max}+P_{min})$$

where P_{max} is the power level of the 3rd peak down from the maximum excursion of the scintillation and P_{min} is the power level of the 3rd peak up from the minimum excursion, measured in dB.

II.2 Equatorial Model

Here, two sets of data were used, one from Huancayo, Peru, the other from Accra, Ghana. The dates of these are:

Huancayo, Peru	ATS-3	May 1969 - April 1976
Huancayo, Peru	LES-6	Dec 1970 - March 1976
Accra, Ghana	ATS-3	Oct 1971 - April 1976

Table 1

Station and Sat.	Date	Subion. Lat. Long.	Geomag. Deg. of Intersection Pt. from Geomag. Eq.	El.	Az.	Iono. Z.A.
Huancayo, Peru A3	5/69-12/71	11.3°S 73.1-75.6°W	0°	51.7-75.9°	71.3-6.4°	36.0-13.9°
	1/72-4/76	11.3°S 74.9-75.1°W	0°	73.6-75.1°	31.8-20.1°	16°
Huancayo, Peru L6	12/70-3/76	11.3°S 72.1-72.7°W	0°	42.2-47.5°	73.5-76.0°	45-40°
Accra, Ghana A3	10/71-4/76	5.2°N 9.5-11.0°W	11°N	10.7-13.7°	268°	67-69°

Table 2

Equatorial Scintillation Index (dB) Models

Huancayo ATS3

$$SI(dB) = 1.+2^{[FA+FB+\{(-1.3FA+2.1FB)\cos(HL+.1-.25K_p)\}+FC\{\cos(2(HL+3.3))-.4\cos(3(HL+1.5))\}]}$$

where $FD = \cos(DA-4.4)-.5\cos(2(DA-4))$ $FA = (-2.9+.6FD)As$ $FB = (.3+FD)+(.1-.2FD)K_p$ $FC = (1.6-.4FD)As+.2K_p$

Huancayo LES6

$$SI(dB) = 2^{[FA+FB+\{(-1.5FA+.8FB)\cos(HL-.2-.25K_p)\}+FC\{\cos(2(HL+3.3))-.4\cos(3(HL+1.5))\}]}$$

where $FD = \cos(DA+1.3)-.6\cos(2(DA-4))$ $FA = (-2.7-.3FD)As$ $FB = (.2+FD)+(.1-.1FD)K_p$ $FC = (1.6+.7FD)As+.1K_p$

Ghana ATS3

$$SI(dB) = -.05+2^{[FA+FB+\{(-3.6FA+1.9FB)\cos(HL-.25K_p)\}+FC\{\cos(2(HL+3.3))-.4\cos(3(HL+1.2))\}]}$$

where $FD = \cos(DA-10.3)-.5\cos(2(DA-4))$ $FA = (-.7+.2FD)As$ $FB = (.4+.5FD)+(0.)K_p$ $FC = (.7-.4FD)As+.15K_p$

DA - Day Number $As = S_f/100$, where

HL - Local Time (hrs.) S_f - 2695 MHz Solar Flux

During these periods, the satellite intersection point at 350 km varied slightly and this range of intersections is seen in Table I, along with related parameters. The 15-minute samples of scintillation index (dB) data for the ATS-3 and LES-6 satellites from the above three stations were augmented into complete data bases on tape. Data associated with each 15-minute sample include: Station ID, Satellite ID, Frequency, Date and UT, Scintillation Index (dB), 3-hourly magnetic index (Kp), 2695 MHz solar flux, (S_f), 4995 MHz solar flux, sub-ionospheric latitude and longitude, and corresponding geomagnetic latitude and magnetic local time.

Various forcing parameters were used in this analysis. They are:

a) Planetary magnetic index, Kp, which was noted previously to increase or decrease scintillation at Huancayo depending on season. At Ghana, increased Kp usually inhibits scintillation activity.

b) Increasing solar flux, which was found to increase scintillation activity.

c) Seasonal occurrence patterns which vary with longitude.

d) The diurnal pattern with start of activity shortly after local sunset and maximum activity before local midnight. The parameters were incorporated into the model but the rapid onset of scintillation activity cannot be duplicated by a simple analytical form. These equations are shown in Table 2. A sample of the behavior of the data and the best

fitting model equations are seen in Fig. II.2.1 for Huancayo A3 and Fig. II.2.2 for Ghana A3 for differing solar flux and K groupings for the month of February.

Both Ghana and Peru data exhibit monthly maximum excursions in the Feb-Mar and Oct-Nov periods, while minimum excursions can be noted in June and July. Both sets of data show clear increases with increasing solar flux (at the same level of magnetic activity). However, both the data and the model indicate little variation with magnetic activity under the same solar flux conditions in Peru. Magnetic activity can be seen to inhibit scintillation excursions at Ghana.

For the LES-6 beacon observed at Huancayo, the data in the time period 22-24 LT, when scintillations were intense, experienced problems which made the data unusable.

Also, the absence of a high signal-to-noise ratio resulted in a limiting value of 16-19 dB excursions peak-to-peak. Graphing of data for February is illustrated in summary form in Fig.II.2.3, the hours 2200-2400 having been omitted.

For the period November thru March, the LES-6 data are of the order of .5 to .6 of the larger values of scintillation excursions of ATS-3.

The behavior of both sets of Huancayo data is similar, though the ratio of scintillation levels between the frequencies varies seasonally. For example, the months of May, June, and July are very low at both frequencies with increasing Kp bringing on increasing SI.

A comparison was made between the average and median values of the data at each station. In general, for low and medium levels of scintillation, the average data tends to be slightly higher than the median while at high scintillation levels, the median data is slightly higher than the average.

II.3 High Latitude Model

For the high latitude model, data from 3 stations were available, providing coverage from the sub-auroral through auroral latitudes. The dates of the data bases used are:

Narssarssuaq	9/17/68 - 9/1/74
Goose Bay	1/1/72 - 12/31/74
Sagamore Hill	12/1/69 - 11/30/74

The three stations are situated near the 70°W meridian and their geomagnetic and geometrical parameters are given in Table 3.

Table 3

Station	Inv. Lat.	Elev.	Az.	Iono. Z.A.
Narssarssuaq	63.2°	18.0°	208°	64°
Goose Bay	60.3°	28.8°	191°	56°
Sagamore Hill	53.5°	40.9°	178°	46°

These 15-minute dB data samples were augmented into complete data bases on tape with the same parameters as described in the equatorial model section.

The forcing parameters used in the high latitude model are:

a) Planetary magnetic index, Kp, which has been associated with increased scintillation activity at high latitudes,

b) solar flux, where influence varies as a function of season,

c) seasonal occurrence patterns,

d) the diurnal pattern.

Initially, separate models for each station were formulated to approximate the data base while smoothing abrupt variations to fit an analytical form.

Table 4 presents the model for each station in terms of local time. The difference between universal time and local time at the sub-ionospheric point (350 km) was taken to be 3.4 hr at Narssarssuaq, 4.1 hr at Goose Bay, and 4.7 hr at Sagamore Hill. In the model equations, the cosine arguments (in radians) that include the terms for day number (DA) and hour (HL) assume a multiplicative term of $2\pi/365$ and $2\pi/24$, respectively. Though not shown in the equation for reasons of convenience, these must be included in the calculations.

To illustrate the behavior of the data and the best fitting model equations, a sample month (March) is shown for each station.

Narssarssuaq data is seen in Fig. II.3.1. It is noted that scintillations increase with increasing Kp, for constant S_F, and scintillations increase with increasing solar flux, for constant Kp.

The behavior of the Goose Bay data and best-fitting model

Table 4

Scintillation Index (dB) Models for Local Time

Narssarssuaq

$$SI(dB) = -6.4+9.2(1-.2FD)[1+.23(1-.3FD)\cos(HL+2.0+.34K_p)+.03\cos(2(HL-0.6))+.02\cos(3(HL+3.0))]^{2[.14K_p(1+.12FD)+.09As(1+1.76FD)]}$$

$$FD = \cos(DA+15.6)+.56\cos(2(DA-22.4))$$

Goose Bay

$$SI(dB) = -1.3+1.1(1-.77FD)[1+.5(1-.2FD)\cos(HL+2.1-.6K_p)+.06\cos(2(HL-2.1))+.02\cos(3(HL+5.2))]^{2[.3K_p(1+.1FD)+.8As(1+1.2FD)]}$$

$$FD = \cos(DA+.5)+.2\cos(2(DA-99))$$

Sagamore Hill

$$SI(dB) = 0.33+.02(1+.2FD)[1+1.2(1-.01FD)\cos(HL-0.4-.15K_p)+.3\cos(2(HL-0.8))-.1\cos(3(HL+6.1))]^{2[.38K_p(1+.3FD)+3.1As(1-.2FD)]}$$

$$FD = \cos(DA+56)+.7\cos(2(DA-143))$$

DA - Day Number

As = $S_f/100$

HL - Local Time (hours) at Sub-Ionospheric Point (350 km)

S_f - Solar Flux at 2695 MHz in Solar Flux Units

THIS PAGE IS BEST QUALITY PRACTICABLE
FROM COPY FURNISHED TO DDC

for March are shown in Fig. II.3.2. Within each particular solar grouping scintillations increase with increasing Kp. For the same Kp grouping, the scintillation excursions increase with increasing solar flux.

Behavior of the Sagamore Hill data and model for March are shown in Fig. II.3.3. For the low solar flux group (0 to 95), a very slight increase in scintillations associated with increasing Kp is seen. The same is true of the solar flux group 96 to 120 while for high solar flux, the increase with Kp becomes more noticeable. In general, within a particular Kp grouping, scintillation index increases with increasing solar flux.

A comparison was made between the average and median data at each of the stations. No substantial differences occurred between these although for low scintillation activity, the average values tended to be slightly higher than the median values.

II.4 Comprehensive Model

Two attempts to combine these individual models into more comprehensive latitudinal models were made. The first, a 3-station model, is restricted to use over the latitude range 53°-63°Λ. It attempts to reproduce the individual station observations at the station invariant latitude and interpolates at latitudes in between. This model, presented in Table 5, is a modified and corrected form of equation B2 in an earlier

Table 5

Revised Mathematical Model

Narssarssuaq - Goose Bay - Sagamore Hill Based

$$SE = -2.8+1.2CL+6.5(1-.2FD)[1+.6(1-.16FD)(1-.45SL)\cos(HL+2-.4K_p)+.05\cos(2(HL-.9))+.02\cos(3(HL+3.5))] \times 2^{[.32(PF-66.1)]}{}_{EXA}$$

where $EXA = 2^{[.2K_p(1+.25CL)(1-.1XD)+As(1-.8SL)(1+.45FD)]}$

and $CL = \cos((PF-54.4)\frac{\pi}{25})$ $\quad$ $CDL = 1+.75SL$ $\quad$ $SL = \sin((PF-54.4)\frac{\pi}{25})$ $\quad$ $SDL = 1-3SL$

PD = cos(DA+16) + .3cos(2(DA-30))
FD = CDL x PD
XD = SDL x PD
PF = Invariant Latitude (in degrees)

HL = Local time
As = $S_f/100$
Kp = Magnetic index
DA = Day number

Table 6

Narssarssuaq-Goose Bay Based

$$SE = -1.3-2.7CL+6.2(1-.17(1+2.6CL)FD)[1+.33(1-.35(1-.8CL)FD)\cos(HL+2.1-.4K_p)+.05\cos(2(HL-.9))+.02\cos(3(HL+3.5))](1-.9CL)EXA$$

where $EXA = 2^{[.2K_p(1+.13FD)+.75AsCL(1+FD)]}$

FD = cos(DA-2.6)+.2cos(2(DA-30))
CL = cos((PF-53.5)π/25)
As = $S_f/100$

HL = Local time (hr.)
PF = Geomag. Lt. (deg.)
[$\frac{2\pi}{365}$ & $\frac{2\pi}{24}$ implied in all annual & diurnal periodic terms (see text)]

published version of the high latitude model (Aarons et al., 1976).

The sub-auroral to middle latitudes present a different morphology from the high latitude ionosphere except during periods of intense magnetic activity when auroral effects at F-layer heights extend into the sub-auroral region. Thus the inclusion of the Sagamore Hill data although serving to extend the model in latitude, does not provide a true picture of this entire scintillation region, since two differing morphologies are joined. Under high Kp cases auroral effects do take place at the latitude of Sagamore Hill in which case the 3-station model may be valid. Therefore a second model, more physically coherent, was postulated which would range over the latitudes 60°-63°Λ, including the Goose Bay and Narssarssuaq data bases but excluding Sagamore Hill which would then simply rely on its single station model. This model, is presented in Table 6 with a sample month, March, shown in Fig. II.4.1. As noted for the individual station models, additional multiplicative terms are assumed in this model.

The standard deviation between the 2-station model values and the individual station models (Aarons et al., 1976) is $\sigma \sim .7$, with the ranges of variation running +1 to 2, 0 to -1 dB. However, the standard deviation between the actual data base and the individual station model runs from $\sigma \sim 1.5$ for Sagamore Hill to $\sigma \sim 2.8$ for Narssarssuaq, with the range of residuals being even higher, since the actual data contains highly

variable scintillations, especially for disturbed magnetic conditions and high solar flux, in which the data base is limited.

II.5 Comparison of Model with Millstone Hill Data

In order to validate the model using an independent set of observations at a higher frequency it was determined that the Millstone Hill data obtained by observing scintillations at 400 MHz tracking Transit satellites would be used. The data base for the comparison was that in the publication "The Millstone Hill Radar Propagation Study: Scientific Results" by J. Evans (1973).

Since Evans' data was in the S_4 format at 400 MHz, a conversion using weak scatter relationships was first made to dB at 137 MHz. The measured S_4 (400 MHz) as a function of invariant latitude is shown in Fig. II.5.1. These values, in three different Kp groupings, at the invariant latitude of Narssarssuaq, Goose Bay and Sagamore Hill, along with the conversion to dB (137 MHz) are shown below.

NSSQ ($\Lambda = 63°$)

	S_4 (400 MHz)	dB (137 MHz)
$Kp \leq 1+$	.0375	2.5
$2_o \leq Kp \leq 3+$	.05	3.6
$Kp \geq 4_o$	.0775	6.3

Goose Bay ($\Lambda = 60°$)

	S_4 (400 MHz)	dB (137 MHz)
Kp $\leq$ 1+	.025	1.5
$2_o \leq$ Kp $<$ 3+	.030	1.9
Kp $\geq 4_o$	.055	4.0

Sagamore Hill ($\Lambda = 54°$)

	S_4 (400 MHz)	dB (137 MHz)
Kp $\leq$ 1+	.016	.8
$2_o \leq$ Kp $\leq$ 3+	.018	1.0
Kp $\geq 4_o$	.021	1.2

This data used by Evans was taken in 1972-1973 and was averaged over local time to include all passes. The model dB values are obtained by using the local time equations for each station for 3 particular Kp values. A solar flux level of $S_f = 108$ was used since solar flux in 1972-73 was of this magnitude. The resulting averages over all hours and all months are:

Narssarssuaq (63°Λ)

	dB (137 MHz)	S_4 (400 MHz)
Kp = .5	2.5	.0375
Kp = 2.5	4.0	.053
Kp = 5.0	6.3	.0775

Goose Bay (60°Λ)

	dB (137 MHz)	S_4 (400 MHz)
Kp = .5	.3	.012
Kp = 2.5	1.6	.026
Kp = 5.0	4.8	.063

Sagamore Hill (54°Λ)

	dB (137 MHz)	S_4 (400 MHz)
Kp = .5	.55	.014
Kp = 2.5	.75	.0155
Kp = 5.0	1.23	.022

The model dB values (converted to S_4) are shown as individual points in Fig. II.5.1 to facilitate comparison with Evans' data. The results of Evans' data and the model dB values predicted are in good agreement for both Narssarssuaq and Sagamore Hill. At Goose Bay, the model values are much lower for the low magnetic activity case, somewhat lower for the case Kp = 2.5 and higher for the case Kp = 5.0.

It is believed that the position of the trough is approximately the invariant latitude of Goose Bay under quiet magnetic conditions, moving farther south as the level of magnetic activity increases. The model data of Goose Bay reflects this picture. Neither the Millstone Hill data nor the model dB values have taken into consideration the viewing geometry.

II.6 Geometrical Considerations at High Latitudes

It has been noted that scintillations maximize both at low angles of elevation and when the signal propagation path is parallel to the lines of force of the earth's field. In order to fully examine the problem of geometry, a model would need to be developed in which the irregularity shape and elongation varied as a function of latitude, time and geomagnetic conditions.

Mikkelsen et al. (1978) has attempted to determine the theoretical scintillation index, S_4, when the irregularities are described by a power-law power spectrum. This utilizes the coordinates of the radio ray in the local coordinate system with set values for the elongation of the irregularities along and perpendicular to the magnetic field lines.

Mikkelsen assumed the approximate dividing line between weak and strong scintillation is ∿9 dB, with SI < 9 dB denoting the weak case. For this case, the geometric variation of S_4 is given by:

$$S_4 \propto \sqrt{z/\cos i \; f(\psi,\phi)}$$

where i = ionospheric zenith angle = angle between radio ray and irregularity layer

ψ = propagation angle = angle between the radio ray and the magnetic field direction,

ϕ = azimuth of the radio ray in local coordinate system of z-axis along magnetic east-west direction and y-axis in magnetic east-west direction

$$f(\psi,\phi) = \alpha\gamma(\gamma^2\cos^2\phi+\sin^2\phi+\cos^2\psi(\cos^2\phi+\gamma^2\sin^2\phi)$$

$$+(\sin^2\psi)/[\gamma^2\cos^2\psi+\alpha^2\sin^2\psi \times (\gamma^2\cos^2\phi+\sin^2\phi)]^{\frac{1}{2}}$$

z = reduced slant range to irregularity layer = $z_1(z_2-z_1)/z_2$ where z_1 = slant range to irregularity layer, z_2 = slant range to satellite

α = elongation of the irregularities along the magnetic field lines

γ = elongation of the irregularities in the magnetic east-west direction

Using his irregularity formulation he found the Narssarssuaq observations of the orbiting satellite, Nimbus-4,

at an altitude of 100 km a best fit of irregularity configuration with 2.5:1.3:1 where the first term is α, elongation of the irregularity along the lines of force of the magnetic field, the second is γ, orthogonal to the elongation along the lines of force, being in the magnetic east-west dimension, and the last term is orthogonal to the other two planes. At high latitudes this last term would lie in the north-south meridian.

Martin and Aarons (1977) interpreted synchronous satellite data in the Narssarssuaq-Goose Bay area using different irregularity equations (Gaussian). They found the dominating irregularities to be elongated along the magnetic field with a 5:2:1 configuration. Theoretically the irregularity model in the N-S meridian is of the order of the Fresnel dimension at 137 MHz and in such cases there is little difference between Gaussian and power-law spectrum for scintillation indices (Rufenach, 1975).

In order to present a simplified solution to this problem, a correction factor for the three high latitude stations under the assumption of the elliptical column model of individual irregularities of 5 km along the lines of force of the earth's magnetic field, 2 km orthogonal to the lines of force (E-W) and of 1 km in the north-south meridian has been calculated. In the publication Aarons et al. (1976) we have illustrated geometrical corrections needed from the three high latitude sites. It was determined that the correction for the S_4 value

derived from each index would be a factor ∿2.0 greater at the azimuth and elevation of the ATS-3 satellite from Narssarssuaq than at zenith. From Goose Bay the correction factor using the same model would be ∿1.3 and from Sagamore Hill it would be ∿1.4 assuming a Gaussian irregularity spectrum.

Turning aside from the general aspects of scintillation, certain periods, especially magnetic storm periods, were studied in detail to examine the extreme scintillation effects. Two examples of this analysis are the Aug. 4-10, 1972 and Oct. 18-19, 1972 storm periods.

For the Aug. 1972 period, orbiting satellite data which was available in addition to the synchronous satellite data, provided a more complete picture of the irregularity development. On August 4, 1972, SSC occurred at 0119 UT. Both the Narssarssuaq and Great Whale River magnetograms show intense activity beginning before 02 UT and peaking between 04 and 06 UT on this day. Nimbus 4 data, that of a low altitude orbiting satellite, was recorded at both Sagamore Hill, Massachusetts and Narssarssuaq, Greenland on this day. Fig. II.6.1 (pass #11398) shows the region of high scintillation (and irregularity development) extending to ∿55°Λ in the 35-45°W longitudinal sector. Further eastward, ∿60°W longitude, the equatorward development of this region is only ∿63°Λ. This is in good agreement with the scintillation data shown in Fig. II.6.2 where the most easterly intersection point (Narssarssuaq at 51°W longitude) shows high scintillation

activity, Goose Bay at 61°W longitude is on the verge of the irregularity region and Sagamore Hill still shows no activity. Passes #11399 and 11400 occurring in the time interval 05-06 UT August 4 show (Fig. II.6.3) this latitudinal and longitudinal development more than the ATS-3 data does since the latter is near saturation for all three stations. The Sagamore Hill data correlates well with the Sagamore Hill pass at ∿05 UT which shows high SI to ∿55°Λ, then falling off in a longitude sector of approximately 90°W longitude. The region seems to be drifting westward as the sector of 120°W longitude shows high SI down to 46°Λ. The time period after 06 UT notes a gradual decrease in magnetic activity. No passes are available at this time to follow the irregularity region movement.

Another aspect of this August storm period is the identification of the storm time component of scintillation.

During this period, an intensive study was begun of the magnetic storms of August 1972. The Nimbus and Transit data available for the initial part of the storm on August 4 were plotted in an effort to provide a picture of the developing irregularity region. Universal time contour plots including Narssarssuaq, Goose Bay, and Sagamore Hill were also generated.

This August data was also used in work done to identify the storm time component of scintillation (Basu, 1974; Aarons et al., 1976).

For large magnetic storms when the plasmapause moves well equatorward of its usual quiettime location, a stormtime

component of scintillations is recognizable at many midlatitude stations with invariant latitudes < 60°. Figs. II.6.4 and II.6.5 show the Dst index and scintillations observed at stations of varying invariant latitudes. The Dst index reached peak values > 100 γ on August 4-6 and August 9. The high latitude stations exhibit high SI values during these periods but the stormtime component is more noticeable at the lower latitude stations of Sagamore Hill, Aberystwyth, and Lindau. Even though these stations are separated 6 hours in local time, all show scintillation peaks ∿0400 UT on August 4, 0000 UT on August 5, and 0500 UT on August 6. These occur at times of Dst index increases and large TEC depletions at Sagamore Hill (Mendillo and Klobuchar, 1974). On August 9 ∿1200 UT, a similar peak occurs at these stations even though the local time of the stations is in the morning - noon sector.

This stormtime analysis, in connection with the intensive study using transiting and synchronous satellites, is helpful in a correlation of the position of the plasmapause with ground-based scintillation.

The second magnetic storm analysis was performed on the Oct. 18-19, 1972 data.

On October 18, 1972 at 1746 UT, a magnetic storm commenced. The magnetic index, K_p, very low prior to the storm reached K_p=3 at SSC, peaked at K_p=5 ∿0000 UT October 19, then fell to K_p=3 again ∿1500 UT October 19.

Fig. II.6.6 is a plot of the 15 min. scintillation index

as observed at Narssarssuaq, Goose Bay, Sagamore Hill and College. Narssarssuaq and Goose Bay exhibit a slightly delayed storm rise at 2030 and 2200 UT October 18, respectively. College scintillation responds with medium activity at ∿0830 UT October 19, while Sagamore Hill shows only a sharp burst of scintillation at ∿2330 UT October 18.

In Fig. II.6.7 is seen the Narssarssuaq and Ottawa magnetograms, and the Dst. Both magnetograms show moderate disturbance levels, peaking in the period 0000-1200 UT October 19. The Dst reaches a maximum value of -75 γ at 0900 October 19. This, combined with a moderate K index, points to the irregularity region developing slowly from a quiet day picture to a moderately expanded version and then fading again. Thus, the College data does not show moderate scintillation activity until the irregularity region becomes developed enough to reach the latitude of its intersection point. Also, College SI seems to show a seasonal response pattern, with the equinox response to magnetic storms differing from the dramatic disturbance pattern seen in winter.

The total electron content plots of Narssarssuaq, Goose Bay, and Sagamore Hill of October 18-19 (Fig. II.6.8) reveal only slightly enhanced values at SSC on October 18. Nighttime TEC values show the increased TEC occurring during many nights with magnetic activity. In addition to somewhat higher values, spiky areas of activity are seen in the polarization records.

There is no clear indication in these records of a trough (DMSP pictures are not available for this period). The scintillation boundary, except for a brief period between 2330 UT October 18 and 0030 UT October 19, in the nighttime along the 75th meridian lies between Goose Bay and Sagamore Hill. This short period is seen in the contour map (Fig. II.6.9) just prior to 2400 October 19. At the same time, the 50% scintillation contour reaches a minimum of $\sim 56°\Lambda$ at ~0400 UT October 19. Perhaps the trough lies between the latitudes of Goose Bay and Sagamore Hill, but the synchronous satellite records cannot be used to determine the trough position in this case. The increase in scintillation index at Sagamore Hill at 2330 on October 18 is accompanied by an increase in TEC on the Sagamore Hill TEC records.

REFERENCES

Aarons, J., Sunanda Basu and E. Martin, The stormtime component of scintillations, in "The Geophysical Use of Satellite Beacon Observations", edited by M. Mendillo, Boston University, June 1976.

Aarons, J., J. Mullen, H. Whitney, E. Martin, K. Bhavnani, and L. Whelan, A high-latitude empirical model of scintillation excursions: Phase 1, AFGL-TR-76-0210, Sept. 17, 1976.

Basu, Sunanda, VHF ionospheric scintillations at L=2.8 and formation of stable auroral red arcs by magnetospheric heat conduction, J. Geophys. Res., 79, 3155, 1974.

Evans, J.V., The Millstone Hill Radar Propagation Study: Scientific Results, Lincoln Lab. Technical Report. ed., 1973.

Martin, E., and J. Aarons, F-layer scintillation and the aurora, J. Geophys. Res., 82, 2717-2722, 1977.

Mendillo, M. and J. Klobuchar, An atlas of the midlatitude F-region response to geomagnetic storms, AFCRL-TR-0065, 1974.

Mikkelsen, I.B., J. Aarons, and E. Martin, Geometrical considerations of 136 MHz amplitude scintillation in the auroral oval, J. Atmos. Terr. Phys., 40, 479-483, 1978.

Rufenach, C.L., Ionospheric scintillation by a random phase screen: spectral approach, Radio Sci., 10, 155, 1975.

Whitney, H.E., C. Malik, and J. Aarons, A proposed index for measuring ionospheric scintillation, Planet. Space Sci., 17, 1069-1073, 1969.

LIST OF FIGURES

Fig. II.2.1 Observational data and best-fitting model for Huancayo A3 for February.

Fig. II.2.2 Observational data and best-fitting model for Ghana A3 for February.

Fig. II.2.3 Observational data and best-fitting model for Huancayo L6 for February.

Fig. II.3.1 Observational data and best-fitting model for Narssarssuaq A3 for March.

Fig. II.3.2 Observational data and best-fitting model for Goose Bay A3 for March.

Fig. II.3.3 Observational data and best-fitting model for Sagamore Hill A3 for March.

Fig. II.4.1 Plots of mathematical model based on Narssarssuaq and Goose Bay (two-station model) for March.

Fig. II.5.1 Mean scintillation index for different levels of magnetic activity for both the model data and Evan's Millstone Hill observations.

Fig. II.6.1 Nimbus pass observed from both Narssarssuaq and Sagamore Hill on Aug. 4, 1972 showing the region of irregularity development.

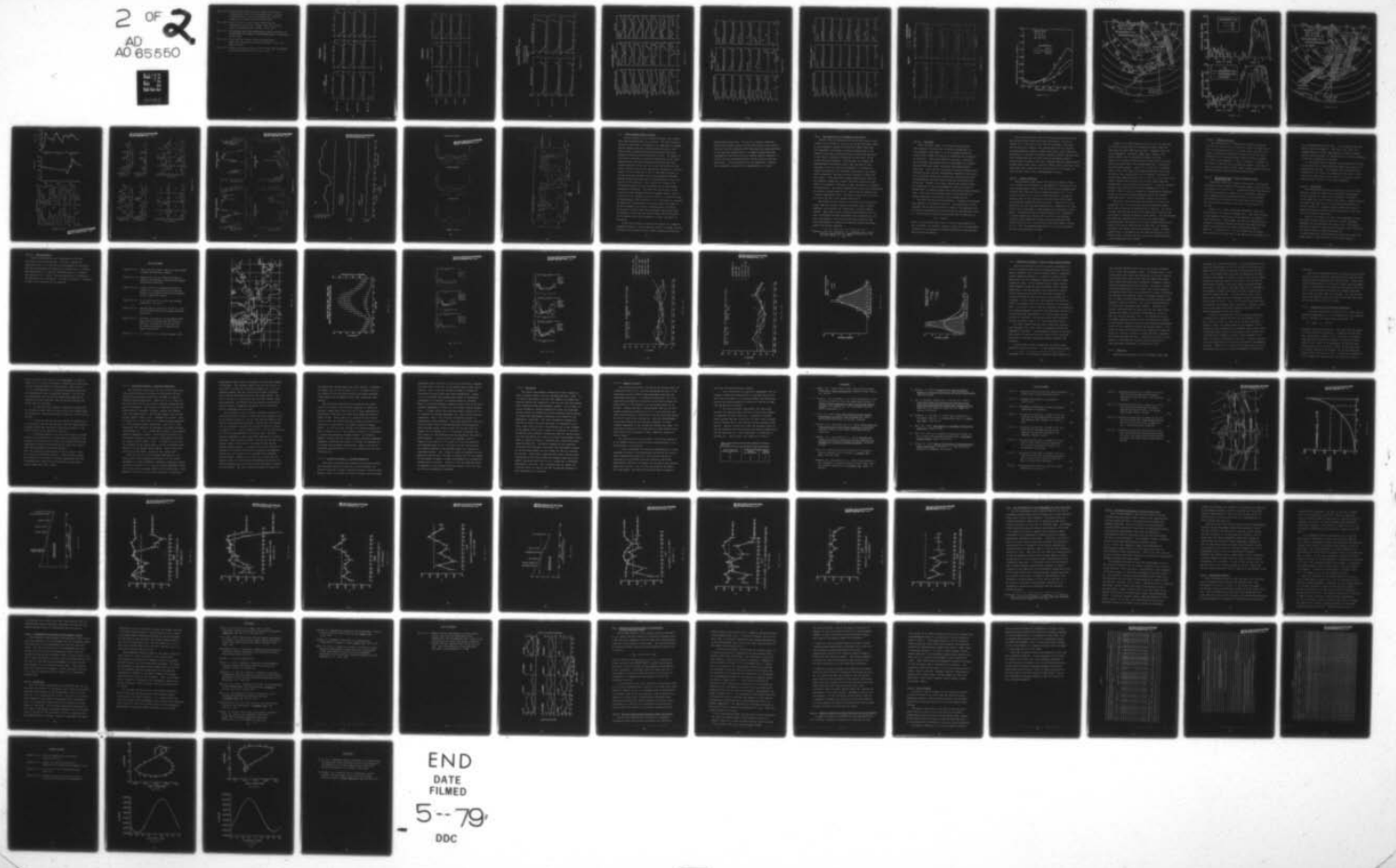
Fig. II.6.2 Scintillation observation from Narssarssuaq, Goose Bay and Sagamore Hill showing high scintillation index during magnetic activity on August 4, 1972.

Fig. II.6.3 A later Nimbus pass on Aug. 4, 1972 observed from Narssarssuaq and Sagamore Hill showing the extension of the irregularity region from that of Fig. 9.

Fig. II.6.4 Dst index and scintillation observations of Narssarssuaq, Goose Bay, and Sagamore Hill for the August 1972 magnetic storm period showing high scintillation values during periods of high Dst.

AD-A065 550 EMMANUEL COLL BOSTON MASS F/G 4/1
STUDY AND ANALYSIS OF EQUATORIAL IRREGULARITIES, TOTAL ELECTRON--ETC(U)
OCT 78 S BASU, S BASU, J JOHANSON F19628-76-C-0003
UNCLASSIFIED AFGL-TR-78-0263 NL

2 OF 2
AD
AD A065550



END
DATE FILMED
5-79
DDC

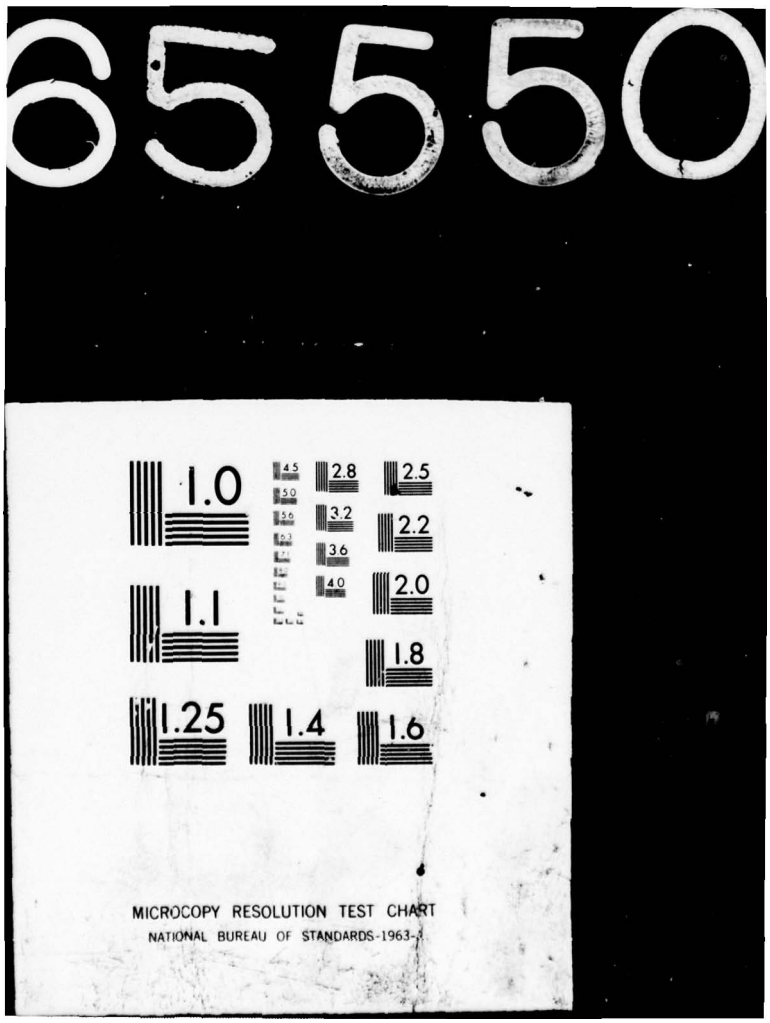

65550
1.0
1.1
1.25
1.4
1.6
1.8
2.0
2.2
2.5
2.8
3.2
3.6
4.0
4.5
5.0
5.6
6.3
MICROCOPY RESOLUTION TEST CHART
NATIONAL BUREAU OF STANDARDS-1963-A

Fig. II.6.5 Scintillation observations for August 1972 magnetic storm period as seen at Narssarssuaq LES-6, and I2F2 at Wales, Athens, and Lindau showing the stormtime component of scintillation (UT-associated).

Fig. II.6.6 Plot of 15 min. scintillation observations of Narssarssuaq, Goose Bay, Sagamore Hill, and College during the magnetic storm of Oct. 18-19, 1972.

Fig. II.6.7 Narssarssuaq and Ottawa magnetograms show correlation of fluctuations with magnetic storm commencement as monitored by D_{st} index.

Fig. II.6.8 Total electron content plots of Narssarssuaq, Goose Bay, and Hamilton during the October 18-19, 1972 magnetic storm.

Fig. II.6.9 Contour map showing variation of SI with time at different invariant latitudes for Oct. 18-19, 1972.

FEBRUARY

HUANCAYO ATS-3

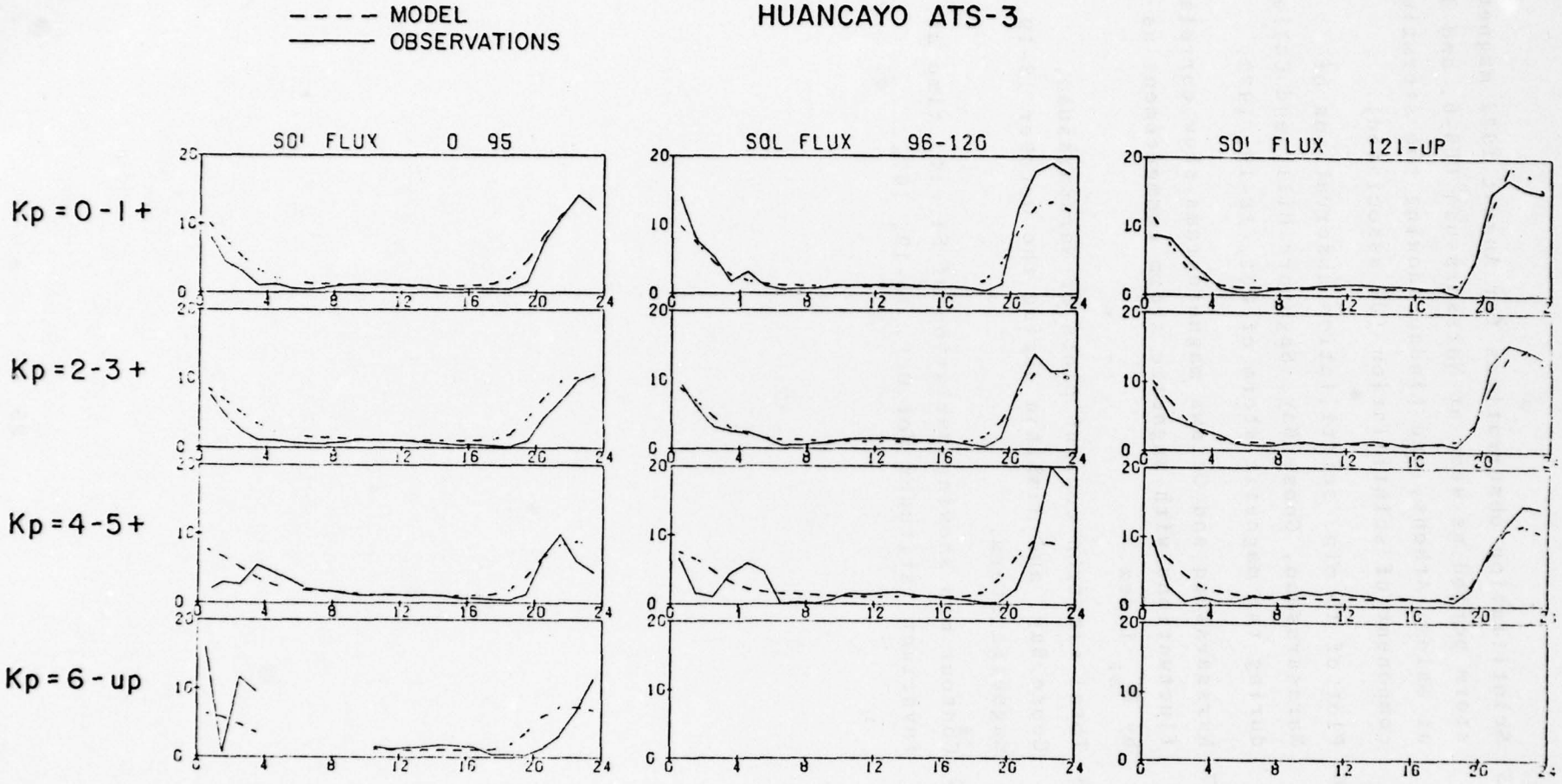


Figure II.2.1

FEBRUARY

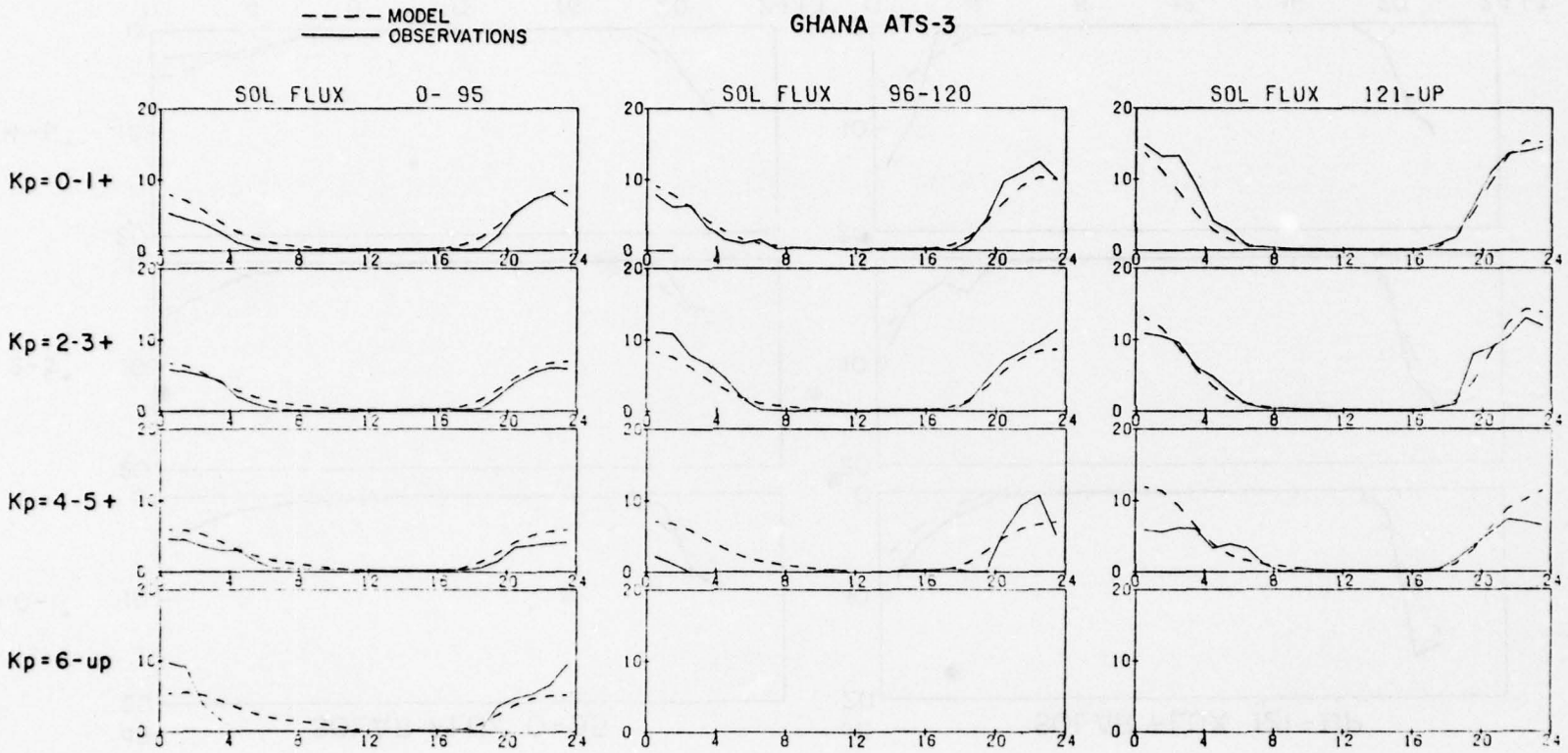


Figure II.2.2

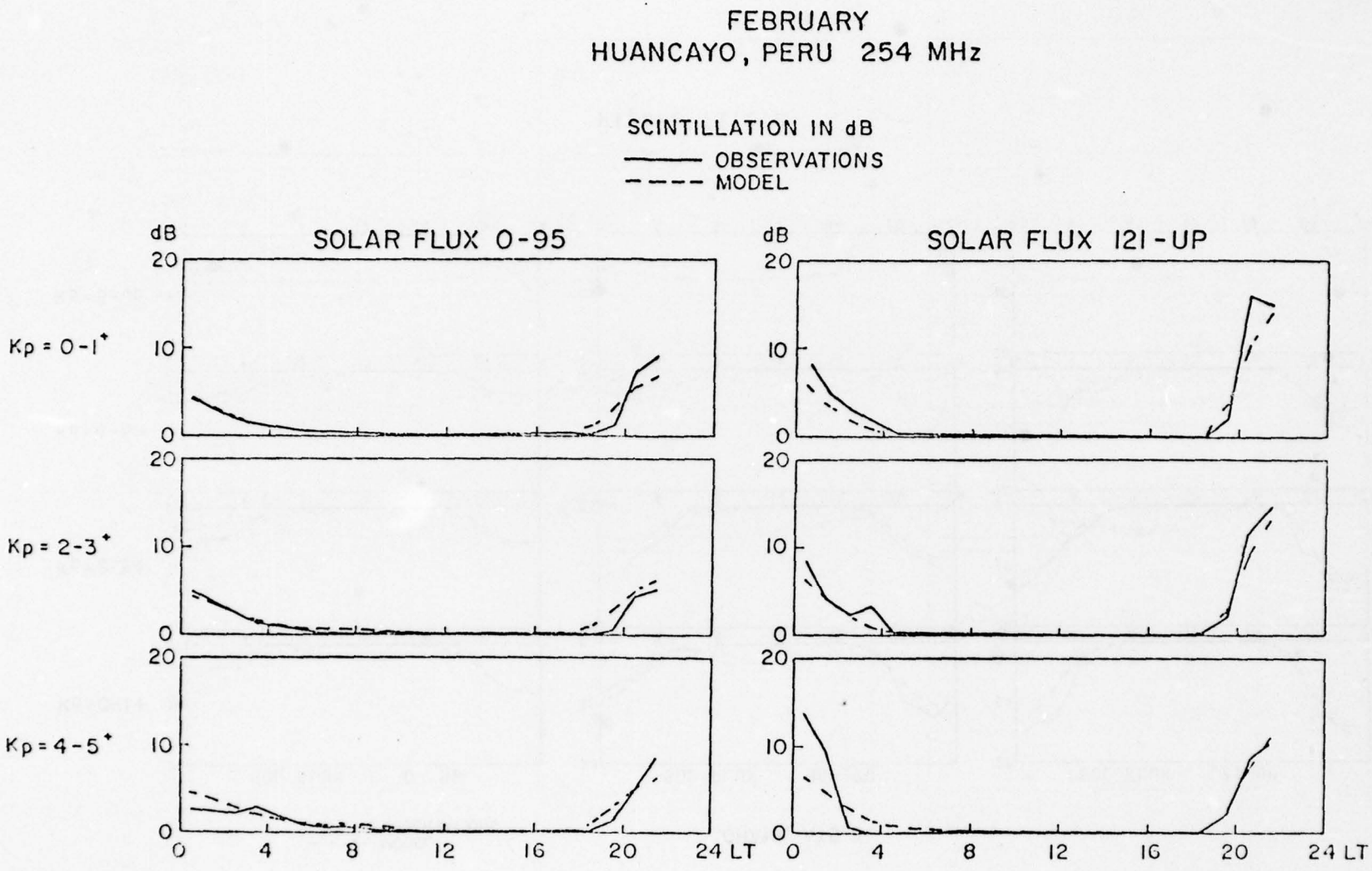

FEBRUARY
HUANCAYO, PERU 254 MHz
SCINTILLATION IN dB
OBSERVATIONS
MODEL
SOLAR FLUX 0-95
SOLAR FLUX 121-UP
dB
Kp = 0-1+
Kp = 2-3+
Kp = 4-5+
20
10
0
0 4 8 12 16 20 24 LT

Figure II.2.3

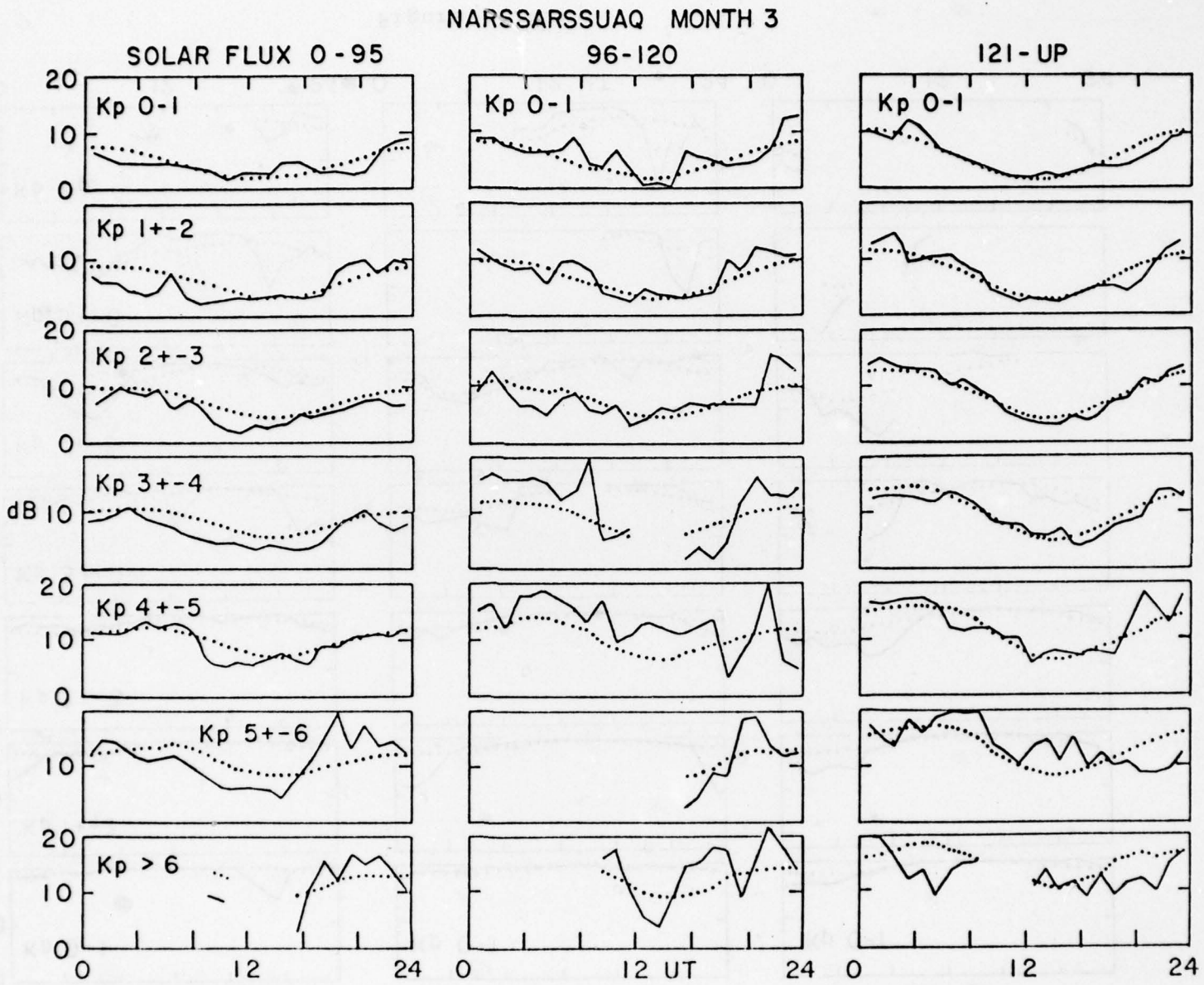

NARSSARSSUAQ MONTH 3
SOLAR FLUX 0-95
96-120
121-UP
Kp 0-1
Kp 1+-2
Kp 2+-3
Kp 3+-4
Kp 4+-5
Kp 5+-6
Kp > 6
dB
20
10
0
0
12
24
12 UT

Figure II.3.1

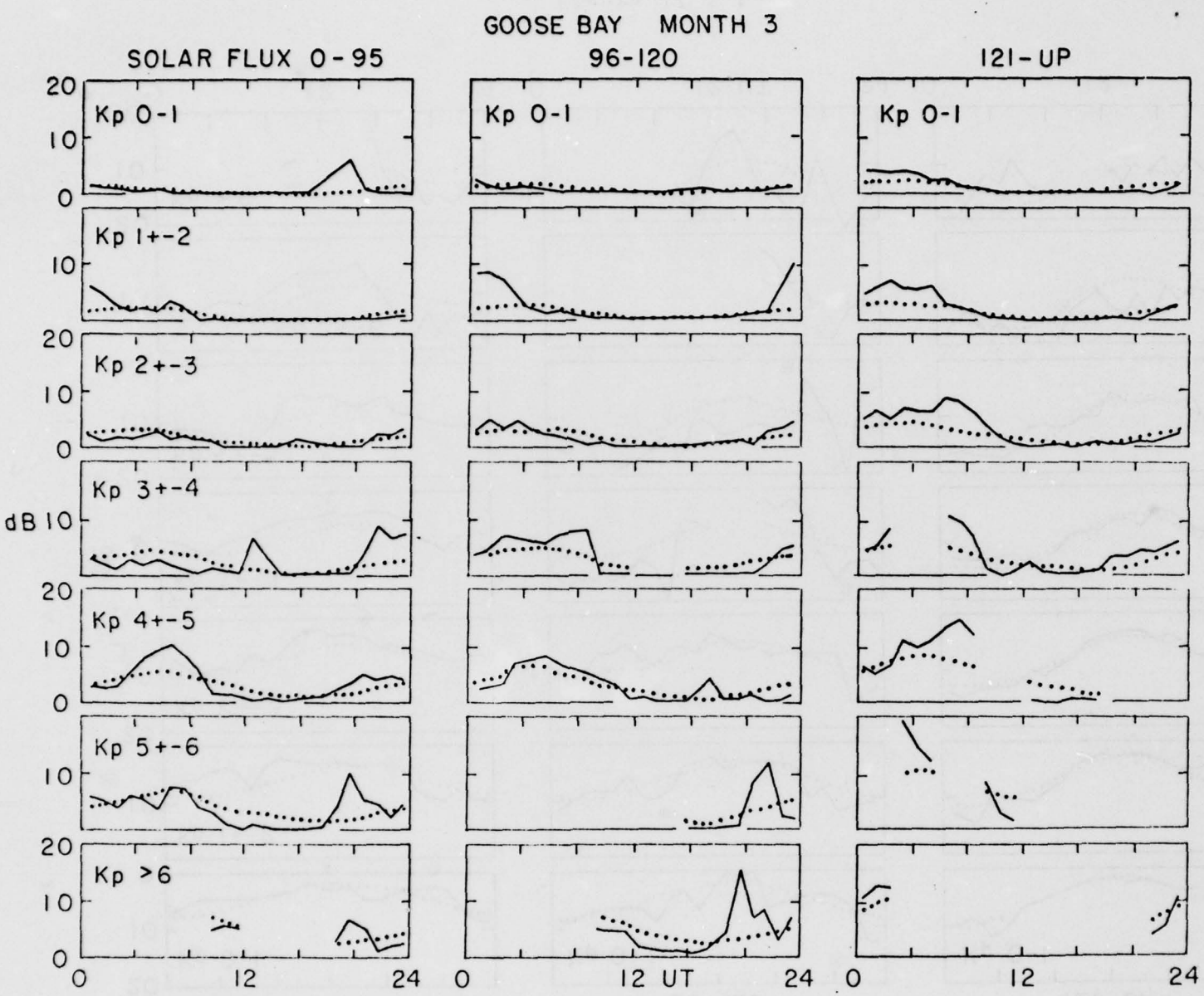

GOOSE BAY MONTH 3
SOLAR FLUX 0-95
96-120
121-UP
Kp 0-1
Kp 1+-2
Kp 2+-3
Kp 3+-4
Kp 4+-5
Kp 5+-6
Kp >6
dB
20
10
0
0
12
24
12 UT

Figure II.3.2

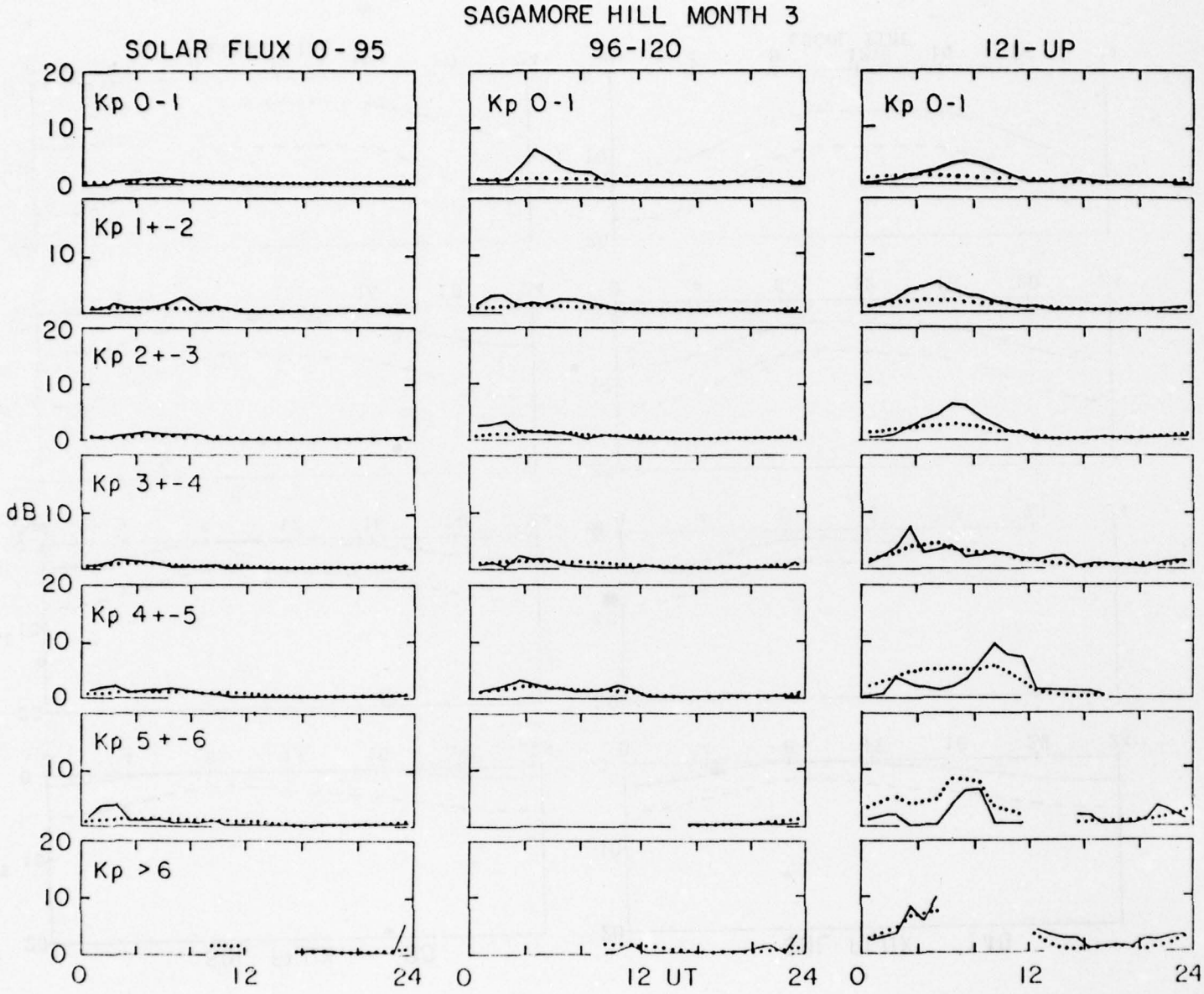

SAGAMORE HILL MONTH 3
SOLAR FLUX 0-95
96-120
121-UP
Kp 0-1
Kp 1+-2
Kp 2+-3
Kp 3+-4
Kp 4+-5
Kp 5+-6
Kp >6
dB
20
10
0
0
12
24
12 UT

Figure II.3.3

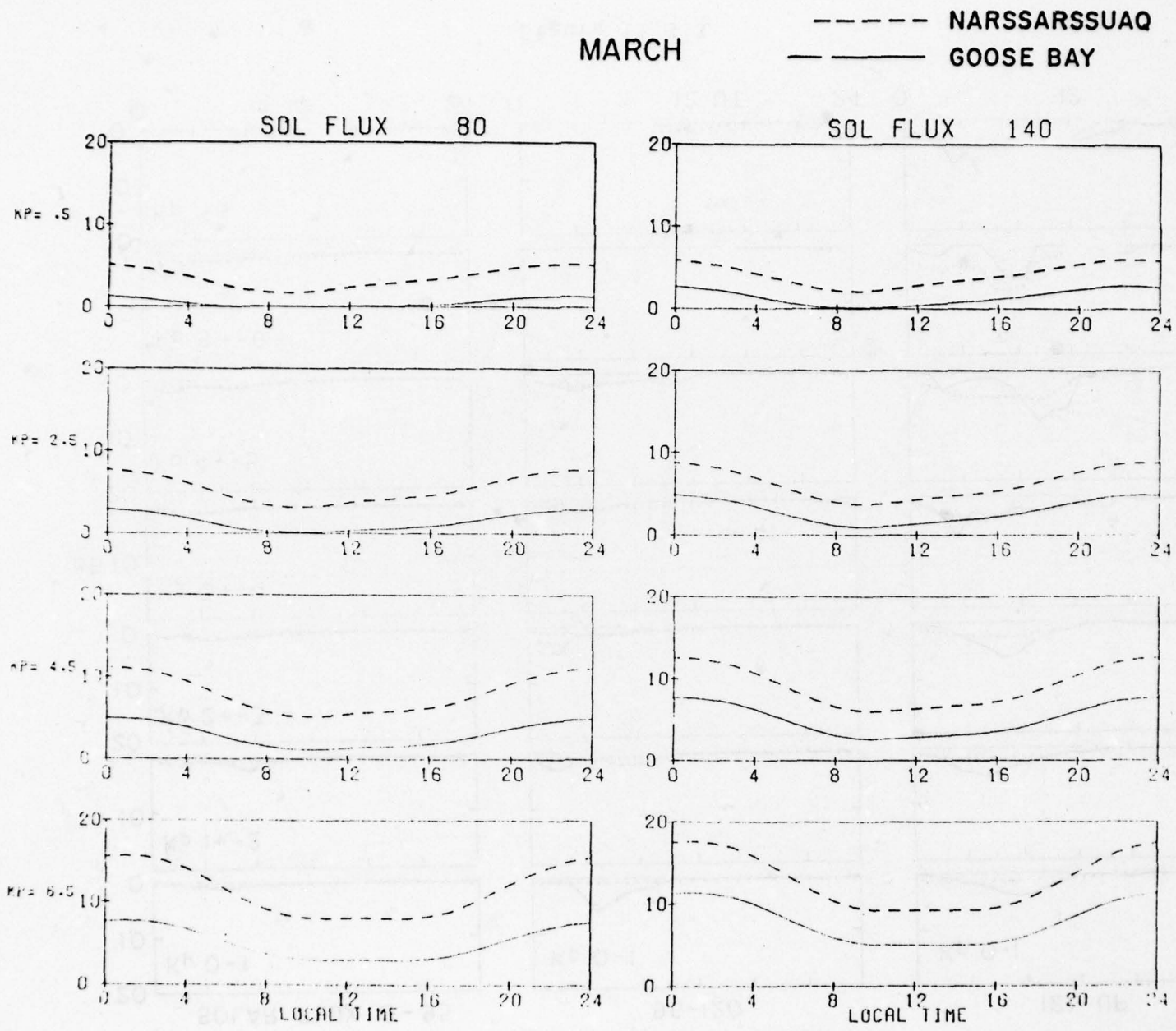

MARCH
NARSSARSSUAQ
GOOSE BAY
SOL FLUX 80
SOL FLUX 140
KP= .5
KP= 2.5
KP= 4.5
KP= 6.5
LOCAL TIME
LOCAL TIME

Figure II.4.1

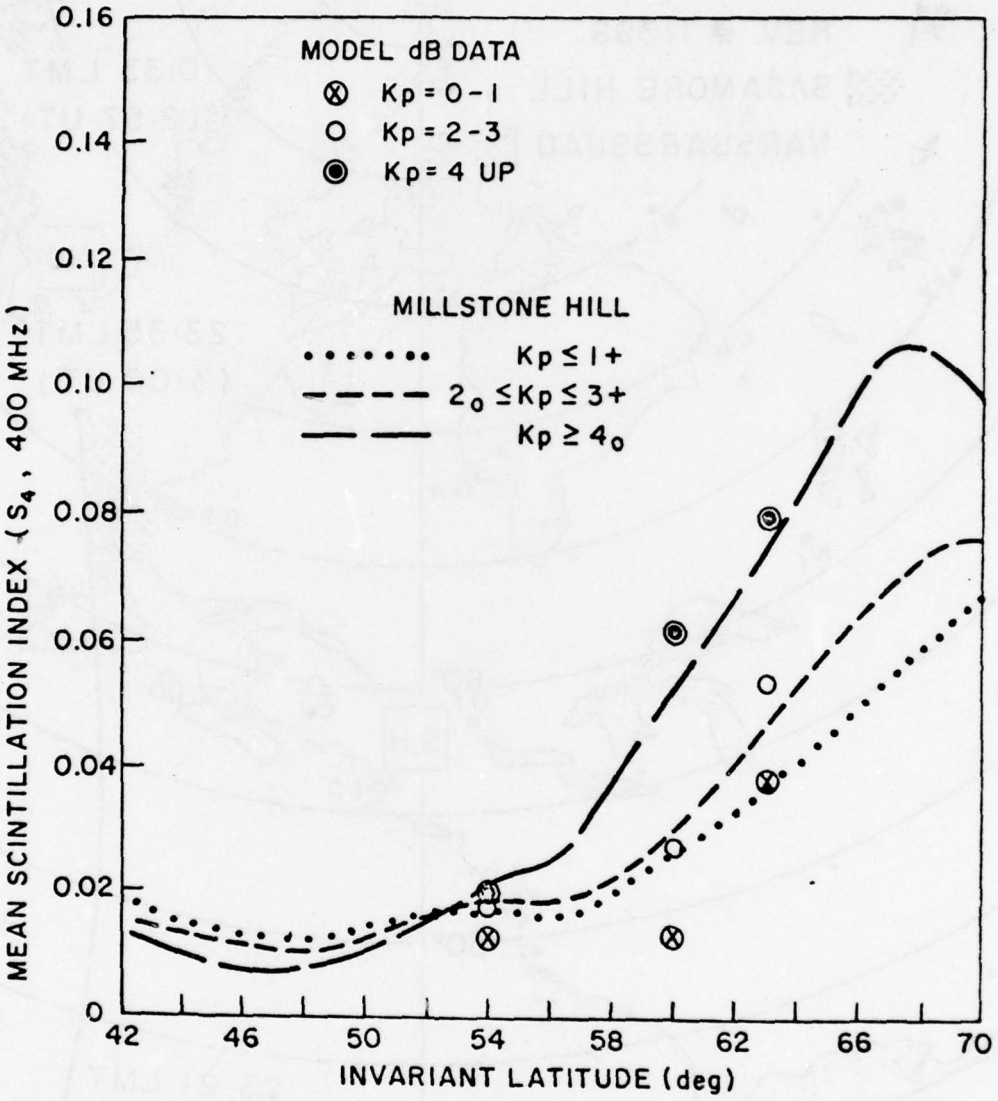

MODEL dB DATA
Kp = 0-1
Kp = 2-3
Kp = 4 UP
MILLSTONE HILL
Kp ≤ 1+
2₀ ≤ Kp ≤ 3+
Kp ≥ 4₀
MEAN SCINTILLATION INDEX (S4, 400 MHz)
0.16
0.14
0.12
0.10
0.08
0.06
0.04
0.02
0
42
46
50
54
58
62
66
70
INVARIANT LATITUDE (deg)

Figure II.5.1

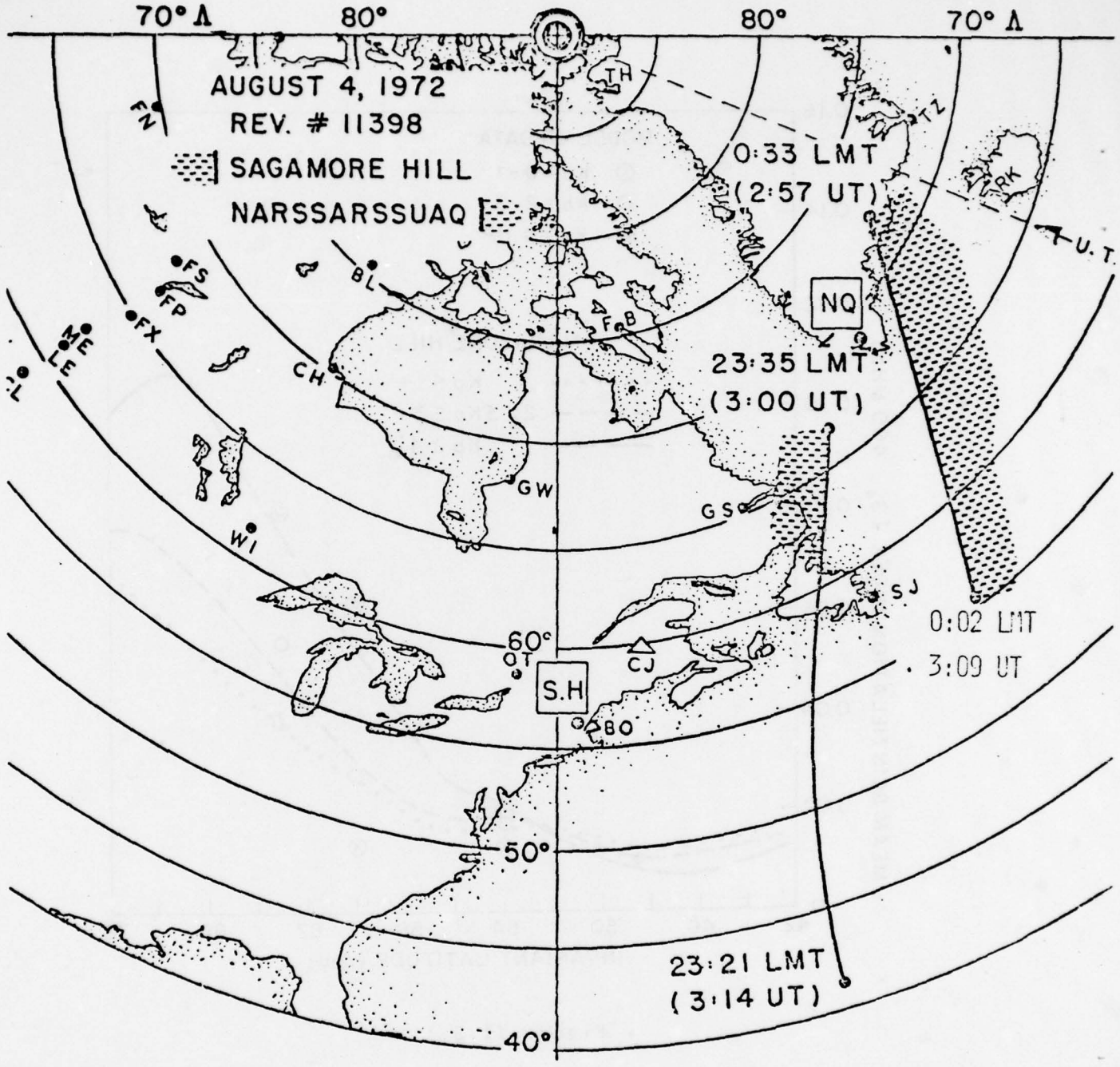

70° Λ
80°
80°
70° Λ
AUGUST 4, 1972
REV. # 11398
SAGAMORE HILL
NARSSARSSUAQ
0:33 LMT
(2:57 UT)
U.T.
23:35 LMT
(3:00 UT)
0:02 LMT
3:09 UT
23:21 LMT
(3:14 UT)
60°
50°
40°
TH
TZ
TRK
FN
FS
FP
FX
ME
LE
CH
BL
FB
NQ
GW
GS
WI
SJ
OT
S.H
CJ
BO

Figure II.6.1

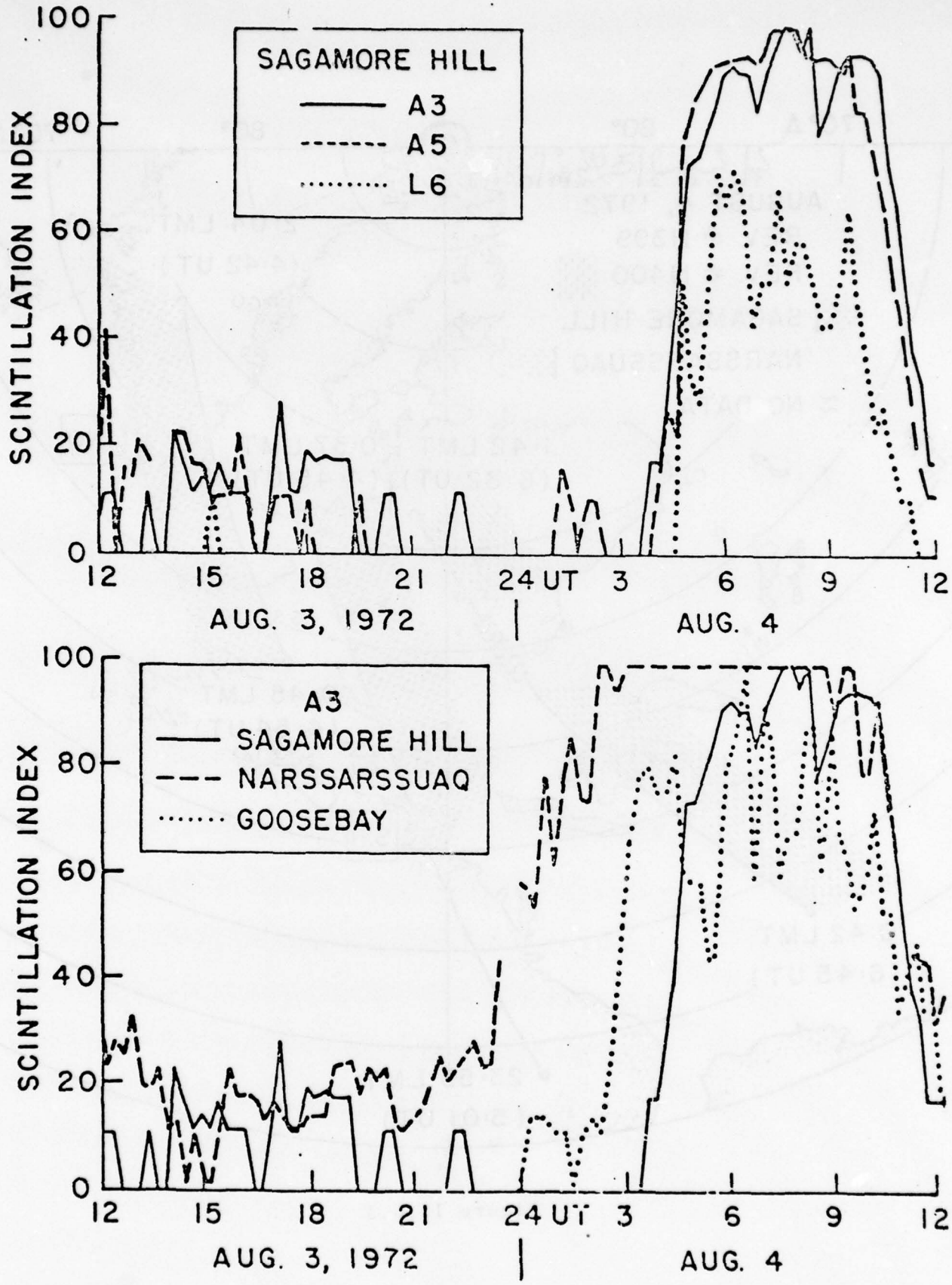

SAGAMORE HILL
A3
A5
L6
SCINTILLATION INDEX
100
80
60
40
20
0
12
15
18
21
24 UT
3
6
9
12
AUG. 3, 1972
AUG. 4
A3
SAGAMORE HILL
NARSSARSSUAQ
GOOSEBAY
SCINTILLATION INDEX
100
80
60
40
20
0
12
15
18
21
24 UT
3
6
9
12
AUG. 3, 1972
AUG. 4

Figure II.6.2

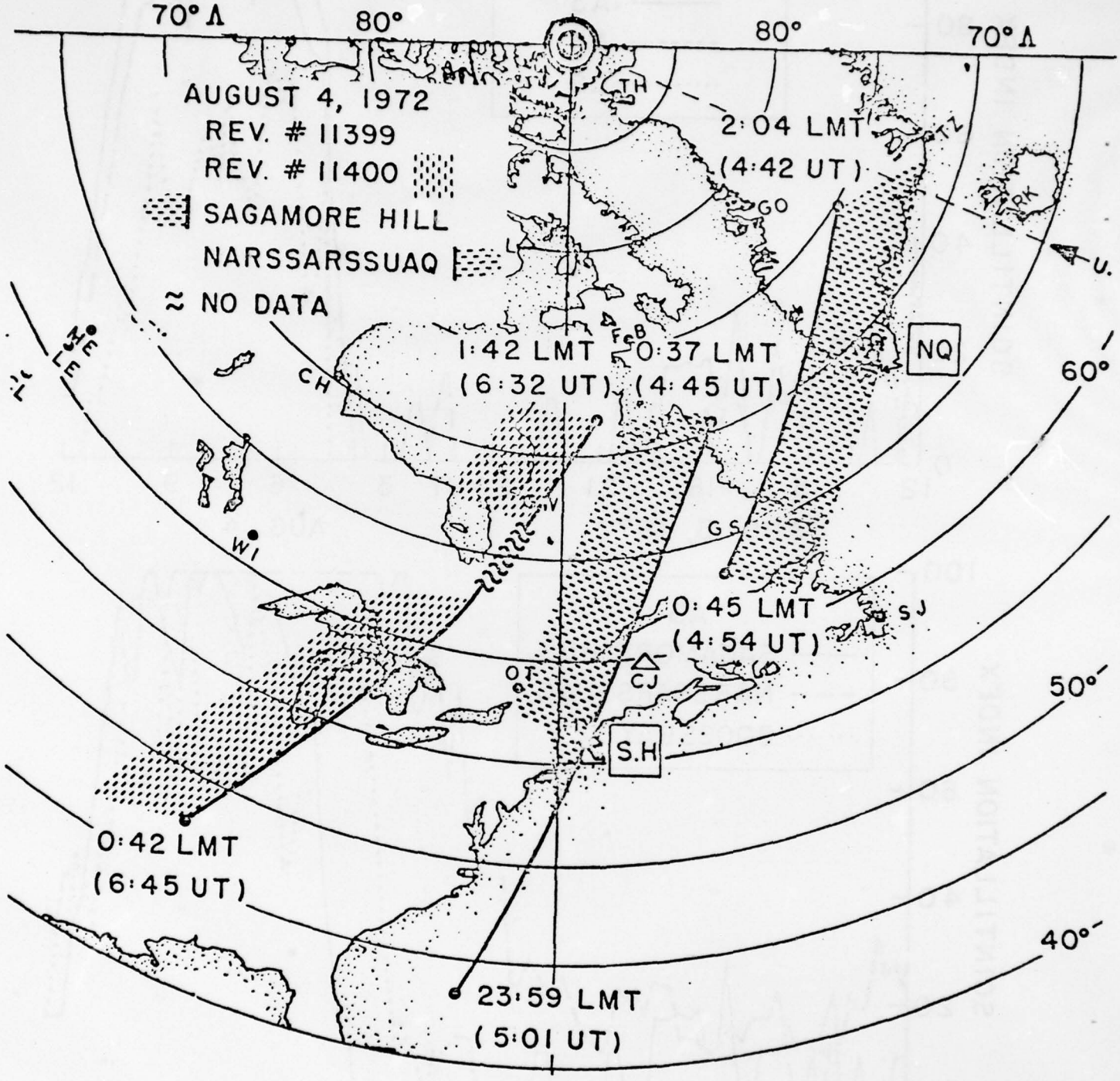

70° Λ
80°
80°
70° Λ
AUGUST 4, 1972
REV. # 11399
REV. # 11400
SAGAMORE HILL
NARSSARSSUAQ
≈ NO DATA
2:04 LMT
(4:42 UT)
1:42 LMT
(6:32 UT)
0:37 LMT
(4:45 UT)
0:45 LMT
(4:54 UT)
0:42 LMT
(6:45 UT)
23:59 LMT
(5:01 UT)
NQ
S.H
60°
50°
40°
TH
GO
FBK
U.
CH
GS
SJ
CJ
OT
WI
LE

Figure II.6.3

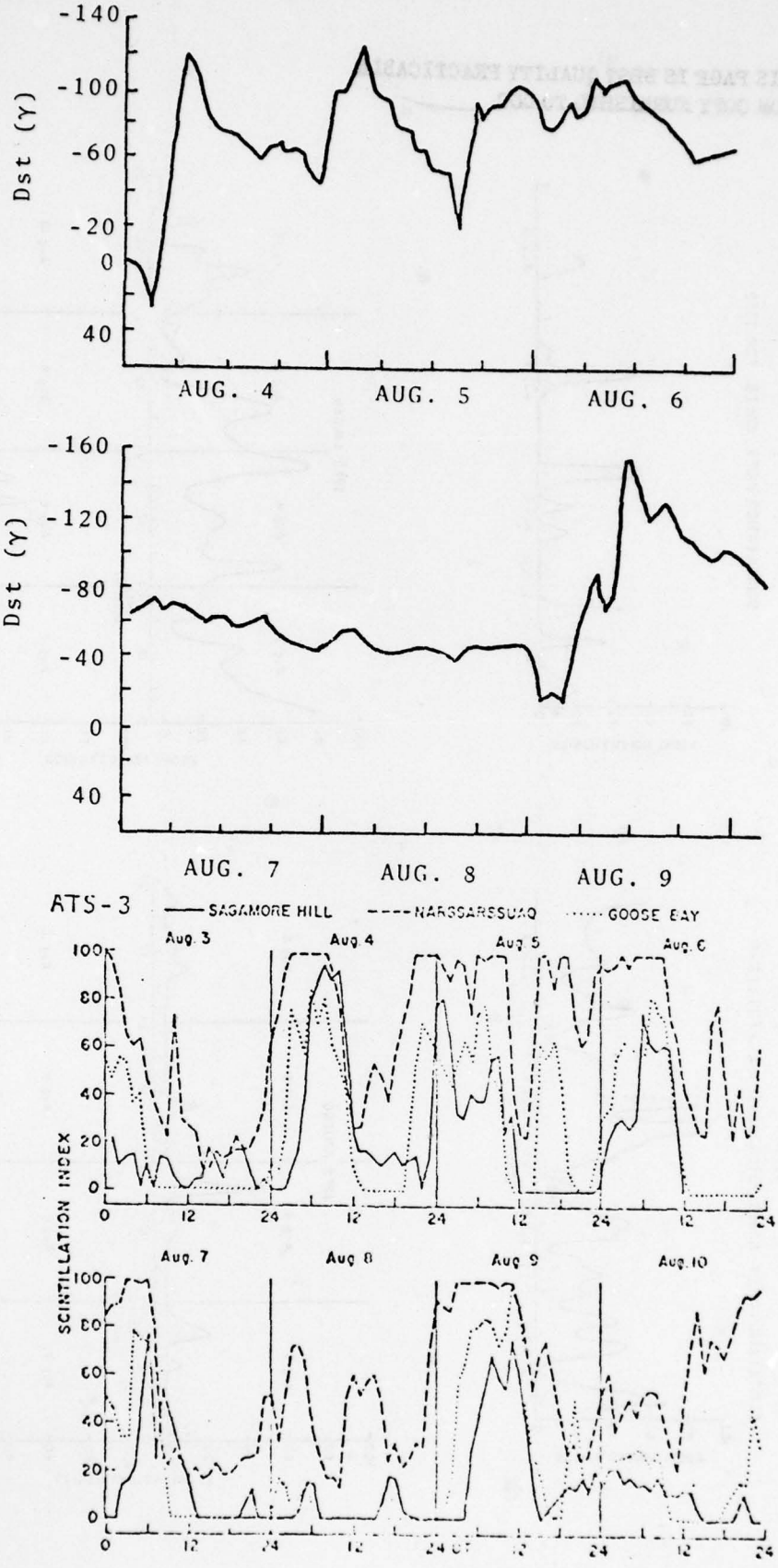


Figure II.6.4

THIS PAGE IS BEST QUALITY PRACTICABLE
FROM COPY FURNISHED TO DDC

THIS PAGE IS BEST QUALITY PRACTICABLE
FROM COPY FURNISHED TO DDC

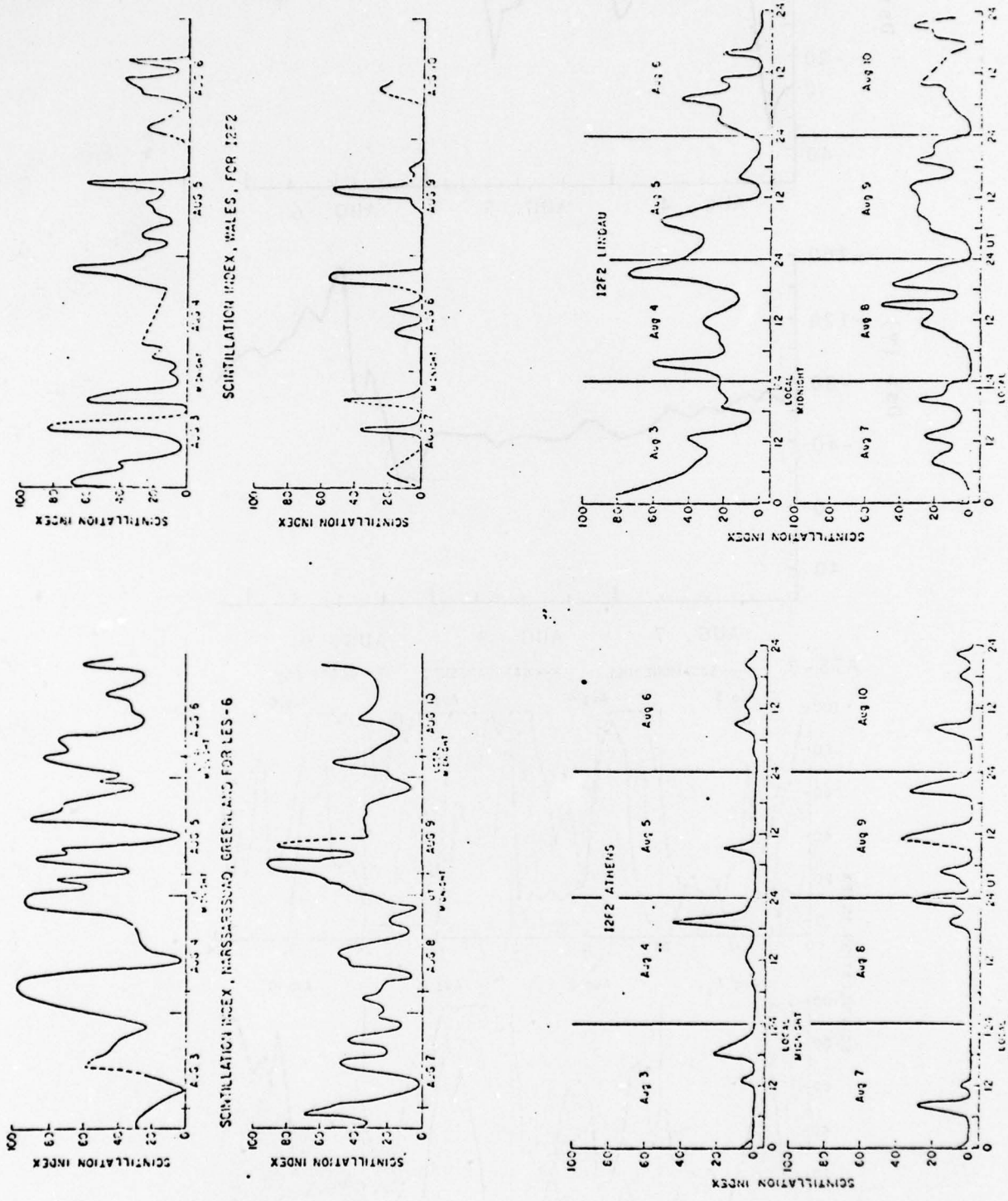


Figure II.6.5

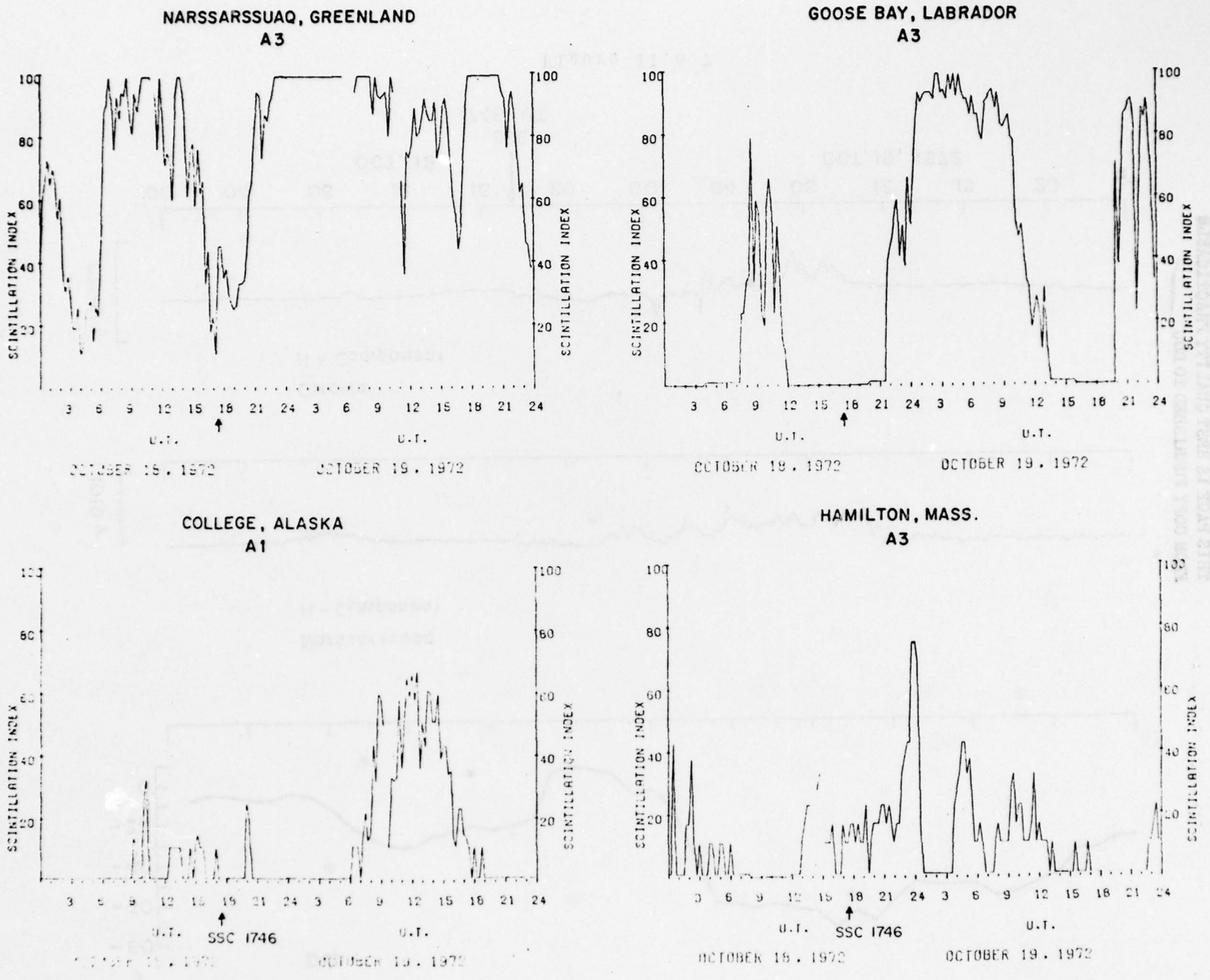


Figure II.6.6

THIS PAGE IS BEST QUALITY PRACTICABLE
FROM COPY FURNISHED TO DDC

THIS PAGE IS BEST QUALITY PRACTICABLE
FROM COPY FURNISHED TO DDC

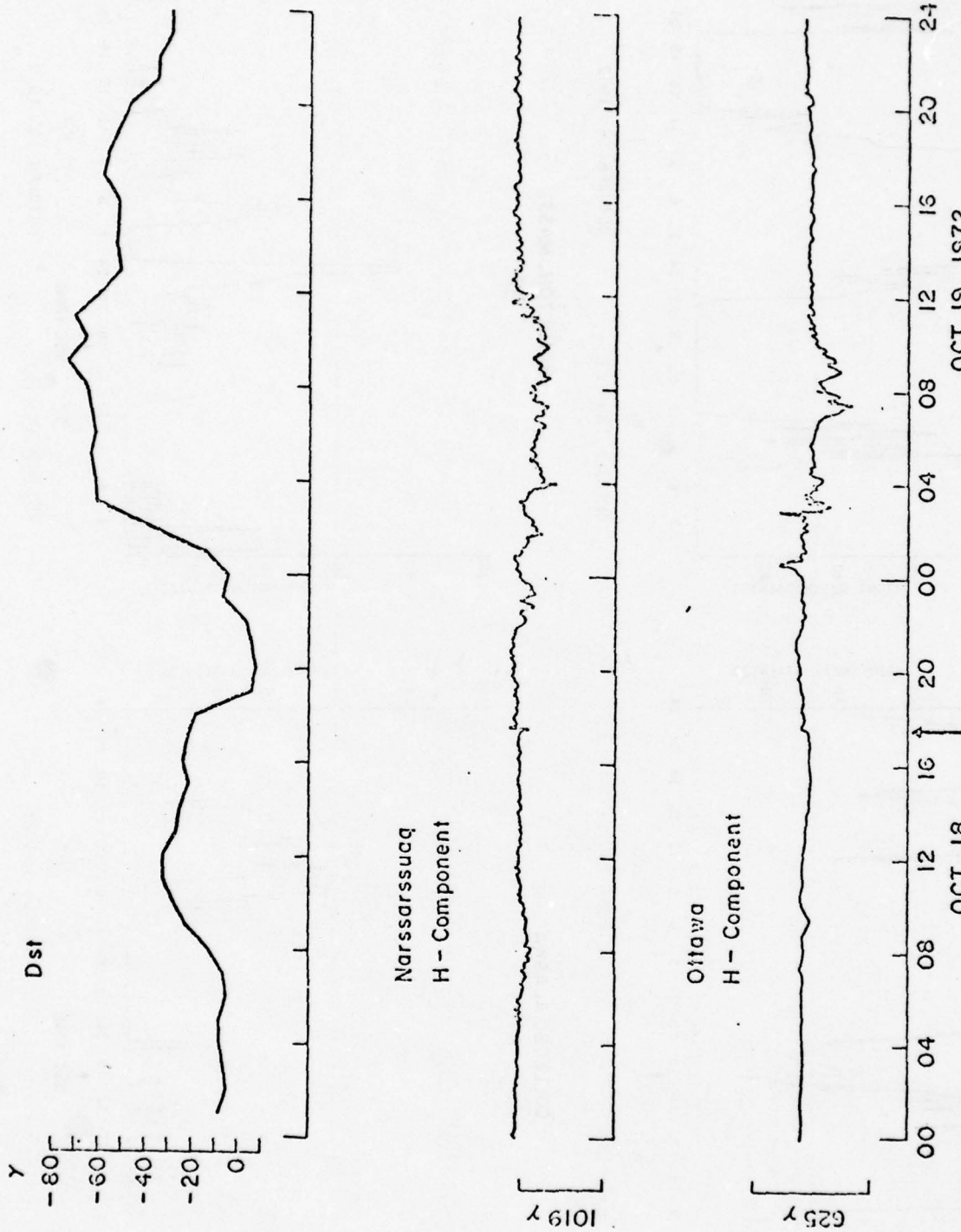
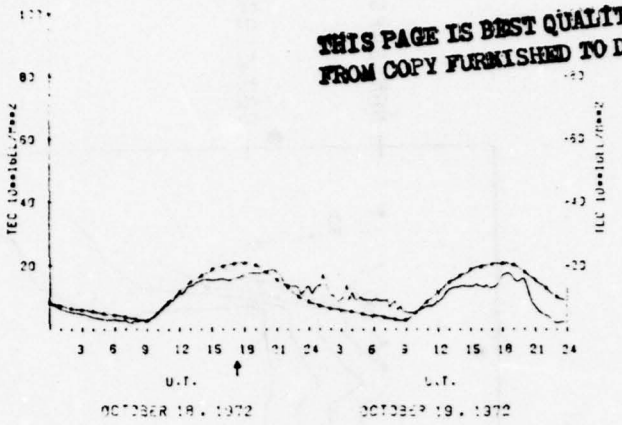


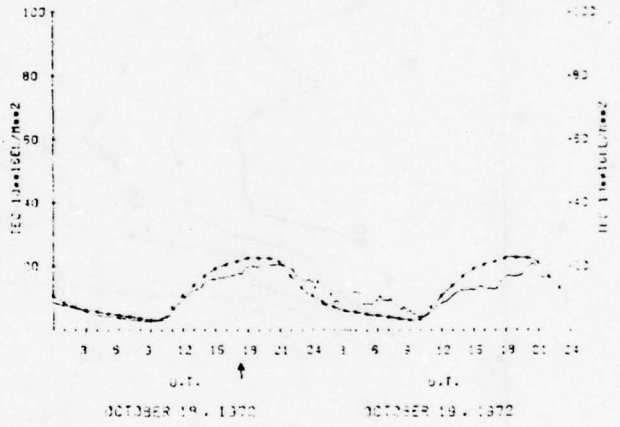
Figure II.6.7

NARSSARSSUAQ, GREENLAND

THIS PAGE IS BEST QUALITY PRACTICABLE
FROM COPY FURNISHED TO DDC



GOOSE BAY, LABRADOR



HAMILTON, MASS.

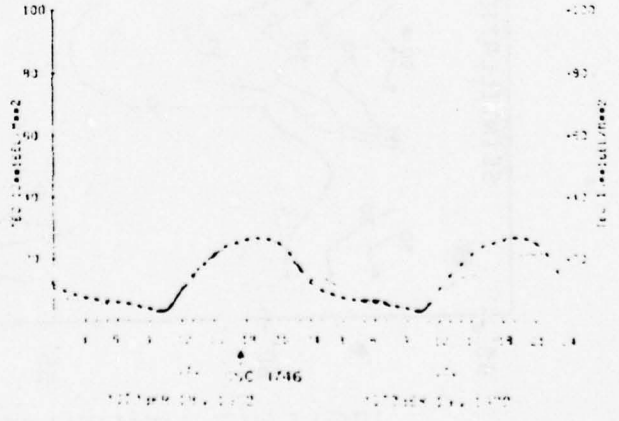


Figure II.6.8

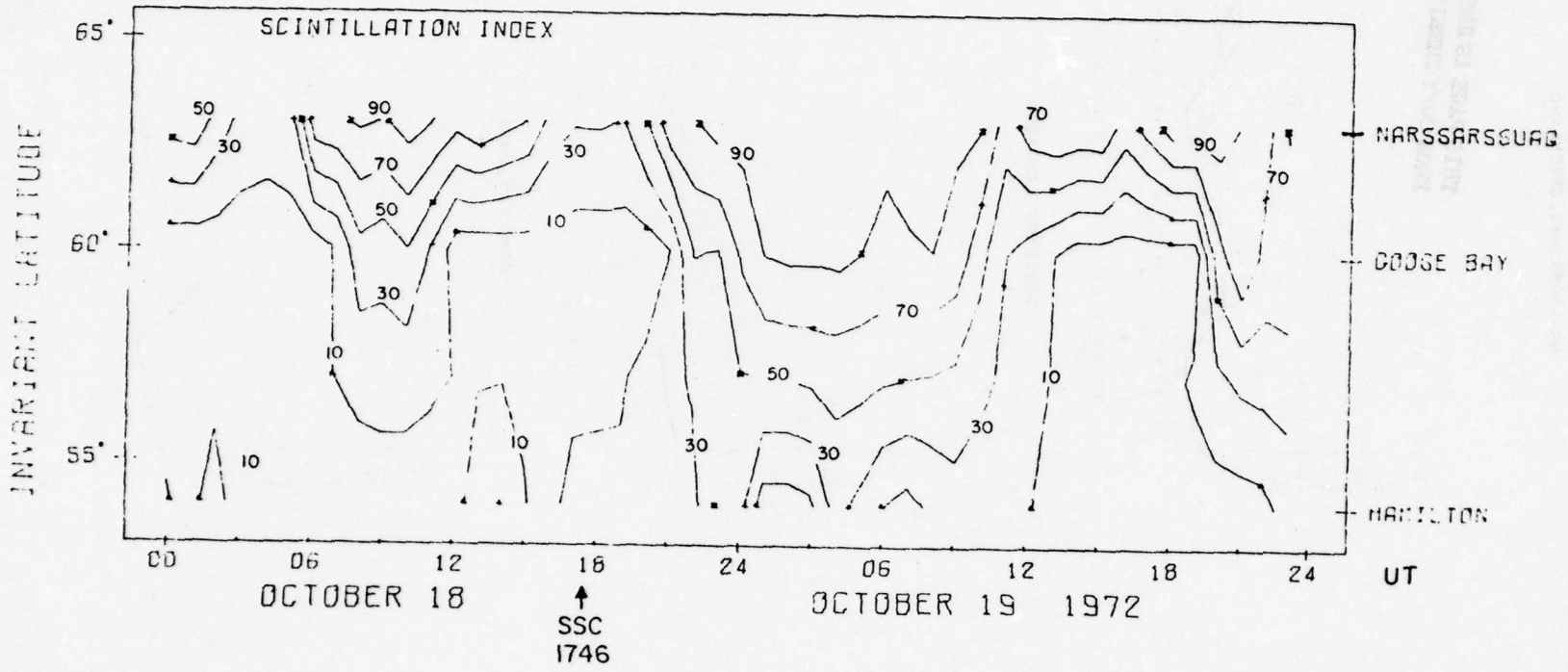

SCINTILLATION INDEX
INVARIANT LATITUDE
65°
60°
55°
NARSSARSSUAQ
GOOSE BAY
HAMILTON
00
06
12
18
24
06
12
18
24
UT
OCTOBER 18
SSC
1746
OCTOBER 19 1972

Figure II.6.9

III. TOTAL ELECTRON CONTENT STUDIES

Several aspects of Total Electron Content (TEC) studies have been performed under this contract. The Total Electron Content of the earth's ionosphere is of importance to ranging system engineers who are concerned about the excess time delay of the ionosphere through which advanced satellite ranging systems must pass from source to user. The amount of this excess time delay is directly proportional to the total number of free electrons encountered along the path from ranging satellite to the user on or near the surface of the earth: therefore, TEC is the appropriate parameter of interest. Studies of the variability of TEC at individual stations at various locations and under both solar maximum and minimum conditions have been done and are presented here in the first portion of this section. Also, results of a study of the correlation distance of the variability of TEC from monthly averages are presented. Since most of the available values of TEC have been determined from the Faraday effect, which is a measure of the columnar electron content to a vertical height of approximately 2500 kilometers, it is of interest to determine the additional contribution of electrons from that height to 36,000 kilometers, the height of geostationary satellites. Using newly available data from ionospheric group path delay, in addition to that from the Faraday effect the contribution of the region above 2,500 kilometers to total time delay is presented.

In the final section we present the results of a computer program developed to convert measured values of Faraday rotation received at the ground from VHF signals transmitted from near-

geostationary satellites. The use of a constant conversion factor from Faraday rotation to final TEC values is not correct when the satellite from which VHF radio waves are being monitored is not precisely geostationary. A computer program has been developed for real time use by Air Weather Service observers to correct for the non-geostationarity of the satellite they are monitoring. A brief description of the importance of making this correction, along with its implementation, is given.

III.1 The Variability of Ionospheric Time Delay*

Modern satellite navigation and satellite detection radar systems can be limited in accuracy due to the time delay caused by the ionosphere through which their RF signals must pass. The ionospheric time delay is directly proportional to the number of electrons encountered along the path from satellite to user and is inversely proportional to the square of the system operating frequency. Some systems, for example the NAVSTAR/Global Positioning System, GPS, are able to take advantage of the fact that the ionosphere is a dispersive medium, by measuring the ionospheric time delay at two widely spaced frequencies and thus are able to directly correct for this effect. Other precision ranging systems do not have the two frequency capability, however, and must instead rely upon models of ionospheric time delay to make corrections to increase system accuracy. Such models generally do a good job of predicting the monthly average behavior but, unless they are updated with a nearby measurement within a few hours of their use, do little to predict the day to day changes which occur.

The purpose of this paper is to outline the errors which result when only monthly average time delay values, without updating, are available for corrections to precise ranging systems. With these results systems design engineers will be able to determine how much improvement can be expected by near-real-time updating or by using a direct two frequency time delay measurement as compared with monthly average time delay models used without updating.

---

*Johanson, J.M., M.J. Buonsanto, J.A. Klobuchar, Proc. of the 1978 Ionospheric Effects Symposium sponsored by NRL and ONR, January 24 - 26, 1978.

III.1.1 Data Base

Since the total number of electrons along the path from satellite to system user is directly proportional to the ionospheric time delay it is this parameter which was studied from a number of stations to determine the variability of time delay. This total number of electrons, called TEC, was determined from Faraday rotation measurements of linearly polarized VHF radio waves transmitted from geostationary satellites. Since the TEC is generally greatest during the mid-afternoon period, and the corresponding ionospheric time delays will be greatest during that period also, the deviations from average behavior are particularly important during this part of the day. Further, since these systems must operate during all conditions of solar and geomagnetic activity we made no attempt here to separate magnetically quiet periods from disturbed times. Data from solar maximum years of 1968 and 1969 were reduced separately from the near solar minimum periods.

The Total Electron Content parameter is capable of describing many features of ionospheric behavior. The variability of this parameter may be easily described in terms of the departure from the monthly mean behavior by constructing the standrard deviation, σ. The percentage standard deviation may then be obtained via:

$$\sigma(\%) = 100\ \sigma/x$$

where x is the monthly mean value. From the large quantity of data available, the diurnal, seasonal, solar cycle, and geographic variations of the percentage standard deviations of monthly mean TEC have been determined.

Total Electron Content data from eleven northern mid-latitude monitoring stations whose world-wide distribution is shown in Figure III.1.1 was used in this study of ionospheric time delay. The TEC data base contains solar maximum data from six stations including Edmonton, Alberta, Canada; Aberystwyth, Wales; Hamilton, Massachusetts; Stanford, California; Honolulu, Hawaii; and Hong Kong. Solar minimum data was collected from the following stations: Narssarssuaq, Greenland; Goose Bay, Labrador; Hamilton, Massachusetts; Kennedy Space Flight Center, Florida; Athens, Greece; and Osan, Korea. Many people were responsible for the data used in this paper and they are each noted in the acknowledegments section.

III.1.2 Diurnal Variation

Typical monthly mean diurnal TEC curves are shown in Figure III.1.2 where data from Hamilton, Massachusetts is plotted for the solar maximum month of March 1969 and for the solar minimum month of March 1975 along with their standard deviations (σ). It is clear in Figure III.1.2 that as the TEC decreases, so does the absolute value of the variability with the result that changes in percentage standard deviation are small. Figure III.1.2 also points out the fact then when operating at a frequency of 1.2 GHz, one TEC unit corresponds to approximately one nanosecond of time delay. It should be noted that while Figure III.1.2 represents a typical monthly mean diurnal TEC curve for a mid-latitude station, a near equatorial station may have monthly mean TEC values which are 2 or 3 times greater than those shown in Figure III.1.2. The corresponding magnitude of σ will also be greater for most near-equatorial stations.

Figure III.1.3 shows diurnal curves of σ (%) for TEC from six stations during the solar maximum year 1969, except for Hong Kong, for which 1968 data was used. Separate curves for winter (November - February), summer (May - August), and equinox (March, April, September, October) are given. Figure III.1.4 shows similar curves for data from six stations during the period April 1974 through March 1975, a period not far from solar minimum. Figures III.1.3 and III.1.4 indicate lowest σ (%) values during the midday period where the curves are fairly flat, ranging from 15 to 25 percent. One must be careful when comparing Figures III.1.3 and III.1.4 for solar cycle effects because data from only one station, namely Hamilton, Massachusetts, was included in both figures. It may be concluded, however, that no obvious solar cycle dependence of σ (%) is evident. There is also no evidence of a geographical dependence except for the winter nighttime period under solar mimimum conditions where a strong latitudinal gradient can be seen.

The data in the two figures seem to fall into one of two categories, the first being those periods exhibiting regular day-to-day variability of approximately 25 percent. The second includes those periods where the extremely high variability can be related to auroral and magnetic storm effects. The Narssarssuaq and Goose Bay nighttime data fall into this second group. At Narssarssuaq, the satellite to station raypath traverses the auroral oval during nighttime and at Goose Bay, the raypath intersects the auroral oval during magnetic storms. We unfortunately have no explanation for the large variability in the Honolulu data, observed especially during the nighttime period in the equinox and winter months.

III.1.3 Monthly Variations

An alternative way of examining the seasonal dependence of σ (%) for the two sets of stations is given in Figure III.1.5. Here the average daytime (12 to 16 hours local time) TEC variability is plotted as a function of month for both the solar maximum and solar minimum periods. Again, we see no evidence of a solar cycle dependence. There is, however, a tendency for the curves to maximize in the equinoctial months. This may be due to the fairly rapid seasonal change between summer and winter diurnal patterns which occurs during those months.

III.1.4 Distribution of Percentage Differences From Monthly Mean TEC

Histograms giving the frequency distribution of percentage differences from the monthly mean daytime values of TEC are given in Figures III.1.6 and III.1.7. Daytime TEC values from Hamilton, June 1971 are plotted in Figure III.1.6 along with a Gaussian curve computed from the standard deviation of the frequency distribution and normalized to the area under the histogram. One can see that the normal curve gives an excellent fit to the data.

Figure III.1.7 shows percentage differences during the daytime period for Hamilton, December 1971. This month includes a large magnetic storm and may be considered as an example of worst case errors. The December 1971 data was chosen because it includes the greatest absolute deviations from monthly average values ever observed in ten years of observations made at Hamilton. In Figure III.1.7, it can be seen that the normal curve (solid line), calculated in the same way as in Figure III.1.6,

is not representative of the data. If we eliminate the three hourly values of December 17, 1971 due to the storm, the standard deviation of the remaining data is greatly reduced, and the resulting normal fit (dashed line) is a better indication of the true distribution of the data.

In the months that we examined, the distribution of errors resulting from use of the monthly mean model were found to be approximately Gaussian. The December 1971 distribution was included only as a worst case example and even here it can be seen that by neglecting 3 hourly values, or 2 percent of the daytime values, the fit is also nearly Gaussian.

III.1.5 Conclusions

We have presented typical errors that a user of a single frequency system can expect when using monthly mean models, without updating, to correct for ionospheric time delays. If one number were to be chosen as the overall standard deviation of monthly mean time delay, one can assume approximately 25 percent variability, although slightly higher values can be expected during the nighttime period when absolute time delay values are genarally much lower.

There is no evidence of a solar cycle dependence of the percentage standard deviation and only a slight geographic dependence as one approaches the auroral zone. The daytime variability exhibits a peak during the equinox and is much more well behaved than the nighttime variability.

We have shown that the distribution of time delays about the monthly mean is nearly Gaussian for the cases examined.

III.1.6 Acknowledgements

Several experimenters were responsible for the data collection from various stations. We wish to express our appreciation for use of the data by acknowledging the following: TEC data from Stanford and Edmonton was provided by A.V. da Rosa; from Aberystwyth by L. Kersley; from Hong Kong by G.O. Walker; from Hawaii by H.T. Roelofs; from Narssarssuaq by I. Mikkelsen; and from Athens by D. Matsoukas. We wish to thank Mr. J. Klobuchar of AFGL for his guidance and co-operation.

LIST OF FIGURES

Figure III.1.1. Total electron content (TEC) data from eleven northern mid-latitude stations.

Figure III.1.2. Monthly mean diurnal variation of TEC at Hamilton, Massachusetts during solar maximum and minimum conditions.

Figure III.1.3. Diurnal curves of standard deviations expressed as a percentage from six stations during solar maximum conditions for northern winter, summer and equinox.

Figure III.1.4. As in Figure III.1.3 during solar minimum conditions, 1974-1975.

Figure III.1.5. Average daytime variability of TEC as a function of month during solar maximum and minimum periods.

Figure III.1.6. Frequency distribution of percentage differences from the monthly mean TEC values at Hamilton, Massachusetts during June 1971. The observed histogram is compared with normal distribution.

Figure III.1.7. As in Figure III.1.6 during December, 1971.

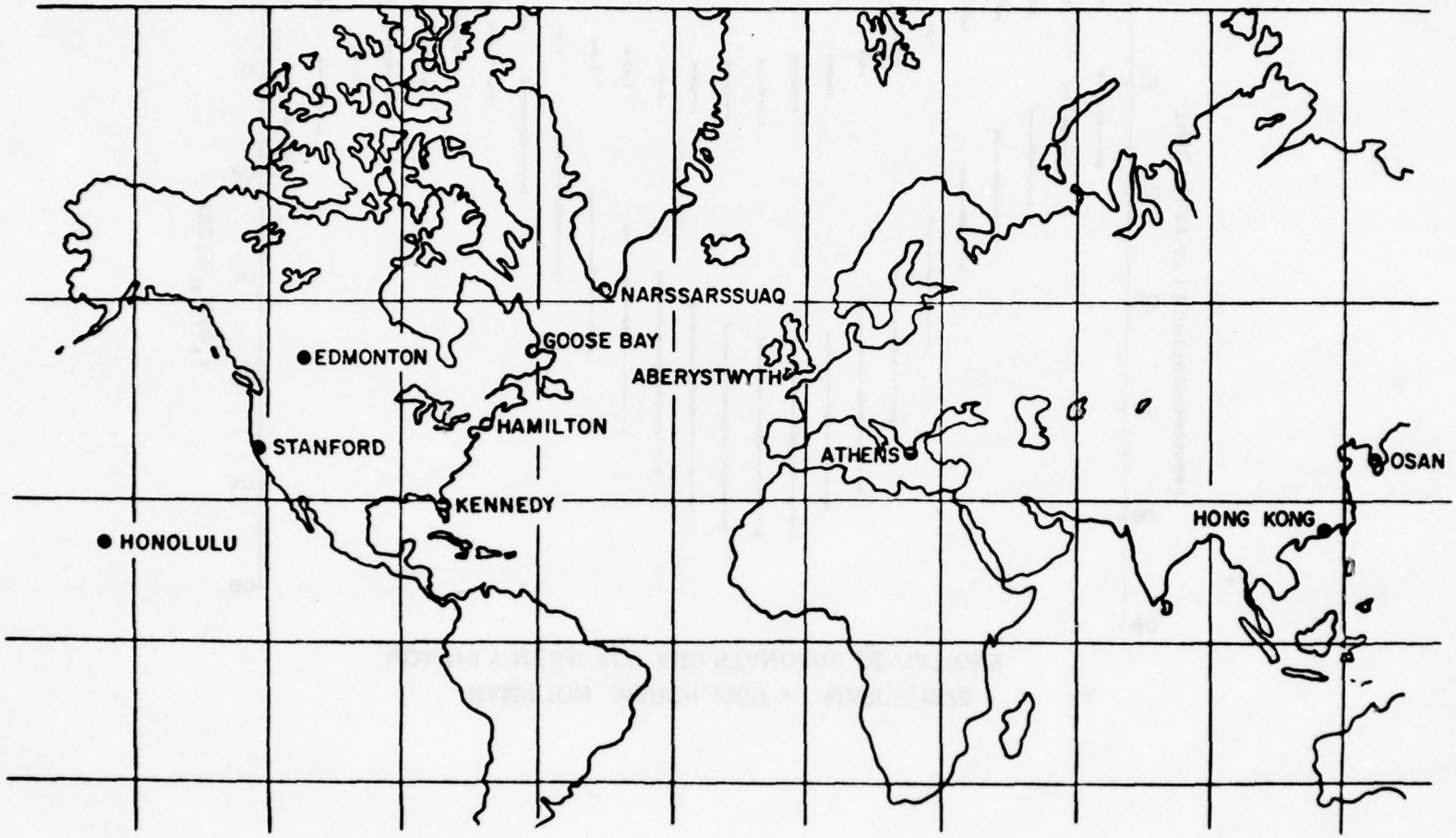

NARSSARSSUAQ
GOOSE BAY
EDMONTON
ABERYSTWYTH
HAMILTON
STANFORD
ATHENS
OSAN
KENNEDY
HONG KONG
HONOLULU

FIG. III. 1.1

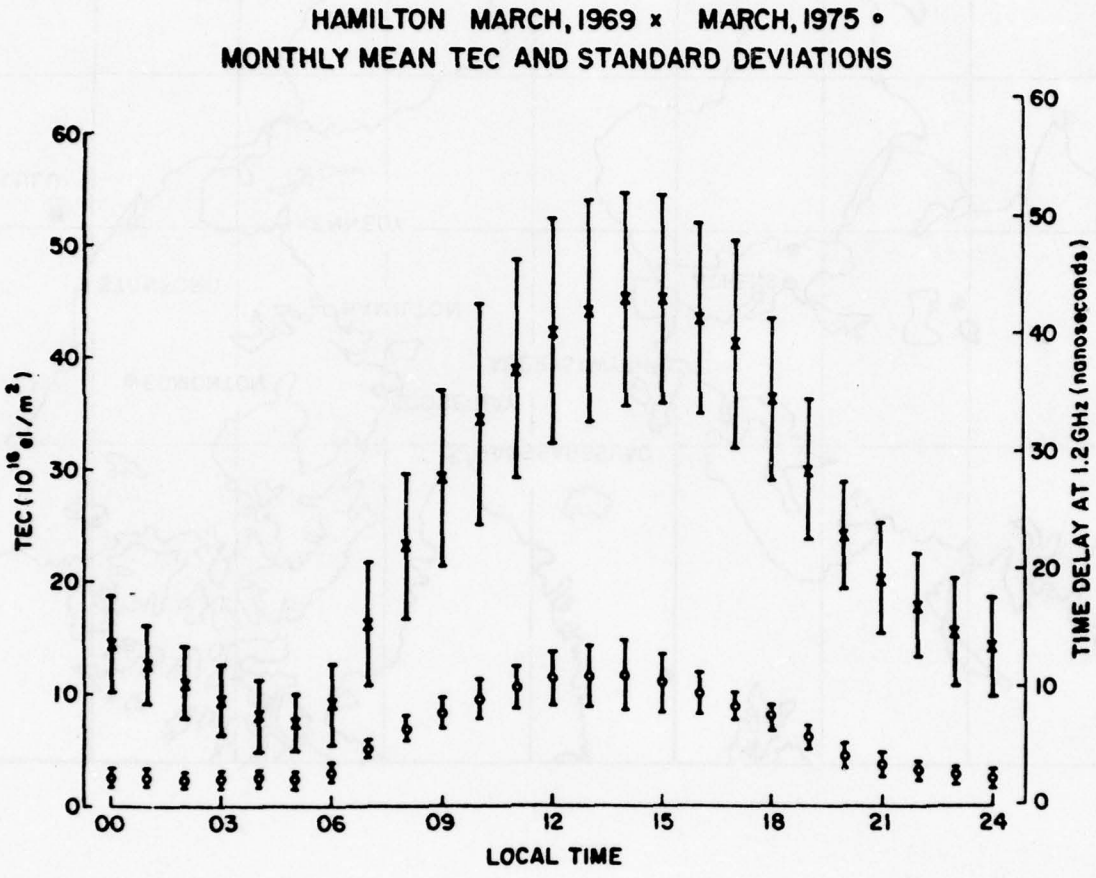

HAMILTON MARCH, 1969 × MARCH, 1975 ∘
MONTHLY MEAN TEC AND STANDARD DEVIATIONS
TEC (10^{16} el/m^2)
TIME DELAY AT 1.2 GHz (nanoseconds)
LOCAL TIME
0
10
20
30
40
50
60
00
03
06
09
12
15
18
21
24

FIG. III. 1.2

THIS PAGE IS BEST QUALITY PRACTICABLE
FROM COPY FURNISHED TO DDC

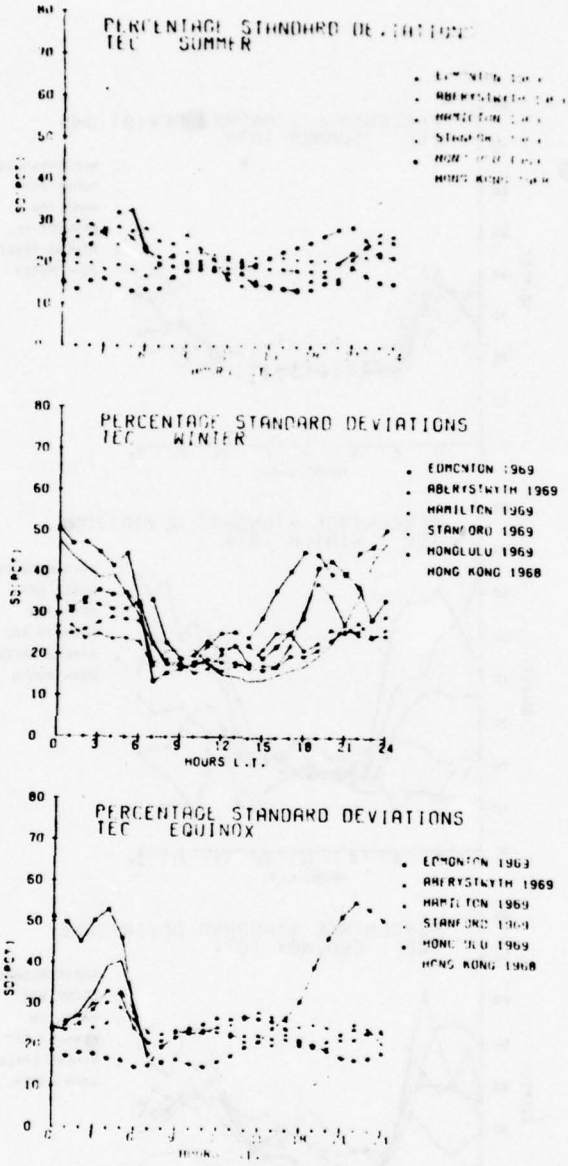


FIG. III. 1.3

THIS PAGE IS BEST QUALITY PRACTICABLE
FROM COPY FURNISHED TO DDC

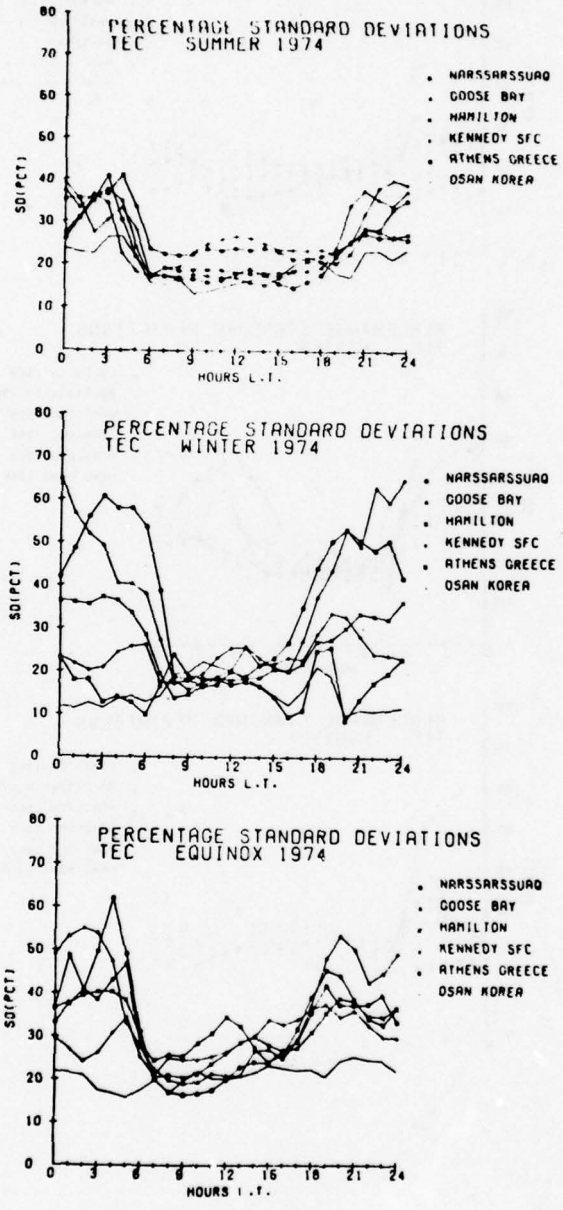


FIG. III. 1.4

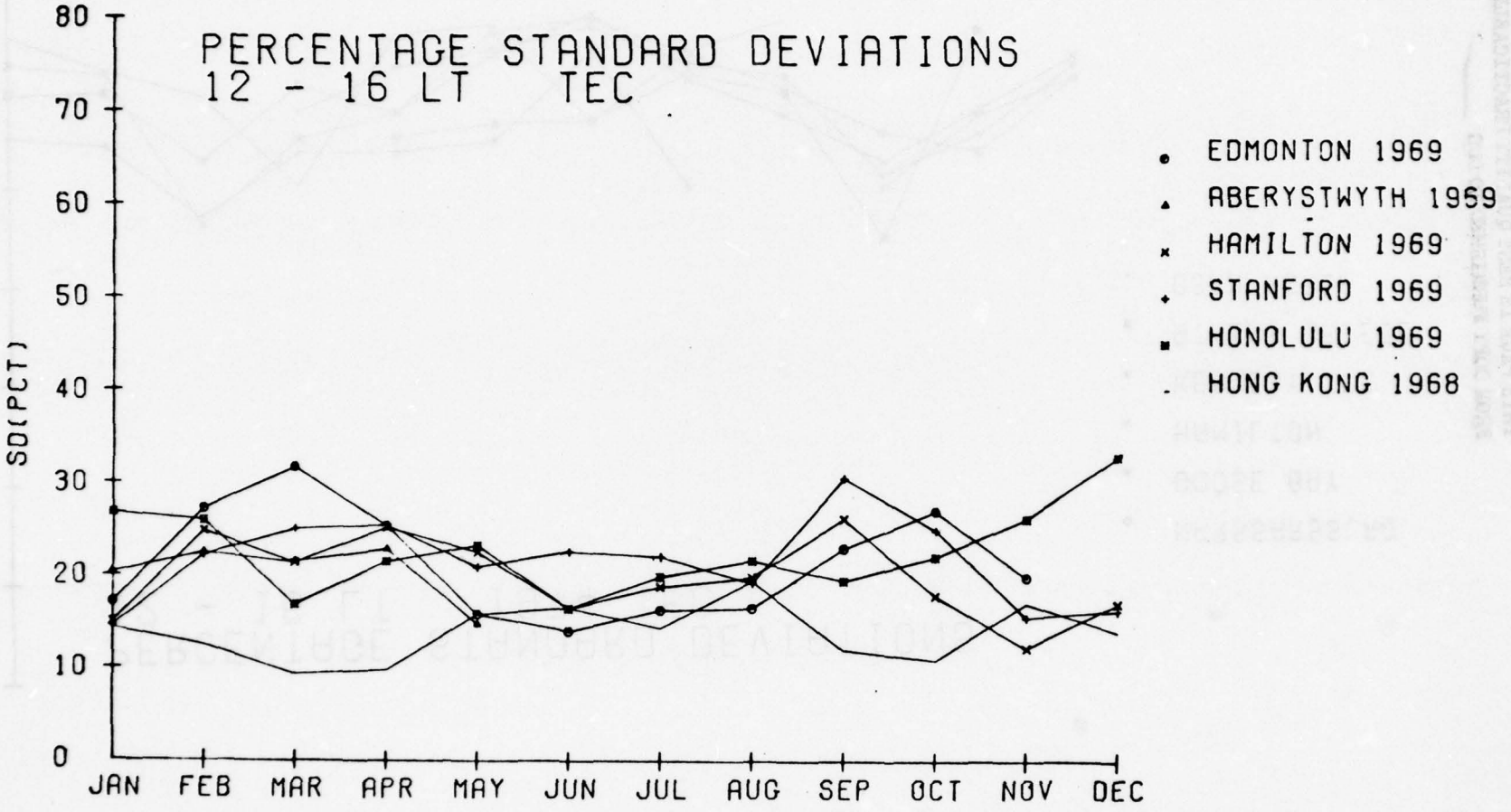

PERCENTAGE STANDARD DEVIATIONS
12 - 16 LT TEC
SD(PCT)
80
70
60
50
40
30
20
10
0
JAN
FEB
MAR
APR
MAY
JUN
JUL
AUG
SEP
OCT
NOV
DEC
EDMONTON 1969
ABERYSTWYTH 1969
HAMILTON 1969
STANFORD 1969
HONOLULU 1969
HONG KONG 1968

FIG. III. 1.5a

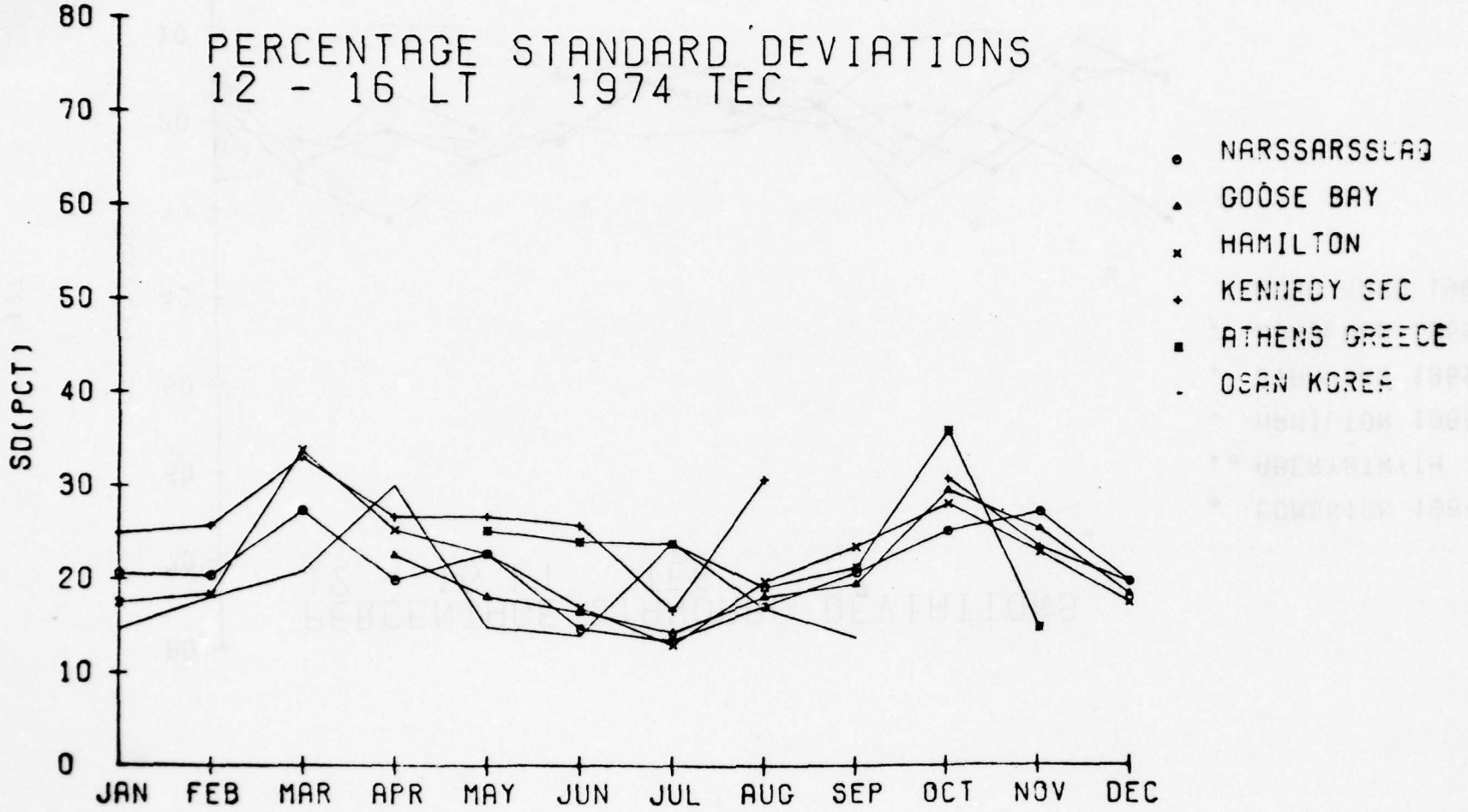


FIG. III. 1,5b

THIS PAGE IS BEST QUALITY PRACTICABLE
FROM COPY FURNISHED TO DDC

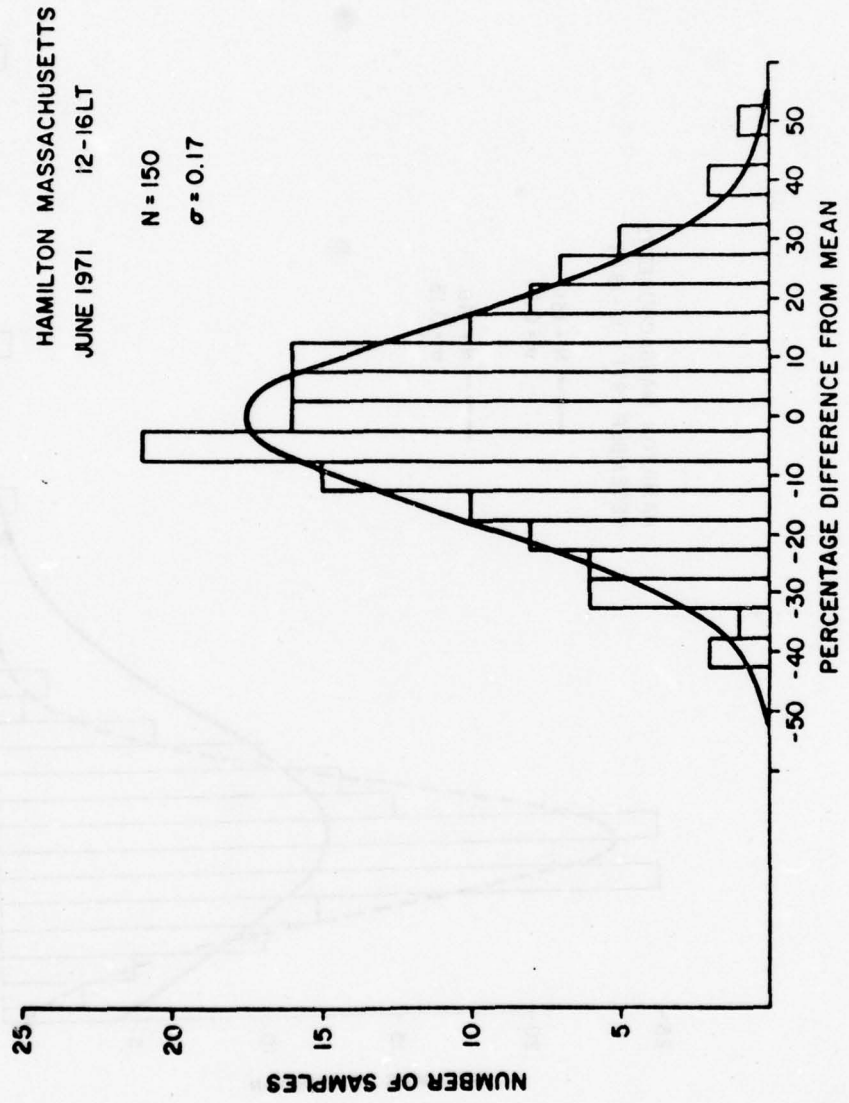

HAMILTON MASSACHUSETTS
JUNE 1971 12-16LT
N = 150
σ = 0.17
NUMBER OF SAMPLES
25
20
15
10
5
-50 -40 -30 -20 -10 0 10 20 30 40 50
PERCENTAGE DIFFERENCE FROM MEAN

FIG. III. 1.6

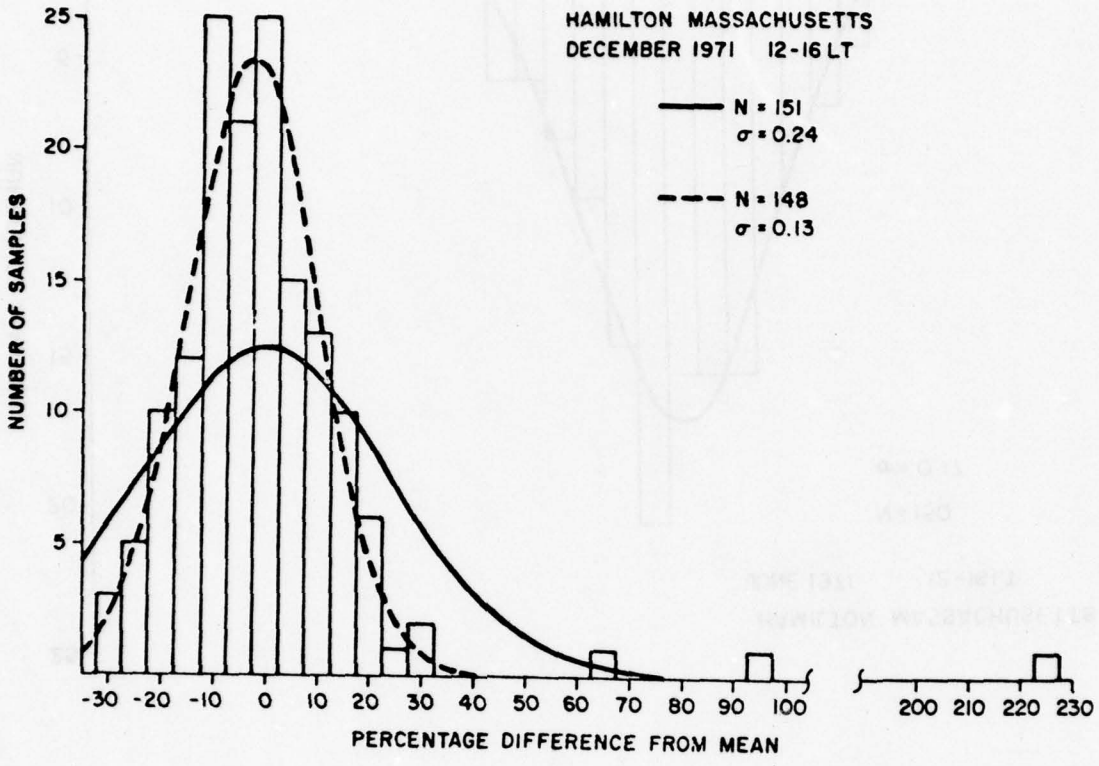

HAMILTON MASSACHUSETTS
DECEMBER 1971 12-16 LT
N = 151
σ = 0.24
N = 148
σ = 0.13
NUMBER OF SAMPLES
25
20
15
10
5
-30 -20 -10 0 10 20 30 40 50 60 70 80 90 100
200 210 220 230
PERCENTAGE DIFFERENCE FROM MEAN

FIG. III. 1.7

III.2 CORRELATION DISTANCE OF MEAN DAYTIME ELECTRON CONTENT*

With the increasing positional accuracy requirements of military navigation and satellite ranging systems, the ionospheric parameter total electron content (TEC) is becoming of greater importance because it is directly related to the group delay that the ionosphere imposes upon the RF signal propagation time. The Air Weather Service, Space Environmental Support System (Flattery and Ramsay, 1975), updates predictions of the TEC parameter for operational military systems using near-real-time TEC data from a network of stations located, for the most part, in the northern mid-latitudes. In this report, we will describe the results of efforts to determine the correlation distance of TEC measurements. The results of this study are important for determining the required geographic spacing of TEC monitoring stations for a given percentage improvement at a location where TEC predictions are required. Preliminary work on TEC correlation distance was done by Rao et al. (1971) and daRosa (1974).

The terms "station spacing" and "correlation distance" used throughout this report refer to distances between subionospheric locations. A subionospheric location is the point below which the slant ray from the station to the satellite intersects a fixed mean ionospheric height, generally 420 kilometers.

In this study, we have assumed that the monthly mean prediction of TEC was correct. In the northern mid-latitudes

---

*Klobuchar, J.A., J.M. Johanson, AFGL-TR-77-0185, August 1977.

this has been generally borne out by the results of Hawkins et al. (1974) and by Mulkern (1976). Of interest here, is the correlation of the day-to-day variability of the TEC, particularly during those times of day when the highest TEC values occur; hence the period when the greatest ionospheric effects influence operational military systems. Accordingly, we have chosen the period from 10 to 16 hours local time to perform correlations of the day-to-day variability at pairs of stations. We refrained from using TEC values over longer intervals of a day, in order to avoid inadvertently correlating diurnal shape changes at pairs of stations. The 24-hour term predominates in a TEC cross correlation power spectra. Therefore, the diurnal correlation will be high, even for very large station spacing, due simply to similar 24-hour behavior of TEC at pairs of stations (Soicher, 1977). The correlation of only the midday component of TEC at pairs of stations was studied, as the absolute values of the day-to-day difference from median values are also generally greatest during this period. A few values of correlation coefficient were computed for nighttime periods as a matter of interest, though the TEC is generally low during the nighttime hours. Daytime values only are used, however, to determine the required station spacing for a given percentage improvement of predictions of TEC.

III.2.1 Data Base

Continuous measurements of the TEC parameter have been

available only since the mid-1960's, as the experimental technique for determination of TEC relies upon the availability of appropriate VHF signals transmitted from geostationary satellites. Such signals from satellites of opportunity are monitored for the changes in Faraday rotation, which can be simply related to equivalent vertical TEC values. The TEC derived from Faraday rotation of VHF radio waves from geostationary satellites is not equal to the group delay of the ionosphere, the parameter normally required by military navigation and satellite ranging systems. A recent study by Fritz (1976), however, has shown that this difference is small during the diurnal peak TEC hours. Also, little actual group delay data are available from geostationary satellites. Faraday rotation data are available from several American longitude sector stations beginning in the late 1960's.

A chain of TEC monitoring stations along an approximate 70 degree west longitude meridian was instrumented in the early 1970's in order to study the latitudinal dependence of magnetic storms; for example Mendillo and Klobuchar (1975). During the solar maximum years of 1968 and 1969, another chain of TEC monitoring stations was operating in the northern mid-latitudes which extended from Wales, United Kingdom in the east, to Stanford, California in the west. Stations along this chain were separated by no more than 20 degrees of geomagnetic latitude. Figure III.2.1 illustrates the locations of the TEC monitoring stations and the mean subionospheric intersection

locations.

Data used in obtaining the cross correlations of TEC from pairs of stations along the longitude chain of stations came from the solar maximum period of 1968 and 1969. Cross correlations of TEC from pairs of stations located along the approximate 70° meridian were calculated for data taken in 1972 and 1974, as many of these stations did not become operational until after the 1968, 1969 solar maximum. All cross correlations were computed using TEC values for the same local time for the same day at pairs of stations.

III.2.2 Significance of Correlation Coefficient

It has been pointed out by Gautier et al. (1965) that the percentage improvement, PI, in the prediction of the parameter f0F2 is related to the correlation coefficient r by:

$$PI = 100[1 - (1 - r^2)^{1/2}] ,$$

assuming a Gaussian distribution. This same relation applies to the TEC uncertainty reduction. A graph of this relationship, illustated in Figure III.2.2, shows that a 50 percent reduction of TEC uncertainty requires a correlation coefficient of 0.87. That is, if measurements of TEC at a monitoring station are to be used to reduce the TEC uncertainty at a second location by 50 percent, the two locations must exhibit a TEC correlation of 0.87. A correlation coefficient of 0.7 between TEC values taken at the same local time at

pairs of stations will result in an improvement, as seen in Figure III.2.2, of only 29 percent in prediction of TEC at one station using data from the second station. This value of r = 0.7, corresponding to a 29 percent uncertainty reduction, is defined here as the "correlation distance." If a 29 percent improvement over the monthly median TEC prediction is required at a given location, then one of the following conditions must be satisfied:

1. If both the station and the location of interest are at the same latitude, then the station must be no greater than one longitudinal correction distance to the east or west of the location.

2. If both the station and the location of interest are to be located along the same meridian, then the station must be available within one latitudinal correlation distance to the north or south of the location of interest.

3. In the more general case, the station must be located within an area defined by an ellipse which is centered on the location of interest, with its major axis defined by twice the longitudinal correlation distance and its minor axis equal to twice the latitudinal correlation distance.

Thus, the required station spacing can be as great as twice the resultant correlation distance. Total electron content data from pairs of stations at various separations were used to determine the limits of this correlation ellipse which satisfy conditions 1 and 2 above.

III.2.3 Correlation Results: Longitude Separation

The correlation coefficient for the 10 to 16 hour local time period for pairs of stations was calculated for each month and these monthly values were averaged, in order to obtain a seasonal mean value. Figure III.2.3 is a plot of r for each season versus station-pair longitude separation distance in kilometers. The seasons are indicated as W for the winter months of November, December, January and February; S for the summer months of May through August; and E for the equinox months of March, April, September and October. Note in Figure III.2.3 that there is no strong seasonal dependence on r for different station separations. Rush (1972, 1976) showed that f0F2 exhibited an East-West correlation distance, corresponding to r = 0.7, significantly greater in the equinox months as compared to summer. Winter gave the poorest E-W correlation distance of all seasons, approximately one third the equinox value in Rush's study. In Figure III.2.3, with the exception of two station pairs, the TEC correlations were greatest also during the equinox months. Winter values are certainly not the lowest, except for one station pair.

With the lack of a clear seasonal dependence on r at various pairs of TEC monitoring stations, only one linear dependence of r upon ionospheric longitude separation distance was drawn in Figure III.2.3, and this linear dependence can be seen to have little seasonal change with available data. From Figure III.2.3, the r=0.7 correlation distance in longitude is

approximately 2900 km which corresponds to 26*cos(lat) degrees of longitude. This distance agrees well with the results of Rush (1972) for f0F2 for the equinox season; but, it is considerably greater than the correlation distance of approximately 1150 km which Rush found for the winter months. Our lack of TEC data at station spacings less than 1500 km longitude separation, and between 1600 and 3200 km, handicaps the present results as compared with Rush's work in which data from 32 ionosondes were available.

In an attempt to see if a clear, seasonal variation of r could be found for stations of relatively close spacing, a plot of the monthly values of r for the year 1969 was made for the Hamilton, Massachusetts and Urbana, Illinois pair of stations, with an ionospheric intersection spacing of 1500 km as shown in Figure III.2.4. Also in Figure III.2.4 is the seasonal behavior of r for the nighttime hours 23-03 local time. The only seasonal dependence in the daytime TEC correlation is shown by the lower values during the months of April, May and June with highest values in late winter, the month of July and the autumnal equinox months. In Figure III.2.5, the seasonal dependence of r between the Stanford, California and Edmonton, Alberta pair of stations also is maximum in the autumnal equinox months. Figures III.2.6 and III.2.7 show that the highest values of r for the Urbana-Stanford pair and for the Hamilton-Stanford pair also occur during the months of September and October. No clear difference between the value of r

for daytime TEC, during summer and winter months, is apparent in Figures III.2.4, III.2.6 and III.2.7. In Figure III.2.5, the values of r for the daytime data of the three available winter months are considerably lower than during the other seasons.

The correlation coefficient for nighttime TEC values from 23 to 03 hours local time was computed as a matter of interest, though these values are not of great importance in predictions of TEC due to the much lower nighttime absolute values of TEC. These values of r, plotted for the station pairs at 1500- and 1600-km spacing as shown in Figures III.2.4 and III.2.5, respectively, are highest during the summer months. For the east-west spacing of the Hamilton-Urbana pair, shown in Figure III.2.4, the nighttime values of r are decidedly lowest from September through December. The Stanford-Edmonton station pair has a fairly large north-south geographic component, exhibiting low values of r during the nighttime of all months from November through March. Again, no clear-cut nighttime seasonal behavior in r can be deduced from the available data base.

III.2.4 Correlation Results: Latitude Separation

While data for determining longitude correlation distance were available during the 1969 year of solar maximum, the stations along the 70 degree longitude meridian, used for determining a value of latitude correlation distance, did not become

operational until late 1971 in the case of Goose Bay, Labrador, and until 1974 in the case of the Kennedy Space Flight Center, Florida. Thus, it was not possible to make an estimate of correlation distance based upon solar maximum data. Figure III.2.8 illustrates the seasonal mean values of correlation coefficient as a function of station spacing in latitude. Again, as with the longitude separation case, there is no clear seasonal dependence in values of r for various station separations. A single linear curve has been drawn in Figure III.2.8 to represent the average dependence of r upon station latitude separation. The r = 0.7 value of correlation distance is approximately 1800 kilometers. This again agrees well with the over-all annual value of 1600 km obtained from averaging the three seasonal values in Rush (1976) for the same value of r. Figures III.2.9 through III.2.12 illustrate the monthly daytime values of r for different station separations from 1300 to 4000 kilometers. For the closest two spacings, shown in Figures III.2.9 and III.2.10, values of r for each month for the nighttime hours of 23 to 03 local time are also plotted. The seasonal behavior of the daytime values of r indicate no consistent pattern. The r value is lowest in September for the Hamilton-Goose Bay pair, as shown in Figure III.2.9, yet highest for the months of August, October and November for the Hamilton-Kennedy pair of stations. Values of r for the nighttime hours are generally lowest during the winter months, as was the case for stations separated in longitude.

III.2.5 Discussion

The spatial and temporal variability of the F region remains of great research interest (Rishbeth and Kohl, 1976). It is unlikely that short term solar EUV changes can produce the observed spatial TEC variability; thus, we are left with neutral wind, composition and electrodynamic effects. In our study, we did not attempt to separate magnetically quiet and disturbed periods because in operational use the required station spacing for prediction improvements would have to be chosen for all geomagnetic conditions. The lower correlation distance for stations at nearly the same longitude, but separated in latitude, could likely be due to the different day-to-day strength of the neutral wind in the F region as a function of latitude. The neutral wind, normally blowing away from the subsolar point, can drive ionization up or down in altitude along magnetic field lines to regions of lower or increased loss, which would significantly change TEC. Different strengths of the equatorial electrojet which transport ionization from the magnetic equator to the low midlatitudes can also change the TEC as a function of latitude. Kane (1975) suggested that erratic neutral winds originating in the polar regions may produce large scale ionospheric turbulence which may act in a random way in different geographical locations. This turbulence may be a major contributing factor in limiting the TEC correlation distance in both longitude and in latitude.

III.2.6 Summary of Results

The correlation distance, defined as the distance where the correlation falls to 0.7, has been determined for pairs of TEC monitoring stations aligned along approximate east-west and north-south directions. A correlation coefficient of 0.7 implies that data taken at one station can be used to reduce the uncertainty in a TEC prediction at the second station by 29 percent. Station spacings of approximately 2900 km, and 1800 km gave correlation coefficients of 0.7 in the east-west and north-south directions, respectively, for TEC data taken during the 10 to 16 hour local time period. With the limited number of stations from which TEC data were available, no clear seasonal dependence of the correlation distance was found. The correlation coefficient for nighttime data taken between 23-03 hours local time was generally lower, especially during the winter season.

The implications of these results, for station spacing in an Air Weather Service TEC monitoring station network, in the mid-latitudes, are as follows:

1. For a 29 percent TEC prediction improvement at a given geographic location, a TEC monitoring station must be located within approximately 2900 km or [26*cos(lat)] degrees of longitude of the required prediction location, and within approximately 1800 km or 16 degrees of latitude of the required prediction location. For the same percentage of TEC prediction improvement, the monitoring stations need be spaced at

twice the correlation distance spacing.

2. For a 50 percent TEC prediction improvement, the correlation coefficient between pairs of stations must be 0.87. This value corresponds to a spacing between a TEC monitoring station and a given prediction location of 1200 km in longitude and 800 km in latitude.

3. For this 50 percent improvement, TEC monitoring stations are required every 2400 km or [22*cos(lat)] degrees of longitude and every 1600 km or 14 degrees of latitude. During periods when the correlation is lower, such as during winter nighttime hours, the required station spacing is much smaller. However, during those times the absolute values of TEC are generally near their diurnal and annual minimum values and the importance of a large improvement in prediction is minimum also. These results are summarized in Table 1.

Table 1. Required Monitor Station Spacing vs Midday TEC Prediction Improvement

Percent midday TEC prediction improvement (%)	Required monitor station spacing	
	Longitude [*cos (lat) degrees]	Latitude (degrees)
29	52	32
50	22	14

REFERENCES

1. daRosa, A.V. (1974) Recent results from satellite beacon measurement, Space Research XIV, Akademie-Verlag, Berlin, pp. 209-226.

2. Flattery, T.W., and Ramsay, A.C. (1975) Derivation of total electron content for real time global applications, in Effects of the Ionosphere on Space Systems and Communications, J.M. Goodman, Ed., U.S. Government Printing Office, Washington, D.C.

3. Fritz, R.B. (1976) ATS-6 Radio Beacon Electron Content Measurements at Boulder, July 1974-May 1975, Report UAG-58 World Data Center A, Boulder, Colorado.

4. Gautier, T.N., and Zacharisen, D.H. (1965) Use of Space and Time Correlation in Short-Term Ionospheric Predictions. Conference Record, First Annual IEEE Communications Convention.

5. Hawkins, G.S., and Klobuchar, J.A. (1974) Seasonal and Diurnal Variations in the Total Electron Content of the Ionosphere at Invariant Latitude 54 Degrees, AFCRL-TR-74-0294.

6. Kane, R.P. (1975) Day-to-day variability of ionospheric electron content at mid-latitudes, J. Geophys. Res. 80(No. 22):3091-3099.

7. Mendillo, M., and Klobuchar, J.A. (1975) Investigations of the ionospheric F region using multistation total electron content observations, J. Geophys. Res. 80(No. 4): 643-650.

8. Mulkern, F.A. (1976) Comparison of Predicted Monthly Medians of Total Electron Content with Field Observations, AFCRL-TR-76-0158.

9. Rao, N. Narayana, Youakim, M.Y., and Yeh, K.C. (1971) Feasibility Study of Correcting for the Excess Time Delay of Transionospheric Navigational Ranging Systems, SAMSO TR71-163, Technical Report No. 43, SAMSO, Los Angeles, California.

10. Rishbeth, H., and Kohl, H. (1976) Topical questions of ionospheric physics: a working group report, J. Atmos. Terr. Phys. 38:775-780.

11. Rush, C.M. (1972) Improvements in Ionospheric Forecasting Capability, AFCRL-72-0138.

12. Rush, C.M. (1976) An ionospheric observation network for use in short-term propagation predictions, Telecommunication Journal 43(No. 8):544-549.

13. Soicher, H. (1977) Spatial Correlation of Transionospheric Signal-Time Delays, ECOM-4483, U.S. Army Electronics Command, Fort Monmouth, New Jersey.

LIST OF FIGURES

III.2.1. Location of Stations and Their Mean Ionospheric Points Used in TEC Correlation Study 147

III.2.2. Percentage Improvement vs Correlation Coefficient r 148

III.2.3. Correlation Coefficient vs Station Longitude Separation in Kilometers 149

III.2.4. Correlation Coefficient vs Month of the Year 1969 for Day and Nighttime TEC Periods for the Hamilton, Mass.-Urbana, Ill. Station Pair 150

III.2.5. Correlation Coefficient vs Month of the Year 1969 for Day and Nighttime TEC Values Measured at Stanford, California, and Edmonton, Alberta, Canada 151

III.2.6. Correlation Coefficient vs Month of the Year 1969 for TEC Values Measured during the 10-16 Local Hour Period at Urbana, Ill., and Stanford, California 152

III.2.7. Correlation Coefficient vs Month of the Year 1969 for Daytime TEC Values Measured during the 10-16 Local Hour Period at Hamilton, Mass., and Stanford, California 153

III.2.8. Correlation Coefficient vs Station Latitude Separation in Kilometers 154

III.2.9. Correlation Coefficient vs Month of the Year 1972 for Day and Nighttime TEC Values Measured at Hamilton, Mass., and Goose Bay, Labrador 155

III.2.10. Correlation Coefficient vs Month of the Year 1974 for Day and Nighttime TEC Values Measured at Hamilton, Mass., and Kennedy Space Flight Center, Florida 156

III.2.11. Correlation Coefficient vs Month of the Year 1974 for Daytime TEC Values Measured during the 10-16 Local Hour Period at Hamilton, Mass., and Narssarssuaq, Greenland 157

III.2.12. Correlation Coefficient vs Month of the Year 1974 for Daytime TEC Values Measured during the 10-16 Local Hour Period at Narssarssuaq, Greenland, and Kennedy Space Flight Center, Florida 158

THIS PAGE IS BEST QUALITY PRACTICABLE
FROM COPY FURNISHED TO DDC

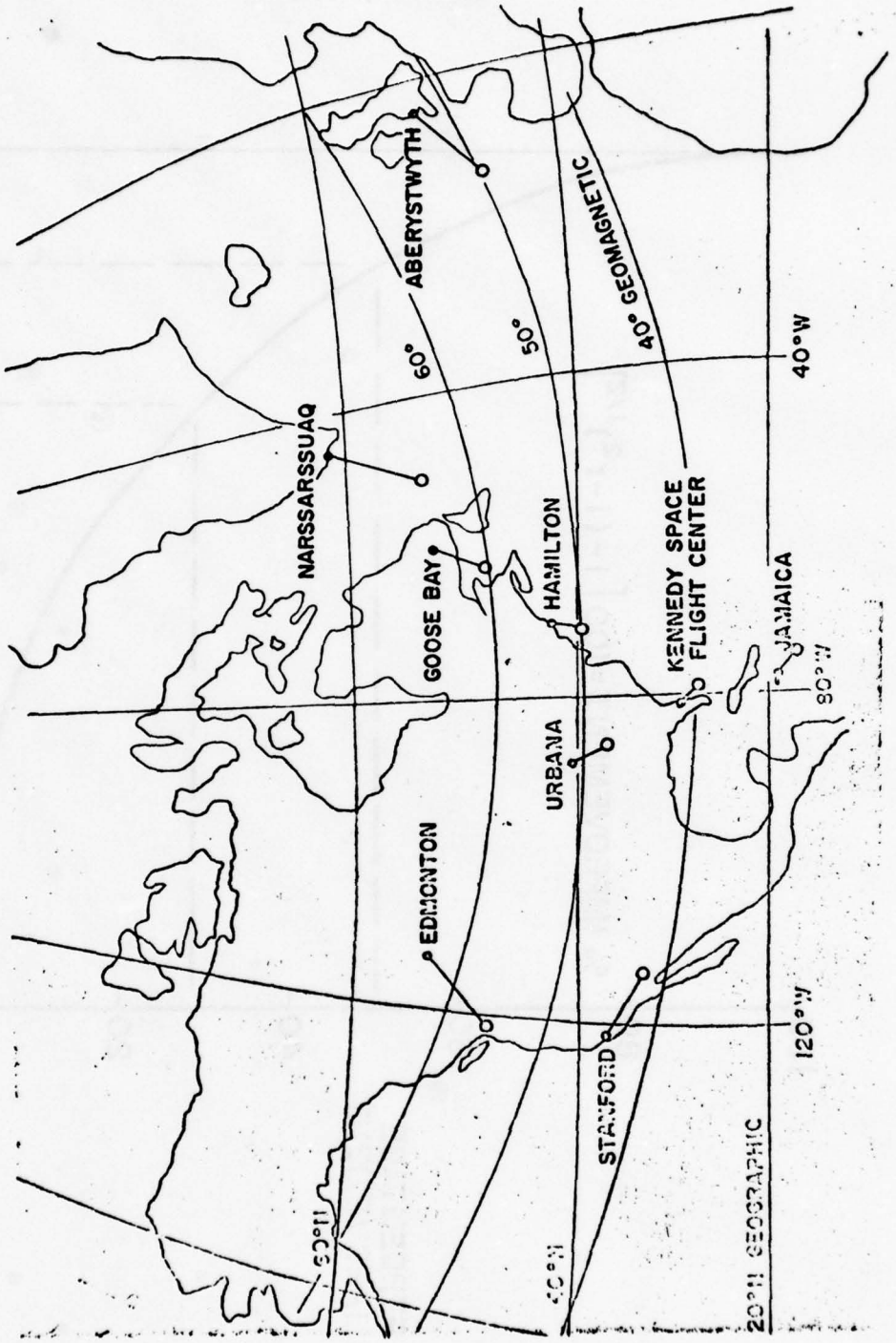


FIG. III. 2.1

THIS PAGE IS BEST QUALITY PRACTICABLE
FROM COPY FURNISHED TO DDC

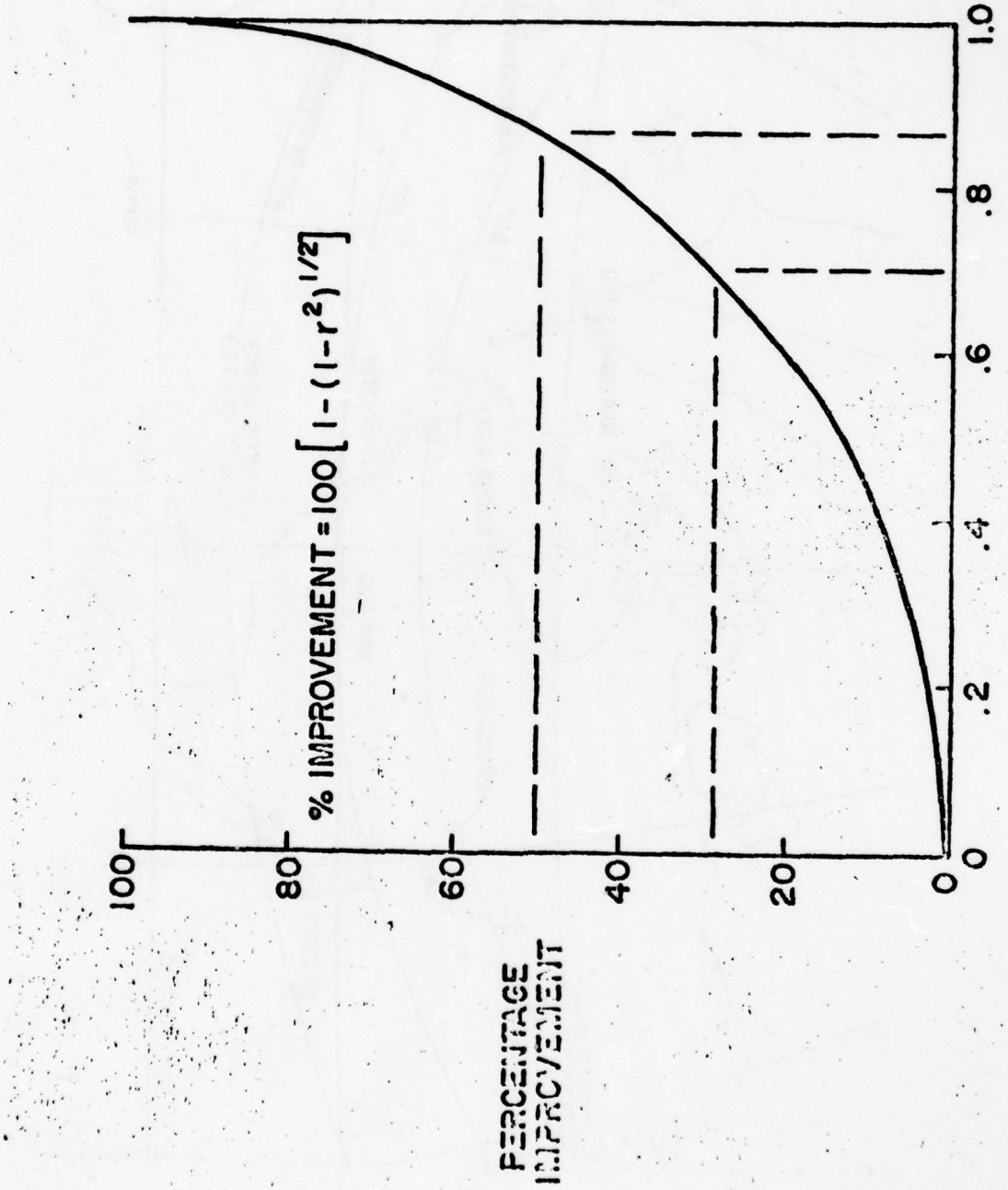


FIG. III. 2.2

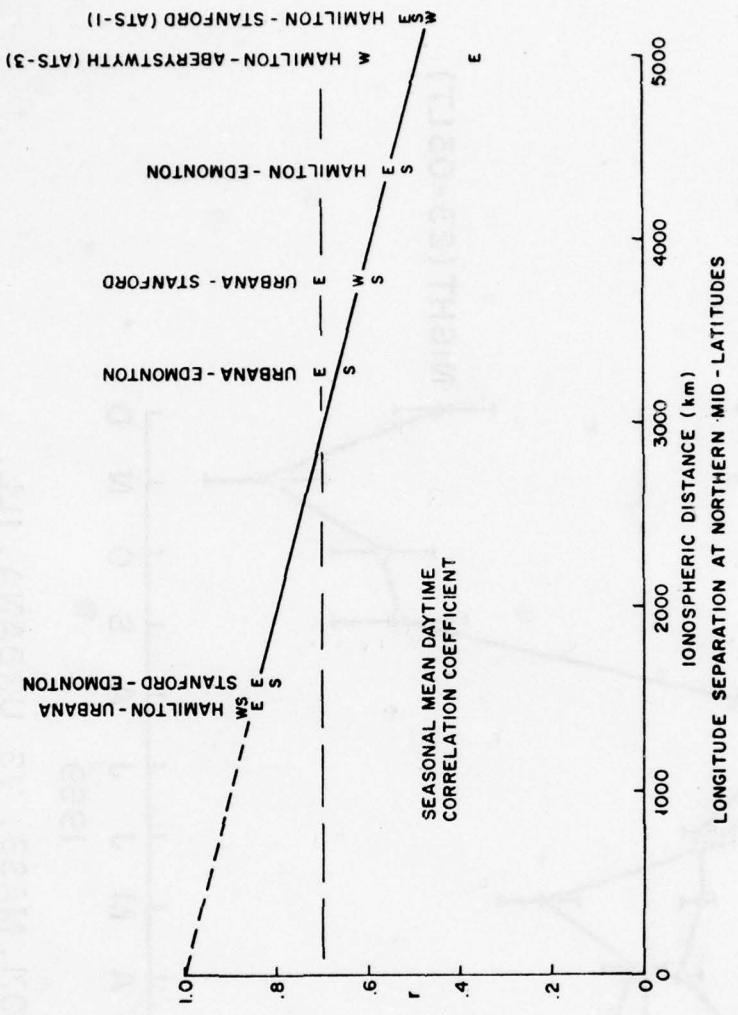

HAMILTON - STANFORD (ATS-1)
HAMILTON - ABERYSTWYTH (ATS-3)
HAMILTON - EDMONTON
URBANA - STANFORD
URBANA - EDMONTON
HAMILTON - URBANA
STANFORD - EDMONTON
SEASONAL MEAN DAYTIME
CORRELATION COEFFICIENT
r
1.0
.8
.6
.4
.2
0
0
1000
2000
3000
4000
5000
IONOSPHERIC DISTANCE (km)
LONGITUDE SEPARATION AT NORTHERN MID-LATITUDES

FIG. III.2.3

THIS PAGE IS BEST QUALITY PRACTICABLE
FROM COPY FURNISHED TO DDC

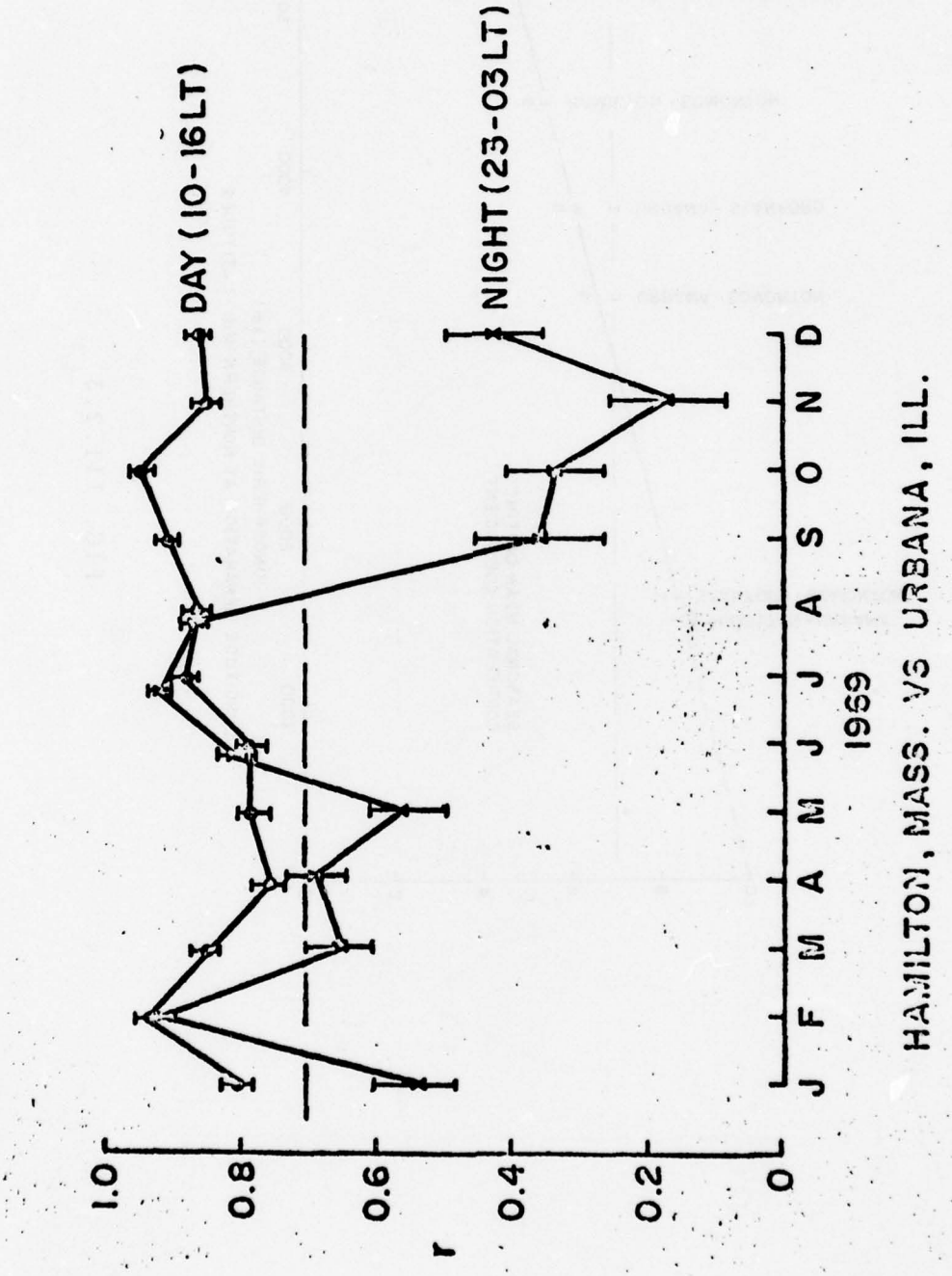


FIG. III. 2.4

THIS PAGE IS BEST QUALITY PRACTICABLE
FROM COPY FURNISHED TO DDC

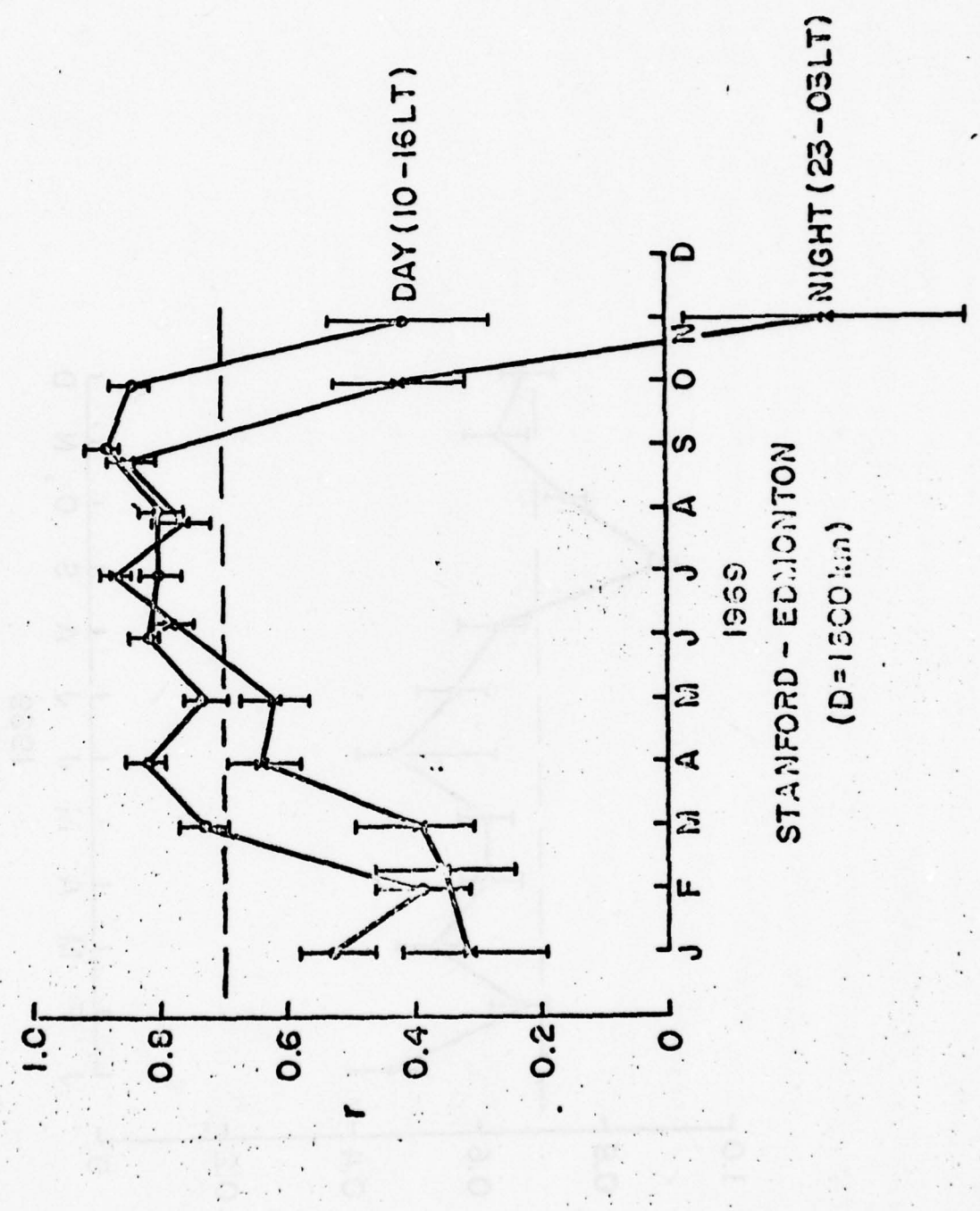


FIG. III. 2.5

THIS PAGE IS BEST QUALITY PRACTICABLE
FROM COPY FURNISHED TO DDC

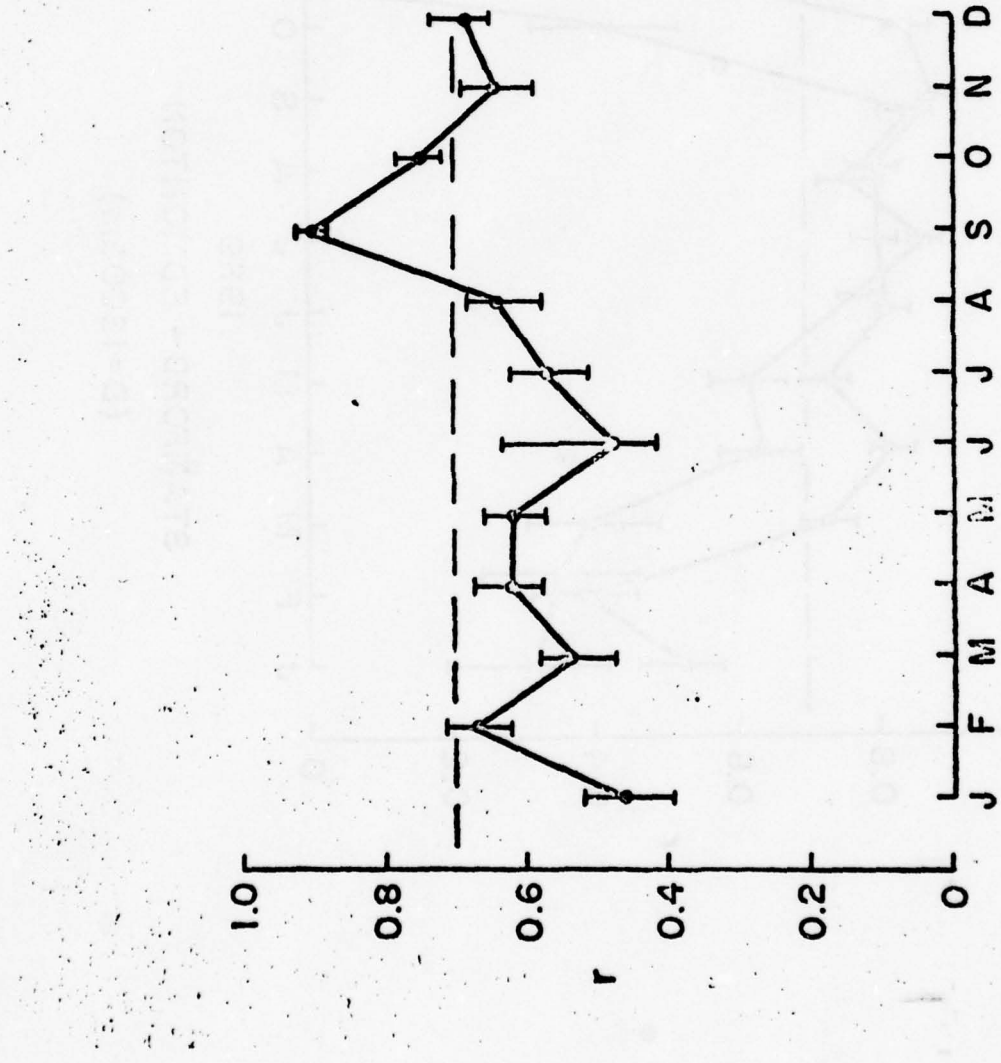


FIG. III. 2.6

THIS PAGE IS BEST QUALITY PRACTICABLE
FROM COPY FURNISHED TO DDC

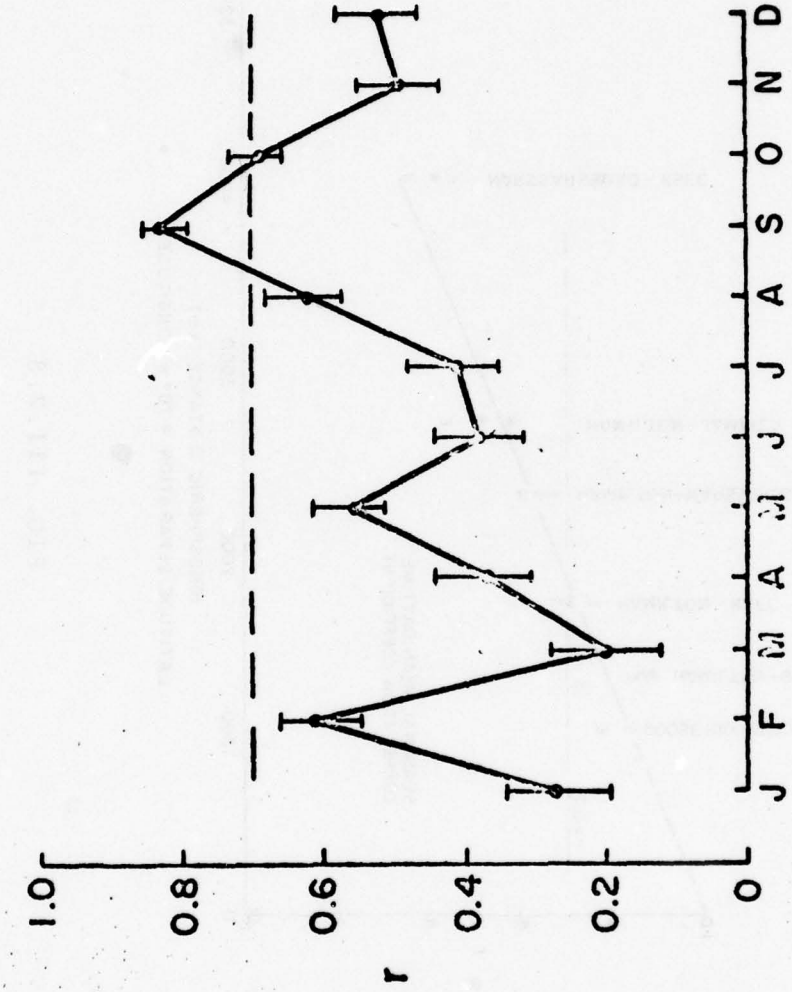


FIG. III. 2.7

THIS PAGE IS BEST QUALITY PRACTICABLE
FROM COPY FURNISHED TO DDC

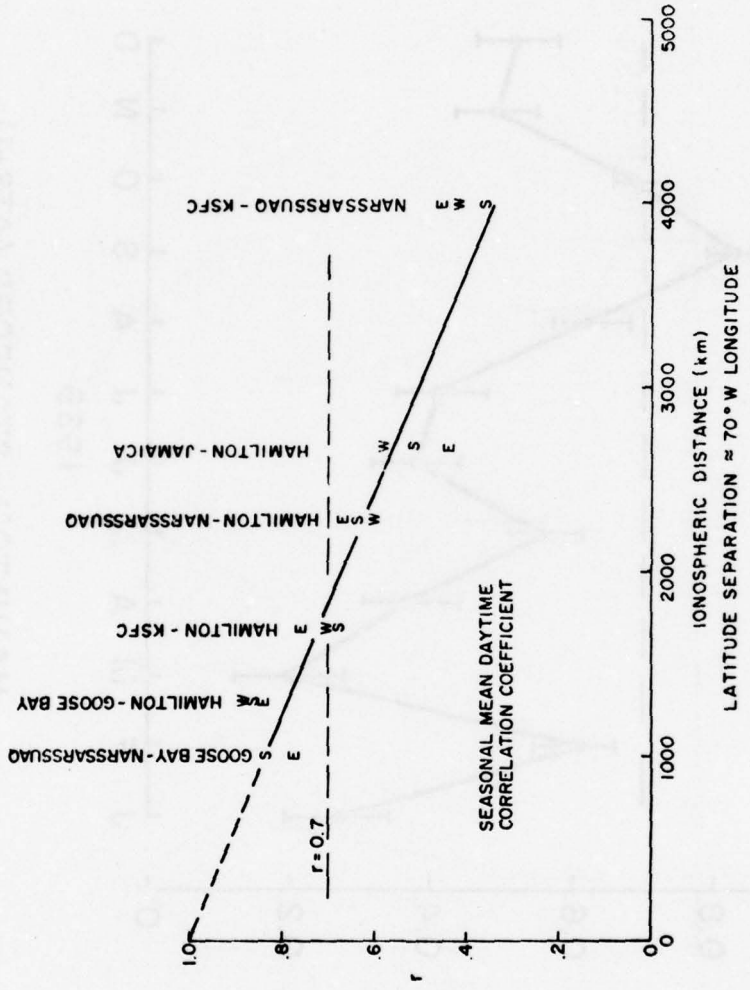


FIG. III.2.8

THIS PAGE IS BEST QUALITY PRACTICABLE
FROM COPY FURNISHED TO DDC

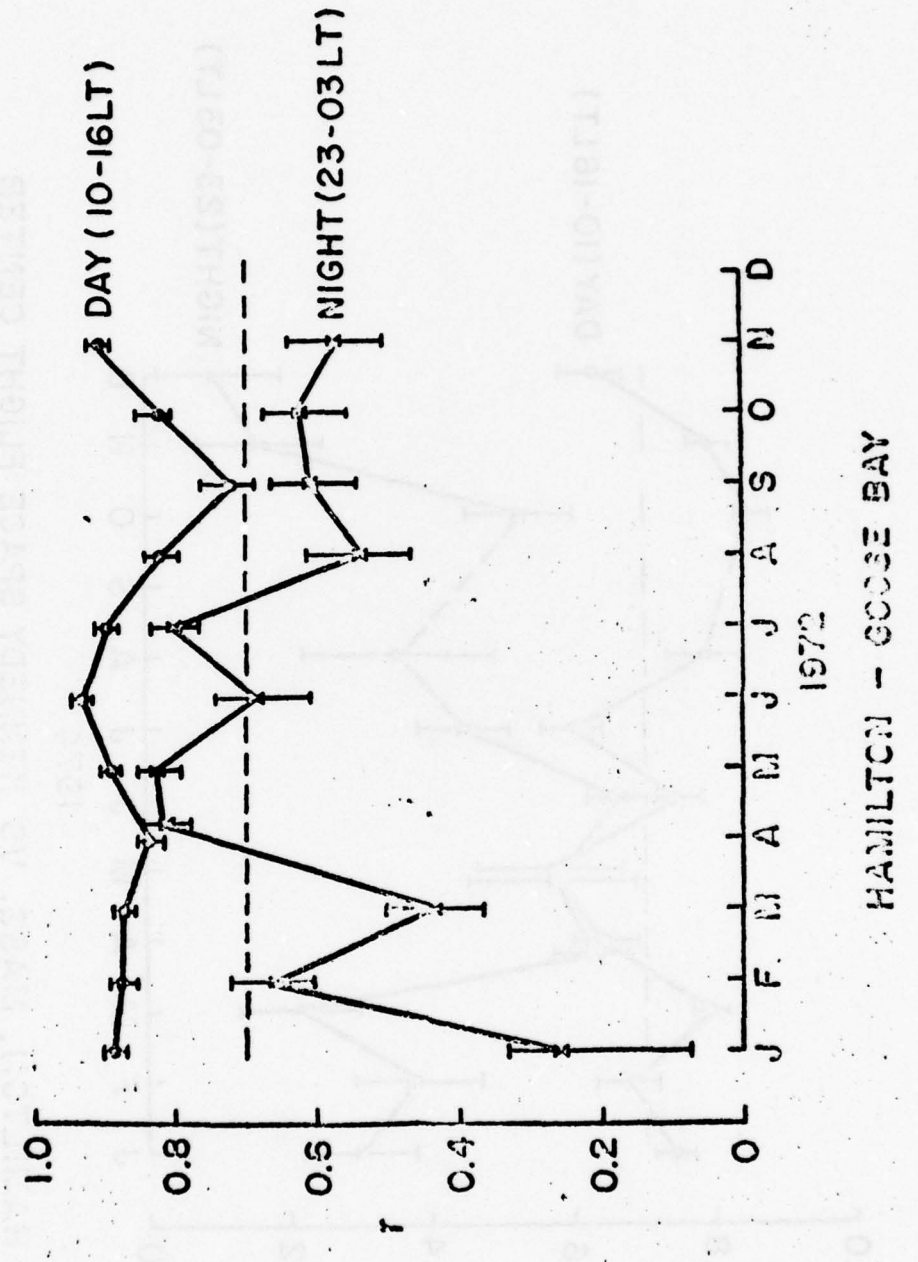
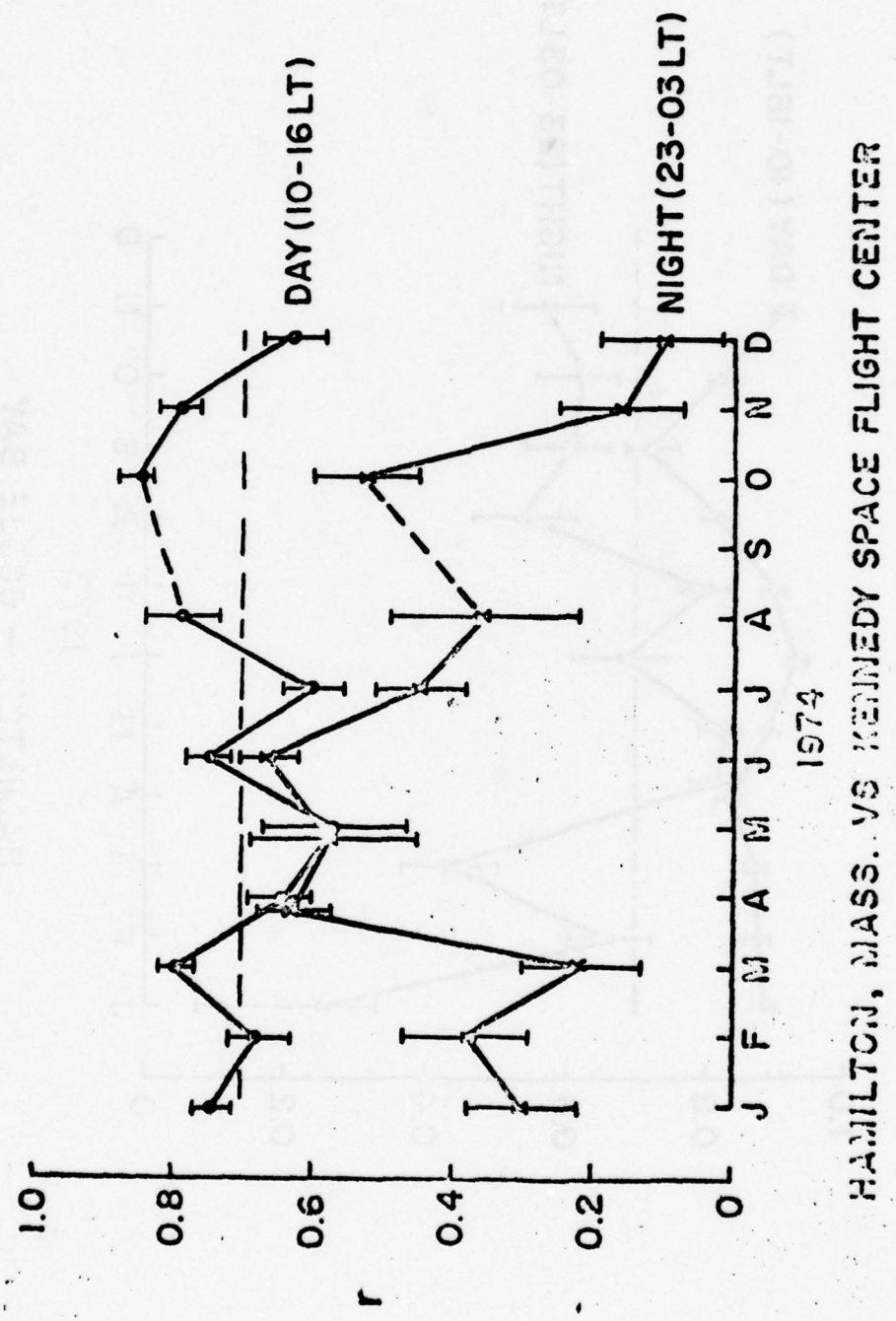


FIG. III. 2.9

THIS PAGE IS BEST QUALITY PRACTICABLE
FROM COPY FURNISHED TO DDC



HAMILTON, MASS. VS KENNEDY SPACE FLIGHT CENTER
(D = 1700 km)

FIG. III. 2.10

THIS PAGE IS BEST QUALITY PRACTICABLE
FROM COPY FURNISHED TO DDC

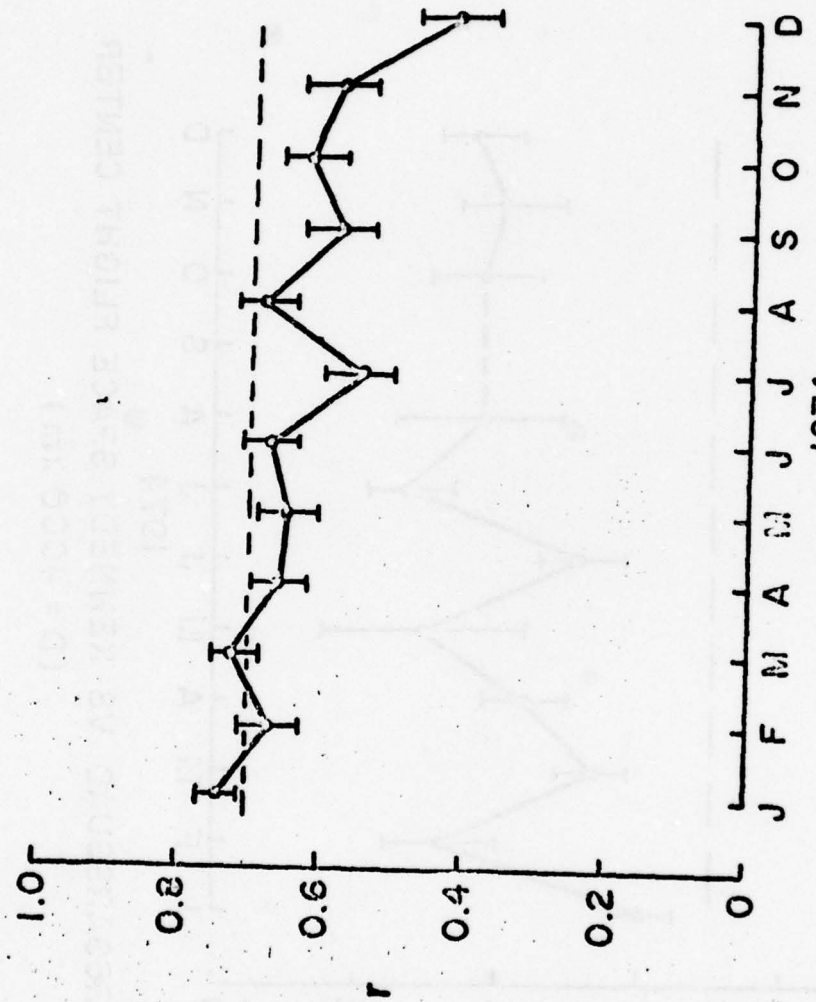


FIG. III. 2.11

THIS PAGE IS BEST QUALITY PRACTICABLE
FROM COPY FURNISHED TO DDC

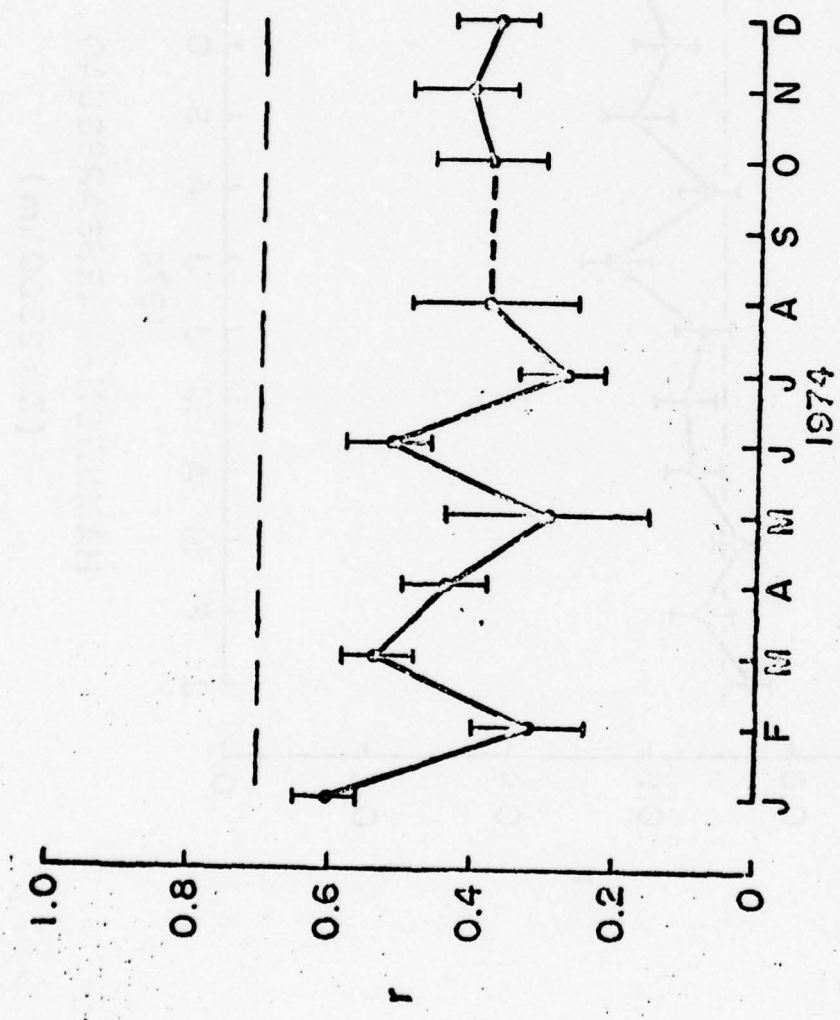


FIG. III. 2.12

III.3 THE CONTRIBUTION OF THE PLASMASPHERE TO TOTAL TIME DELAY*

The Total Columnar Electron Content (TEC) of the earth's ionosphere produces group delay of modulation of radio frequency waves which traverse the ionosphere. This group delay can produce significant range errors in advanced systems which require accuracies of a few feet in measured range. The NAVSTAR-Global Positioning System (Lassiter and Parkinson, 1977) (GPS) is an example of a precise ranging system currently under development by the Department of Defense which will undergo significant ionospheric group delay. Fortunately, the GPS will have two, widely spaced frequencies available from which the group delay of the ionosphere can be directly measured and subtracted from the apparent range to yield the true range from satellite to user. Some users may not choose the sophistication of the two frequency version of the system, however, and may instead choose to use an analytic model representation of the ionospheric time delay. To construct and to test such models and to enable advanced ranging system designers to obtain estimates of the magnitude of the ionospheric group delay error, use has been made of the available Faraday rotation data which is a measure of the TEC to a height of approxiamtely 2,500 kilometers, 20,000 kilometers in the case of the GPS, it is of interest to determine the additional contribution to ionospheric time delay not measurable from the available Faraday TEC data.

---

*Klobuchar, J.A., M.J. Buonsanto, M.J. Mendillo, J.M. Johanson, Proc. of the 1978 Ionospheric Effects Symposium sponsored by NRL and ONR, January 24 - 26, 1978.

III.3.1 Available Plasmaspheric Electron Content Data

There are approximately 1000 station-months of TEC data obtained from the Faraday effect available from representative stations around the world, covering both solar maximum and minimum conditions. Until the launch of the geostationary satellite ATS-6 in mid-1974, there were no simultaneous Faraday and group delay measurements from which the additional contribution to TEC not measurable from the available Faraday TEC data could be determined. The ionospheric beacon transmitter carried on the ATS-6 geostationary satellite, Davies, et al., (1975), was designed to enable the measurement of simultaneous Faraday rotation and true group delay from its multi-frequency beacon transmissions. This is the first satellite to carry a beacon transmitter specifically designed for simultaneous Faraday and group delay measurements.

The difference between the group delay measurement of slant TEC, minus the Faraday electron content, defined here as a measure of the electrons in the region up to approximately 2,500 kilometers in vertical height, is called the plasmaspheric electron content, N_p. The currently available published monthly mean values of N_p are relatively few and consist of approximately 11 months of data from Boulder, Colorado, Fritz (1976), a few months from Ft. Monmouth, New Jersey, Soicher (1976a), one month each from Natal, Brazil and from Kiruna, Sweden, Soicher (1976b), and nine months of N_p monthly median values from Aberystwyth, Wales, Hajeb-Hosseinieh (1977). In addition, Soicher (1976c), Webb and Lanzerotti (1977), Poletti-Liuzzi, et al.(1977) and Hajeb-Hosseinieh (1977) have published studies of the behavior of N_p during a few magnetic

storms, and Klobuchar and Johanson (1977) presented a comparison of the monthly average N_p results at Boulder with those from Hamilton, Massachusetts. Since all the available N_p data is from the period later than May 1974 it is representative of solar minimum conditions only.

Kersley (p.com.) has recently pointed out that plasmaspheric electron content measurements taken from stations at nearly the same latitude, but differing in longitude, while viewing the ATS-6 satellite at the same satellite location, actually probe nearly the same plasmaspheric region even though the stations may have relatively large longitudinal differences. This is simply because the ray paths from the ground stations all converge at the satellite at 36,000 kilometers and in the plasmasphere they are also not significantly different. Klobuchar and Johanson (1977) indeed showed that the difference in monthly behavior between data sets taken at Hamilton, Mass. and Boulder, Col. was small. In view of this we shall take the Hamilton, Mass. data as being typical of the U.S. region and the data from Aberystwyth, Wales as typical of the European sector.

III.3.2 Experimental Results

With a substantial amount of data available only from Wales from the European sector and with the Hamilton, Mass. data representative of the U.S. data it is of interest to compare the absolute values of the monthly average N_p values versus local time. Data from Hamilton are from July 1974 through May 1975, taken when ATS-6 was at 94°W longitude, while data from Aberystwyth are from November 1975 through July 1976 during which time ATS-6

located at 35°E longitude. The scale on the left in Figure III.3.1 is in TEC units of $m^{-2}x10^{16}$, while the right hand scale is in nanoseconds of group delay at a system operational frequency of 1.6 GHz, the single frequency mode GPS system operational frequency. Also plotted in Figure III.3.1 is the one month's available N_p data from Kiruna, Sweden for October 1975.

It is immediately obvious from Figure III.3.1 that the Wales data is significantly higher than the values from the U.S. Kersley and Klobuchar (prep.) have attributed the difference between the N_p values in the American and European sectors as being due to the lower geomagnetic latitudes reached by the Aberystwyth ray path to ATS-6 as opposed to the ray from Hamilton, Mass. to ATS-6. At the lower geomagnetic latitudes the scale height at the base of the plasmasphere is predominantly controlled by H^+ ions, with consequent greater scale heights, as opposed to the higher magnetic latitudes where more O^+ ions yield smaller scale heights. The Wales ray path reaches a minimum L shell of 1.7 as opposed to 2.2 for the Hamilton ray path.

While the difference in the diurnal behavior of the two sets of data shown in Figure III.3.1 can be explained by their different minimum geomagnetic latitudes, for the systems engineer it is of more interest to point out that the day-to-night variation for both sets of data is less than the difference between the two data sets. The absolute value of the time delay is small in terms of present system accuracy requirements. In view of the small absolute values of time delay no attempts were made to fit diurnally changing functions to the monthly average data from the station. Simple constant values of

2 nanoseconds for the Wales data and 1 nanosecond for the U.S. representative data are probably sufficient to account for the monthly average values of plasmaspheric electron content.

III.3.3 Plasmaspheric Group Delay During Magnetic Storms

Major magnetic storms produce electrodynamical effects which cause the emptying of the plasmasphere into the ionosphere and/or the peeling off of the plasmasphere away from the near-earth region. The time for refilling of the plasmasphere has been studied by use of whistler measurements by Park (1974) and recently for the N_p data by Soicher (1976), Poletti-Liuzzi et al. (1977), Webb and Lanzerotti (1977), and by Hajeb-Hosseinieh (1977). The time for refilling of the plasmasphere as viewed from the mid-latitudes is on the order of several days. These results from a few representative magnetic storms illustrate that from 3 to 8 days are required for N_p to return to its approximate average value.

III.3.4 Conclusions

With the limited plasmaspheric data available thus far the additional contribution to ionospheric group delay not previously available from Faraday rotation measurements of TEC is of the order of 1 to 2 nanoseconds at 1.6 GHz. This value is certainly small compared to the present system operational requirements, but it is an additional amount which can be added to existing models of time delay. The difference between the European and U.S. data is significant and perhaps represents the two limiting cases of N_p from the mid-latitudes as the U.S. longitudes have the highest magnetic latitudes compared to geographic latitudes.

Insufficient data are presently available from higher latitudes to determine whether either of these regions will have values of N_p significantly different from those in the mid-latitudes. The one month of data available from Kiruna, Sweden compares well with the Aberystwyth data. The Sao Paulo data is at a much lower latitude than any of the other stations, yet it is consistant with the other data sets.

During magnetic storms N_p drops to very small values and takes from 3 to 8 days to recover to the average value. If information on occurrence of magnetic storms is available the model value of N_p can be modified accordingly. Of course, during magnetic storms much greater changes occur in the TEC of the ionosphere and the N_p depletions will be generally insignificant compared to the greater changes from average conditions which occur in the ionosphere. Thus, any TEC model must be capable of representing the ionospheric changes from average conditions, before the much smaller N_p values need be of concern.

All available N_p data are for solar minimum conditions and are from only two representative mid-latitude regions of the world, with small exception. It is expected that the electron content of the plasmasphere will increase with increasing solar activity as does the electron content of the ionosphere. Measurements of N_p using signals from ATS-6 are continuing.

References

Davies, K., R.B. Fritz, R.N. Grubb, and J.E. Jones, Some early results from the ATS-6 radio beacon experiment, Radio Sci., 10, Nos.8 & 9, 185-799, 1975.

Fritz, R.N., ATS-6 radio beacon electron content measurements at Boulder, July 1974-May 1975, Report UAG-58, World Data Center A for Solar-Terrestrial Physics, Boulder, Colo., Sept. 1976.

Hajeb-Hosseinieh, H., Ionospheric studies using geostationary satellites, Thesis submitted to the University of Wales, Aberystwyth, Wales, June 1977.

Kersley, L., private communication.

Kersley, L., and J. Klobuchar, Comparison of photonospheric electron content measurements from the American and European sectors, in preparation.

Klobuchar, J.A. and J.M. Johanson, A comparison of average plasmaspheric electron content at two mid-latitude stations, presented at Spring meeting of American Geophysical Union, Washington, D.C., June 1977.

Lassiter, E.M., and B. Parkinson, The status of the development of the NAVSTAR/Global Positioning System, Navigation, Vol.XXV, 97, 13-26, January 1977.

Park, C.G., Some features of plasma distribution in the plasmasphere deduced from Antarctic Whistlers, J. Geophys. Res., 79, 169-173, 1974.

Poletti-Liuzzi, D.A., K.C. Yeh, and C.H. Liu, Radio beacon studies of the plasmasphere, J. Geophys. Res., 82, 1106-1114, 1977.

Soicher, H., Diurnal, day-to-day, and seasonal variability of N_f, N_t, and N_p at Fort Monmouth, New Jersey, Cospar Satellite Beacon Symposium, Boston MA, Boston Univ., Ed. by M. Mendillo, June 1976.

Soicher, H., Comparative ionospheric and plasmaspheric electron contents from the three world regions, Nature, 264, 46-48, 1976.

Soicher, H., Response of electrons in ionosphere and plasmasphere to magnetic storms, Nature, 259, 33-35, 1976.

Webb, D.C. and L.J. Lanzerotti, Temporal variations in total equatorial plasmasphere content and their relationships to the ring current intensity and the plasmapause, presented at Spring meeting of American Geophysical Union, Washington, D.C., June, 1977.

List of Figures

Fig. III.3.1 Monthly average plasmaspheric electron content versus local time for Aberystwyth, Wales, (dashed line) and for Hamilton, Mass. (solid line). Also plotted are values from Kiruna, Sweden for October 1975 and from Sao Paulo, Brazil for May 1975. The right hand axis is the equivalent time delay in nanoseconds at 1.6 GHz.

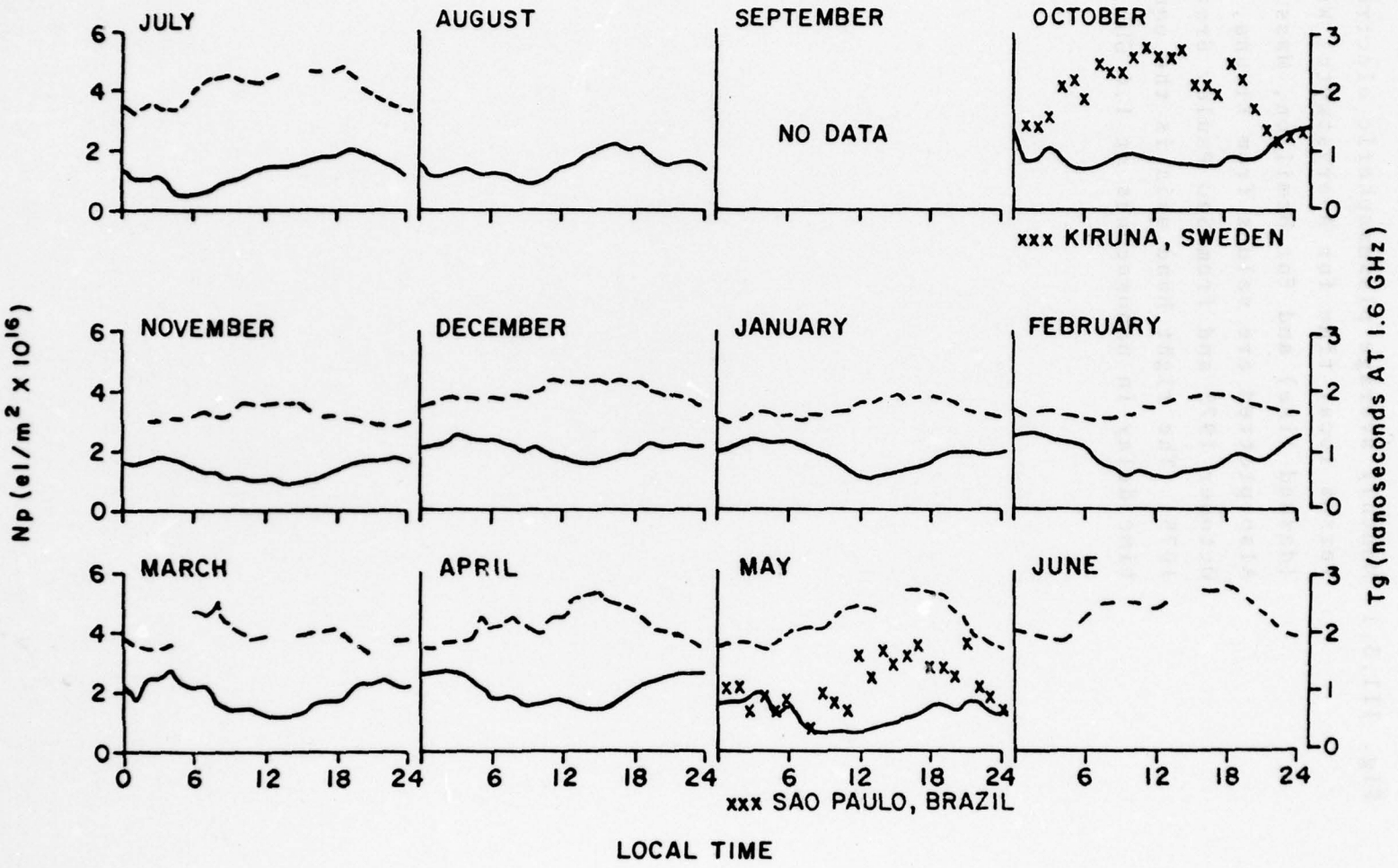

JULY
AUGUST
SEPTEMBER
OCTOBER
NO DATA
xxx KIRUNA, SWEDEN
NOVEMBER
DECEMBER
JANUARY
FEBRUARY
MARCH
APRIL
MAY
JUNE
xxx SAO PAULO, BRAZIL
Np (el/m² X 10¹⁶)
Tg (nanoseconds AT 1.6 GHz)
LOCAL TIME
0
6
12
18
24
0
2
4
6
0
1
2
3

FIG. III. 3.1

III.4 CONVERSION OF FARADAY ROTATION MEASUREMENTS TO TOTAL ELECTRON CONTENT

The measured quantity in the Faraday rotation experiment is, of course, the total amount of polarization rotation which a VHF radio wave undergoes along the path from a geostationary satellite to the observer on the ground. The relation between the observed Faraday rotation and the equivalent vertical TEC is given by

$$\Omega = \frac{K}{f^2} \int B \cos \theta \sec i \, N dh$$

where in practice the quantity B cos θ sec i is replaced by a mean vertical value $\overline{B \cos \theta \sec i}$, called $\overline{M}$, which equals the actual value at a height of approximately 420 kilometers in the ionosphere. Titheridge (1972) has shown that for a large number of ground stations and satellite locations 420 kilometers is an appropriate mean height to use for the conversion factor $\overline{M}$.

It was pointed out by Fritz (1972) that the diurnal motion of a so called "geostationary satellite" is in some cases large enough to require the use of a changing value of the $\overline{M}$ factor, if accurate values of TEC are required. Here we present the results of a brief study illustrating the potential error caused by neglecting the diurnal change in satellite motion, due primarily to the non-zero inclination of the satellite orbital plane with respect to the earth's equatorial plane.

III.4.1 Non-zero Geostationary Satellite Orbit Inclination

For an ideal geostationary satellite in a perfectly synchronous orbit with orbital inclination an eccentricity

exactly equal to zero the $\overline{M}$ value is indeed a constant and needs to be determined only once. In practice, however, even if the ideal orbit is initially achieved it soon becomes perturbed due to the gravitational forces of the sun, moon, and variations in the earth's gravitational field.

A non-zero inclination in the satellite's orbit results in a diurnal oscillation in latitude of the sub-satellite point around a mean value of latitude. Any ellipticity in the orbit will produce a similar oscillation in longitude. Examples of this are shown in Figure III.4.1 and Figure III.4.3. Figure III.4.1 is a plot of the actual hourly variation in latitude and longitude of the sub-satellite position of I2F3 which has an inclination of 6.6 degrees and eccentricity of .002 degrees. The corresponding $\overline{M}$ values for an observer at Lunping, Taiwan are shown in Figure III.4.2. A plot of the sub-satellite position of ATS-3 which has an inclination of 5.9 degrees and eccentricity of .002 appears in Figure III.4.3 and the corresponding $\overline{M}$ values for an observer at Hamilton, Massachusetts are shown in Figure III.4.4. The amplitude of the diurnal variation in $\overline{M}$ value for I2F3 as observed from Lunping is ±8.8% from the constant mean value which would traditionally be used in the Faraday computation. The amplitude of the diurnal variation in $\overline{M}$ value for ATS-3 as observed from Hamilton is ±5.5%. There are several effects to be noted:

1. For a near-geostationary satellite with a given inclination the relative diurnal change in the $\overline{M}$ factor will be in general larger for a lower latitude station, where the value of M is smaller than for a high latitude station.

The smaller $\overline{M}$ value is due to the angle θ being near 90 degrees for the low latitude station; for a given angular change in θ due to satellite diurnal positional changes the cosine of the angular change will be greater.

2. Since the line of constant $\overline{M}$ factor for most stations looking towards geostationary satellites lies in the east-west direction, north-south motion of the near-geostationary satellite will result in greater change in $\overline{M}$ than east-west satellite motion. The largest component of motion of a near-geostationary satellite due to its non-zero inclination is in the north-south direction.

3. Satellite launch techniques have improved to the point where the initial orbital inclination can be made non-zero, but in a phase such that the effects of the sun and the moon cause an initial decrease in the orbital inclination, which later goes through zero and then increases with time. Older "geostationary" satellites have fairly large inclination angles of their obbital plane; for instance the inclination of the orbit of ATS-1, launched in 1966 is over nine degrees. As the inclination of the orbital plane of a satellite increases with time the sub-satellite position will have greater latitudinal oscillations and thus a larger duirnal variation in the $\overline{M}$ value will occur.

III.4.2 Computer Program for Diurnal $\overline{M}$ Calculation Called ROPLOK

A computer program called ROPLOK has been developed which will calculate a satellite's position as a function of time

for a given set of orbital elements and will also calculate the corresponding $\overline{M}$ value for an observer at a given station as shown in Table 1. The program provides a set of relatively simple correction tables which can be used by the monitoring stations for obtaining more accurate TEC values. These tables, illustrated in Tables 1, 2, and 3, convert Faraday rotation angles expressed in the polarimeter polarization channel strip chart units of π values and millimeters into corrected TEC values. These tables have been designed to minimize the amount of time and effort that is required for an observer. The conversion tables are currently in use at observing stations in Athens, Greece; Goose Bay, Labrador; Hamilton, Massachusetts; Kennedy Space Flight Center, Florida; Ramey Air Force Base, Puerto Rico; Osan, Korea; Lunping, Taiwan; Shemya, Alaska; and Palehua, Hawaii.

III.4.3 Use of Program

In order to use the Faraday to TEC conversion correctly an observer should first verify that the station location, operating frequency, satellite being observed, and reference polarization value match those listed on the computer table headings.

The observer then turns to the page of the conversion tables with the proper π value and finds the millimeter reading which matches the polarization channel chart reading. He then scans across the table to find the final TEC value in the column which corresponds to the time of the observation.

For example, referring to the sample output in Table 3

one can easily see that for an observer at Lunping, Taiwan monitoring the satellite IS2F3 which has a nominal longitude of -161.9 degrees east, on a frequency of 136.44 MHz, with a reference polarization value of 13.5 millimeters during the month of September, 1976, a polarization chart reading of 2π, 15 millimeters at 14 hours universal time corresponds to a TEC value of 13.8×10^{16} el/m^2.

These TEC conversion tables were designed for real time use by weather observers. If the conversion is to be done by computer at a later time, the recommended procedure is to read the chart recordings in π's and millimeters and use an analytical conversion algorithm probably of sine wave shapes made from the hourly values of tabulated $\overline{M}$ given on the first page of the TEC conversion table output. Use of this procedure has become standard at AFGL as a result of this program development.

TABLE I

M-VALUE OUTPUT

LOOK ANGLES FOR A GEOSTATIONARY SATELLITE (EQUATORIAL ORBIT) AS A FUNCTION OF SATELLITE LATITUDE AND LONGITUDE.

DATE	STATION	LATITUDE	E.LONGITUDE
SEPTEMBER 15, 1976	TAIWAN	25.00	121.00

TIME (UT)		SUB-SATELLITE LAT	SUB-SATELLITE E.LONG	SUB-IONOSPHERIC LAT	SUB-IONOSPHERIC E.LONG	M	PSOP ANGLE	SEC Z	G	ELEV	AZIM	RANGE	HOUR ANGLE HR	HOUR ANGLE MIN	HOUR ANGLE SEC	DECLIN DEG	DECLIN MIN	ALPHA
0	0	4.7	-161.7	23.6	138.5	-29419.	108.5	2.822	3.69	4.7	91.5	41229.	18	19	41	0	39.0	-65.0
1	0	2.8	-161.9	23.1	138.9	-30711.	109.5	2.837	3.95	4.2	92.9	41278.	18	20	6	-0	-50.1	-64.9
2	0	1.2	-162.0	22.6	139.3	-32136.	110.5	2.852	4.34	3.6	94.5	41329.	18	20	38	-2	-30.7	-64.7
3	0	-.6	-162.1	22.0	139.8	-33682.	111.5	2.868	4.71	3.0	96.1	41380.	18	21	10	-4	-16.0	-64.6
4	0	-2.2	-162.2	21.3	140.2	-34329.	112.5	2.876	5.04	2.3	97.7	41431.	18	21	34	-5	-59.1	-64.6
5	0	-3.9	-162.3	20.8	140.7	-36064.	113.4	2.885	5.39	1.7	99.1	41478.	18	21	46	-7	-32.8	-64.5
6	0	-5.1	-162.3	20.2	141.1	-36924.	114.1	2.890	5.55	1.1	100.3	41521.	18	21	41	-8	-50.7	-64.5
7	0	-6.0	-162.2	19.6	141.5	-37457.	114.6	2.893	5.70	.6	101.1	41554.	18	21	20	-9	-47.4	-64.5
8	0	-6.5	-162.1	19.4	141.6	-37613.	114.8	2.894	5.73	.3	101.5	41576.	18	20	47	-10	-19.0	-64.5
9	0	-6.6	-161.9	19.5	141.4	-37520.	114.8	2.895	5.69	.1	101.5	41583.	18	20	9	-10	-23.2	-64.5
10	0	-6.2	-161.8	19.7	142.0	-37209.	114.5	2.895	5.74	.2	101.1	41571.	18	19	33	-9	-59.7	-64.6
11	0	-5.4	-161.7	20.4	141.8	-36735.	114.1	2.894	5.61	.4	100.3	41541.	18	19	6	-9	-10.1	-64.6
12	0	-4.2	-161.6	20.9	141.8	-36060.	113.4	2.892	5.42	.9	99.2	41494.	18	18	52	-7	-50.1	-64.6
13	0	-2.7	-161.5	21.1	141.9	-34930.	112.6	2.887	5.15	1.5	97.9	41433.	18	18	51	-6	-26.4	-64.6
14	0	-1.1	-161.6	21.7	142.4	-33656.	111.6	2.877	4.84	2.3	96.4	41364.	18	19	1	-4	-47.3	-64.7
15	0	.7	-161.7	22.4	142.8	-32434.	110.7	2.863	4.47	3.1	94.8	41293.	18	19	16	-3	-1.5	-64.7
16	0	2.4	-161.7	22.9	143.2	-31454.	109.7	2.845	4.08	3.9	93.3	41228.	18	19	30	-1	-12.6	-64.8
17	0	3.9	-161.8	23.4	143.7	-29753.	108.9	2.827	3.71	4.6	91.9	41174.	18	19	39	0	14.8	-64.9
18	0	5.1	-161.8	23.8	144.2	-28948.	108.1	2.811	3.39	5.1	90.7	41136.	18	19	39	1	32.1	-65.0
19	0	6.0	-161.8	24.1	144.8	-27823.	107.6	2.800	3.15	5.5	89.8	41116.	18	19	30	2	27.9	-65.1
20	0	6.5	-161.7	24.2	145.4	-27354.	107.3	2.794	2.99	5.8	89.3	41115.	18	19	17	2	58.3	-65.2
21	0	6.6	-161.7	24.2	145.9	-27310.	107.2	2.795	2.98	5.8	89.3	41130.	18	19	5	3	1.2	-65.2
22	0	6.2	-161.6	24.1	146.3	-27679.	107.4	2.802	3.10	5.4	89.6	41159.	18	18	58	2	36.4	-65.1
23	0	5.4	-161.6	23.9	146.3	-28414.	107.9	2.813	3.32	5.1	90.4	41196.	18	19	1	1	45.8	-65.1

FOR A SATELLITE AT THE EQUATOR...

	0.0	-161.9	22.1	139.8	-33035.	111.1	2.865	4.60	3.0	95.5	41426.	18	20	6	-3	-41.7	-64.7

NSAT=12F3 FREQ= 136.440 DETAT= 7.00 DETAR= 13.5

THIS PAGE IS BEST QUALITY PRACTICABLE
FROM COPY FURNISHED TO DDC

TABLE 2

TEC CONVERSION TABLE OUTPUT

CONVERSION TABLES FROM REFERENCE POLARIZATION CHANNEL CHART READINGS TO FINAL T.E.C. VALUES

********** WARNING **********

MAKE CERTAIN THAT STATION, SATELLITE, FREQUENCY, MONTH, AND REFERENCE POLARIZATION VALUE ARE CORRECT BEFORE USING THESE TABLES.

TO OBTAIN THE REFERENCE POLARIZATION VALUE:

1. INITIALLY ADJUST THE POLARIZATION CHANNELS FOR 45 MILLIMETERS (DIVISIONS) DEFLECTION.
2. CONNECT A SIGNAL GENERATOR INTO R.F. SWITCH INPUT "B" WITH INPUT "A" TERMINATED WITH WITH A MATCHED LOAD.
3. READ REFERENCE POLARIZATION VALUE ON POLARIZATION REFERENCE CHANNEL.

DIFFERENCES BETWEEN THE ACTUAL REFERENCE POLARIZATION VALUE AND THAT LISTED IN THE TABLE HEADINGS CAN BE ACCOMODATED BY ONE OF THE FOLLOWING:

1. TAKE THE DIFFERENCE BETWEEN THE ACTUAL REFERENCE POLARIZATION VALUE MINUS THE COMPUTER LISTED VALUE. ADD THIS VALUE TO THE FINAL CHART READINGS BEFORE LOOKING UP FINAL T.E.C. IN THE FOLLOWING TABLES.
2. NEW TABLES WITH CORRECT VALUES MAY BE OBTAINED FROM AFGL-LIR BY NOTIFYING THEM OF THE CORRECT REFERENCE POLARIZATION VALUE (IN MILLIMETERS).

THIS PAGE IS BEST QUALITY PRACTICABLE
FROM COPY FURNISHED TO DDC

TABLE 3

FARADAY TO TEC CONVERSION TABLE

DATE: SEPTEMBER 1976 | STATION: TAIWAN | SATELLITE (NOMINAL LONGITUDE): I2F3 -161.9 | FREQUENCY (MHZ): 136.440 | REFERENCE POLARIZATION VALUE (MM): 13.5

CHIRP PERIOD	HR	TIME (U.T.) 0	1	2	3	4	5	6	7	8	9	10	11	12	13	14	15	16	17	18	19	20	21	22	23
2	0	13.1	12.9	12.6	11.5	11.0	10.7	10.4	10.3	10.2	10.2	10.3	10.5	10.7	11.0	11.4	11.9	12.4	12.9	13.4	13.8	14.0	14.1	13.9	13.5
2	1	13.2	12.7	12.1	11.6	11.2	10.8	10.6	10.4	10.4	10.4	10.5	10.5	10.9	11.2	11.6	12.0	12.5	13.1	13.6	14.0	14.2	14.3	14.1	13.7
2	2	13.4	12.9	12.3	11.8	11.4	11.0	10.8	10.7	10.6	10.6	10.6	10.8	11.1	11.3	11.7	12.2	12.7	13.3	13.8	14.2	14.5	14.5	14.3	13.9
2	3	13.6	13.1	12.5	11.9	11.5	11.1	10.9	10.7	10.6	10.7	10.8	10.9	11.2	11.5	11.9	12.4	12.9	13.5	14.0	14.4	14.6	14.7	14.5	14.1
2	4	13.9	13.4	12.8	12.1	11.6	11.3	11.0	10.9	10.8	10.8	10.9	11.1	11.3	11.6	12.0	12.5	13.1	13.6	14.2	14.6	14.8	14.9	14.7	14.3
2	5	14.0	13.6	12.8	12.3	11.8	11.4	11.2	11.0	10.9	11.0	11.1	11.2	11.5	11.8	12.2	12.7	13.3	13.8	14.4	14.8	15.0	15.1	14.9	14.5
2	6	14.2	13.6	13.0	12.4	12.0	11.6	11.3	11.2	11.1	11.1	11.2	11.4	11.8	12.0	12.4	12.9	13.6	14.0	14.6	15.0	15.2	15.3	15.1	14.7
2	7	14.4	13.8	13.2	12.6	12.1	11.7	11.5	11.3	11.2	11.3	11.3	11.5	11.8	12.1	12.5	13.0	13.6	14.2	14.8	15.2	15.4	15.5	15.3	14.9
2	8	14.5	13.9	13.3	12.8	12.3	11.9	11.6	11.4	11.4	11.5	11.5	11.7	11.9	12.3	12.7	13.2	13.9	14.4	14.9	15.4	15.6	15.7	15.5	15.1
2	9	14.7	14.1	13.5	12.9	12.4	12.0	11.8	11.6	11.5	11.5	11.6	11.9	12.1	12.4	12.9	13.4	14.0	14.6	15.1	15.6	15.8	15.9	15.7	15.3
2	10	14.9	14.3	13.7	13.1	12.6	12.2	11.9	11.7	11.7	11.7	11.9	12.0	12.2	12.6	13.0	13.5	14.1	14.8	15.3	15.8	16.0	16.1	15.9	15.5
2	11	15.1	14.5	13.9	13.3	12.7	12.3	12.1	11.9	11.8	11.8	11.9	12.1	12.4	12.7	13.2	13.7	14.3	14.9	15.5	16.0	16.2	16.3	16.1	15.6
2	12	15.3	14.7	14.1	13.5	13.0	12.5	12.3	12.0	12.0	12.0	12.1	12.4	12.8	13.2	13.7	14.3	14.9	15.5	16.0	16.4	16.5	16.5	16.3	15.8
2	13	15.5	14.9	14.2	13.6	13.1	12.7	12.4	12.2	12.1	12.1	12.2	12.4	12.7	13.1	13.6	14.1	14.7	15.3	15.9	16.4	16.6	16.7	16.5	16.0
2	14	15.7	15.0	14.4	13.7	13.2	12.8	12.5	12.3	12.3	12.3	12.4	12.6	12.8	13.2	13.7	14.2	14.9	15.5	16.1	16.6	16.8	16.9	16.7	16.2
2	15	15.9	15.2	14.6	13.9	13.4	13.0	12.7	12.5	12.4	12.4	12.5	12.7	13.0	13.4	13.9	14.4	15.0	15.7	16.3	16.8	17.0	17.1	16.9	16.4
2	16	16.0	15.4	14.7	14.1	13.5	13.1	12.8	12.6	12.5	12.6	12.7	12.9	13.2	13.5	14.0	14.6	15.2	15.9	16.5	17.0	17.2	17.3	17.1	16.6
2	17	16.2	15.6	14.9	14.2	13.7	13.3	13.0	12.8	12.7	12.7	12.8	13.0	13.3	13.7	14.2	14.7	15.4	16.1	16.7	17.2	17.5	17.5	17.3	16.8
2	18	16.4	15.7	15.0	14.4	13.8	13.4	13.1	12.9	12.8	12.8	12.9	13.0	13.2	13.6	14.3	14.9	15.6	16.2	16.9	17.4	17.7	17.7	17.5	17.0
2	19	16.5	15.9	15.2	14.6	14.0	13.6	13.3	13.1	13.0	13.1	13.3	13.6	14.0	14.5	15.1	15.7	16.4	17.1	17.6	17.9	17.9	17.7	17.5	17.2
2	20	16.6	16.1	15.4	14.7	14.2	13.7	13.4	13.2	13.2	13.3	13.5	13.8	14.2	14.7	15.2	15.9	16.6	17.3	17.8	18.1	18.1	17.9	17.6	17.4
2	21	17.0	16.3	15.6	14.9	14.3	13.9	13.6	13.4	13.3	13.4	13.5	13.9	14.3	14.8	15.4	16.1	16.8	17.4	18.0	18.3	18.3	18.1	17.8	17.6
2	22	17.2	16.5	15.7	15.1	14.5	14.0	13.7	13.5	13.4	13.4	13.6	13.9	14.3	14.9	15.5	16.2	17.0	17.6	18.2	18.5	18.5	18.3	18.1	17.8
2	23	17.4	16.6	15.9	15.2	14.6	14.2	13.9	13.7	13.6	13.6	13.7	13.9	14.2	14.6	15.1	15.8	16.4	17.2	17.8	18.4	18.7	18.7	18.5	18.0
2	24	17.5	16.8	16.1	15.4	14.8	14.3	14.0	13.8	13.7	13.7	13.8	14.1	14.4	14.8	15.3	15.8	16.4	17.3	18.0	18.5	18.9	18.9	18.7	18.2
2	25	17.7	17.0	16.2	15.6	15.0	14.6	14.2	14.0	13.8	13.9	14.0	14.2	14.5	14.9	15.5	16.1	16.8	17.5	18.2	18.7	19.1	19.1	18.9	18.4
2	26	17.9	17.2	16.4	15.7	15.2	14.8	14.5	14.3	14.2	14.2	14.3	14.5	14.8	15.1	15.6	16.3	17.0	17.7	18.5	19.0	19.3	19.3	19.1	18.6
2	27	18.1	17.4	16.6	15.9	15.3	14.8	14.4	14.2	14.2	14.2	14.3	14.6	14.8	15.3	15.8	16.4	17.2	17.9	18.6	19.1	19.5	19.5	19.2	18.7
2	28	18.3	17.5	16.8	16.0	15.4	14.9	14.6	14.4	14.3	14.3	14.4	14.7	15.0	15.4	16.0	16.6	17.3	18.1	18.9	19.3	19.7	19.7	19.4	18.9
2	29	18.5	17.7	16.9	16.2	15.6	15.1	14.7	14.5	14.4	14.5	14.6	14.8	15.1	15.6	16.1	16.8	17.5	18.3	19.0	19.5	19.9	19.9	19.6	19.1
2	30	18.7	17.9	17.1	16.4	15.7	15.3	14.9	14.7	14.6	14.6	14.7	15.0	15.3	15.7	16.3	16.9	17.7	18.5	19.2	19.7	20.1	20.1	19.9	19.5
2	31	18.8	18.1	17.3	16.5	15.9	15.4	15.1	14.8	14.7	14.8	14.9	15.1	15.4	15.9	16.4	17.1	17.9	18.6	19.4	19.9	20.3	20.3	20.0	19.5
2	32	19.0	18.3	17.4	16.7	16.1	15.6	15.2	15.0	14.9	14.9	15.0	15.3	15.6	16.0	16.6	17.3	18.0	18.8	19.6	20.1	20.5	20.5	20.2	19.7
2	33	19.2	18.4	17.6	16.9	16.2	15.7	15.4	15.1	15.0	15.1	15.2	15.4	15.8	16.2	16.8	17.5	18.2	19.0	19.7	20.3	20.7	20.7	20.4	19.9
2	34	19.4	18.6	17.8	17.0	16.4	15.9	15.5	15.3	15.2	15.2	15.3	15.5	15.9	16.4	16.9	17.6	18.4	19.2	19.9	20.5	20.9	20.9	20.6	20.1
2	35	19.5	18.8	18.0	17.2	16.6	16.0	15.6	15.4	15.3	15.3	15.5	15.9	16.4	16.9	17.6	18.4	19.2	19.9	20.5	21.0	21.3	21.3	21.0	20.5
2	36	19.6	19.0	18.1	17.4	16.7	16.2	15.8	15.6	15.5	15.5	15.6	15.9	16.2	16.7	17.3	18.0	18.8	19.6	20.3	20.9	21.3	21.3	21.0	20.5
2	37	20.0	19.1	18.2	17.5	16.8	16.3	15.9	15.7	15.6	15.6	15.8	16.0	16.4	16.8	17.4	18.1	18.9	19.8	20.5	21.1	21.5	21.5	21.2	20.7
2	38	20.2	19.3	18.5	17.7	17.0	16.5	16.1	15.9	15.8	15.8	15.9	16.2	16.5	17.0	17.6	18.3	19.1	19.9	20.7	21.3	21.7	21.7	21.4	20.9
2	39	20.4	19.6	18.8	17.8	17.2	16.8	16.2	16.0	15.9	15.9	16.1	16.3	16.7	17.1	17.8	18.5	19.3	20.1	20.9	21.5	21.9	21.9	21.6	21.1
2	40	20.5	19.7	19.0	18.0	17.3	16.8	16.4	16.2	16.1	16.1	16.2	16.5	16.8	17.3	17.9	18.6	19.5	20.3	21.1	21.7	22.1	22.1	21.8	21.3
2	41	20.7	19.9	19.2	18.2	17.5	16.9	16.5	16.3	16.2	16.2	16.4	16.6	17.0	17.5	18.1	18.8	19.6	20.5	21.3	21.9	22.3	22.3	22.0	21.5
2	42	20.9	20.0	19.2	18.3	17.6	17.1	16.7	16.5	16.3	16.4	16.5	16.8	17.1	17.6	18.2	19.0	19.8	20.7	21.5	22.1	22.5	22.5	22.2	21.7
2	43	21.1	20.2	19.4	18.5	17.9	17.2	16.8	16.6	16.5	16.5	16.7	16.9	17.3	17.8	18.4	19.2	20.0	20.9	21.7	22.3	22.7	22.7	22.4	21.8
2	44	21.3	20.4	19.5	18.7	18.0	17.4	17.0	16.7	16.6	16.7	16.8	17.1	17.4	17.9	18.6	19.3	20.2	21.0	21.9	22.5	22.9	22.9	22.6	22.0

THIS PAGE IS BEST QUALITY PRACTICABLE
FROM COPY FURNISHED TO DDC

FIGURE CAPTIONS

Figure III.4.1 Locus of INTELSAT 2F3 sub-satellite position versus UT.

Figure III.4.2 Diurnal variation of M factor for INTELSAT 2F3 as observed from Lunping, Taiwan.

Figure III.4.3 Locus of ATS-3 sub-satellite position versus UT.

Figure III.4.4 Diurnal variation of M factor for ATS-3 as observed from Hamilton, Massachusetts.

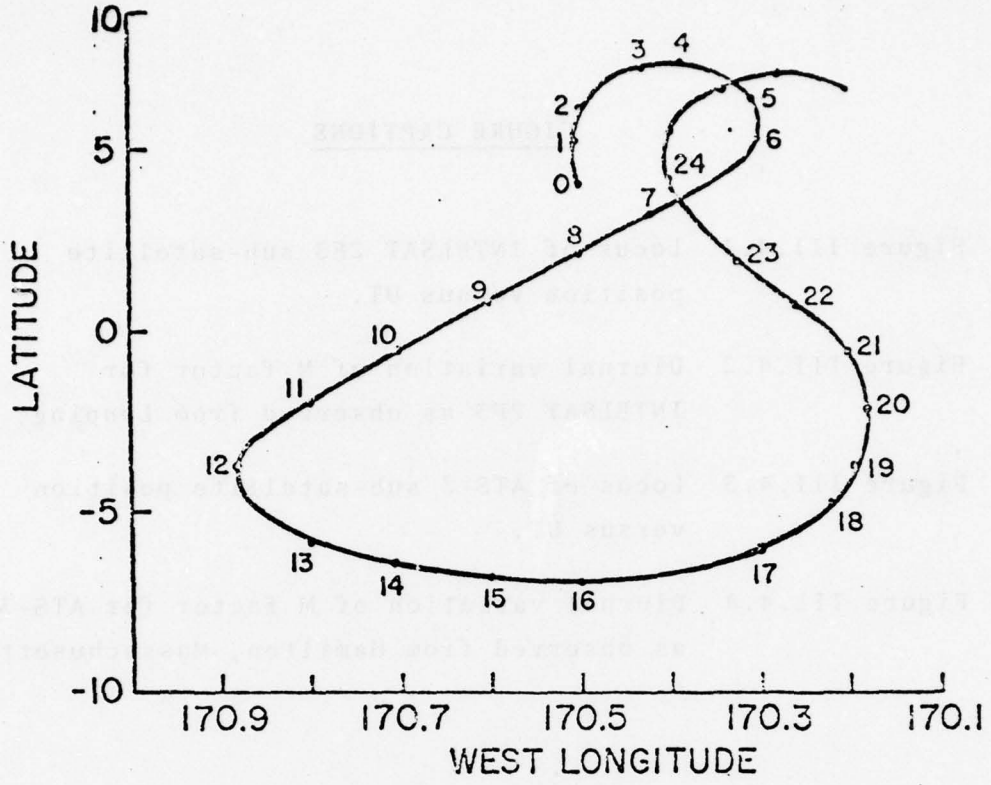


Fig. III.4.1

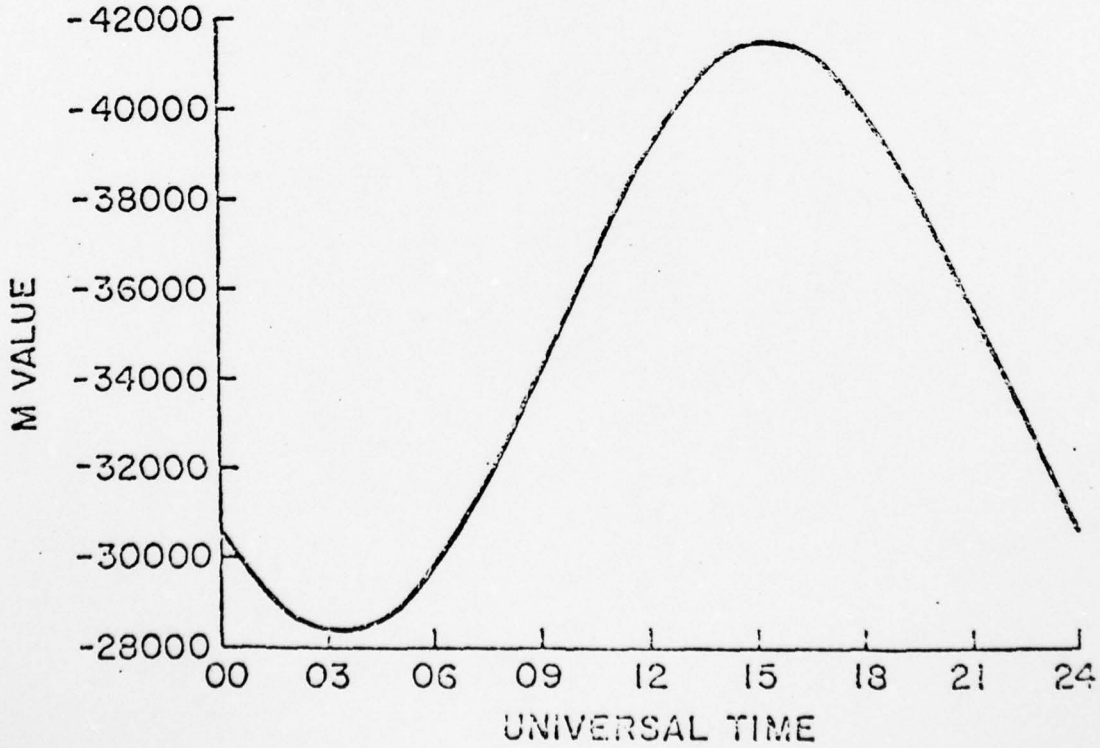


Fig. III.4.2

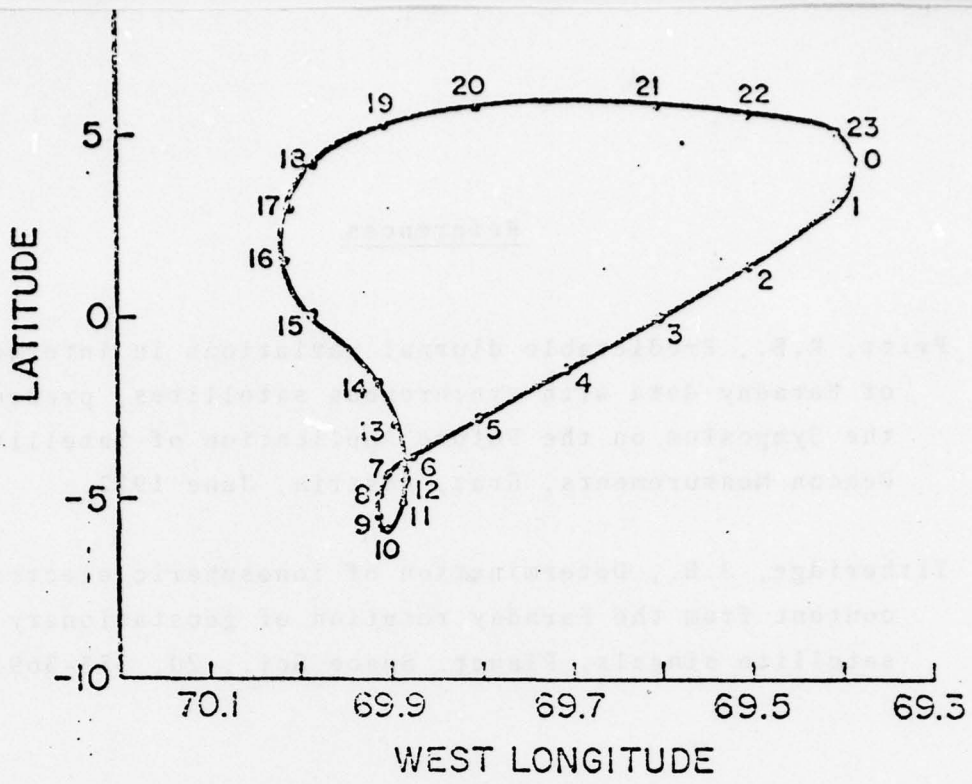


Fig. III.4.3

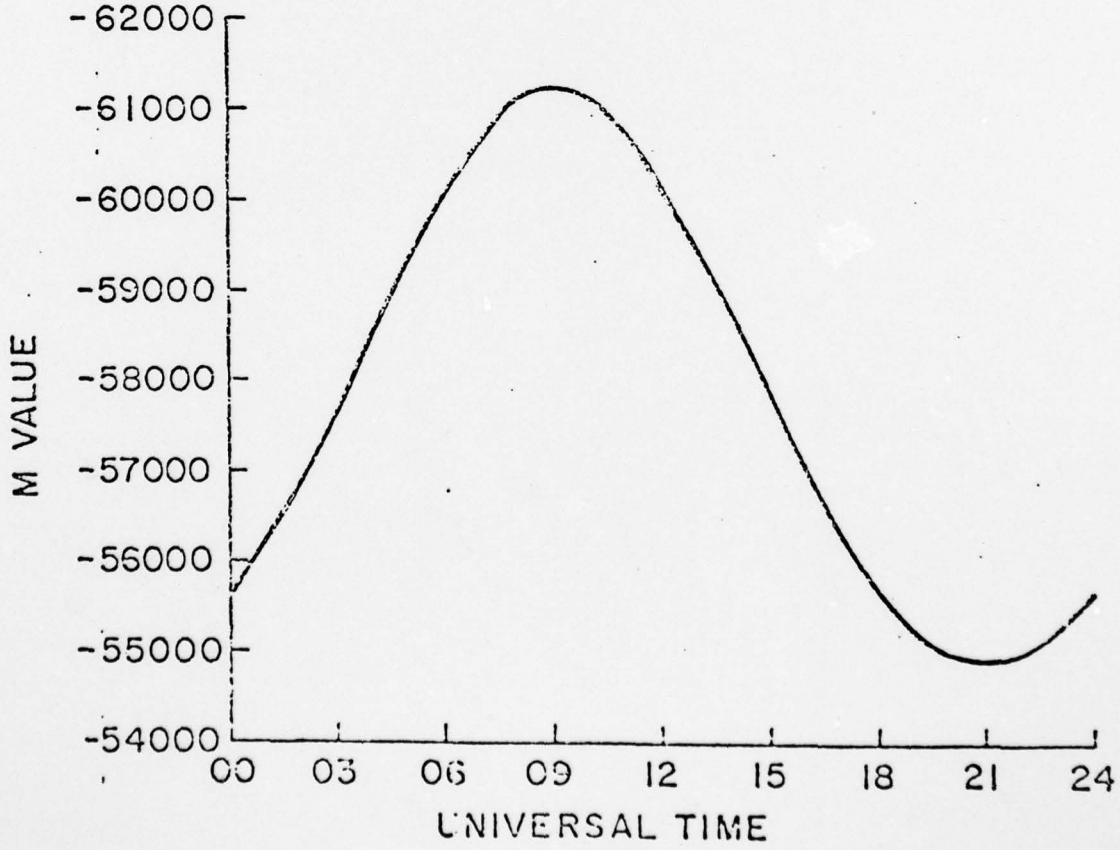
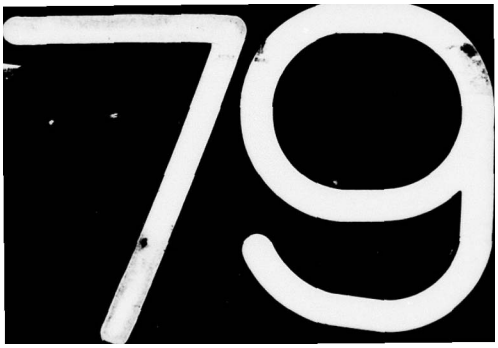


Fig. III.4.4

References

Fritz, R.B., Predictable diurnal variations in interpretation of Faraday data with synchronous satellites, presented at the Symposium on the Future Application of Satellite Beacon Measurements, Graz, Austria, June 1972.

Titheridge, J.E., Determination of ionospheric electron content from the Faraday rotation of geostationary satellite singals, Planet. Space Sci., 20, 353-369, 1972.


79